Scientific Inquiry and Review (SIR)
Volume 7 Issue 1, 2023
ISSN (P): 2521-2427, ISSN (E): 2521-2435
Homepage: https://journals.umt.edu.pk/index.php/SIR

Article QR

Title:	**Measuring the Awareness of Polycystic Ovarian Syndrome (PCOS) among Women in Punjab, Pakistan**
Author (s):	Alina Rafique[1], Um E Salma[1], Hafiz Ghulam Murtaza Saleem[2]
Affiliation (s):	[1]University of Lahore, Pakistan [2]QIE Lahore Campus, Riphah International University, Pakistan
DOI:	https://doi.org/10.32350/sir.71.01
History:	Received: September 5, 2022, Revised: December 1, 2023, Accepted: December 2, 2022, Published: March 15, 2023
Citation:	Rafique A, Salma U, Saleem HGM. Measuring the awareness of polycystic ovarian syndrome (PCOS) among Women in Punjab, Pakistan. *Sci Inq Rev.* 2023;7(1):1–16. https://doi.org/10.32350/sir.71.01
Copyright:	© The Authors
Licensing:	This article is open access and is distributed under the terms of Creative Commons Attribution 4.0 International License
Conflict of Interest:	Author(s) declared no conflict of interest

A publication of
The School of Science
University of Management and Technology, Lahore, Pakistan

Measuring the Awareness of Polycystic Ovarian Syndrome (PCOS) among Women in Punjab, Pakistan

Alina Rafique[1*], Um E Salma[1], Hafiz Ghulam Murtaza Saleem[2]

[1]University Institute of Medical Lab Technology, Faculty of Allied Health Sciences, University of Lahore, Pakistan
[2]Department of Medical Laboratory Technology, Faculty of Rehabilitation & Allied Health Sciences, QIE Lahore Campus Riphah International University, Pakistan

ABSTRACT

Polycystic ovarian syndrome (PCOS) is the most prevailing endocrine disorder among women of reproductive age, worldwide. Its prevalence is 52% in Pakistani women and the rate of infertility is gradually increasing. It can be treated through early diagnosis, management of symptoms, and a healthy lifestyle. This cross-sectional study aimed to determine the level of awareness and knowledge regarding PCOS in the women of Punjab, Pakistan. For this purpose, a total of 350 women between the ages of 16 and 50 years were included in the current study. The data was obtained through a questionnaire and analyzed through SPSS (version 25). The results determined that 56% of women were found to have the knowledge of PCOS, while 44% had never heard about it. Furthermore, about 67% of 196 PCOS-aware women were unaware of its signs and symptoms. Moreover, in 14% of the cases, a friend was the source of knowledge regarding PCOS. Whereas, approximately 10% of these women had heard about the syndrome through education, 9% through their family, 7% through various media such as newspapers, television, and social media, and 17% through other sources including general physicians and gynecologists. It was concluded that only 33% of the participants who claimed to have heard of PCOS were aware of its symptoms, whereas 67% were unaware of them. A total of 152 women, out of 350, had never heard about PCOS.

Keywords: endocrine disorder, infertility, healthy lifestyle, polycystic ovarian syndrome (PCOS), women of reproductive age

1. INTRODUCTION

Polycystic ovary syndrome (PCOS) is known worldwide as a common syndrome affecting the women of reproductive age and causing

* Corresponding Author: dr.alinarafique@gmail.com

reproductive, endocrine, and metabolic abnormalities. PCOS is delineated as a heterogeneous disorder associated with hormonal changes, a deranged reproductive system, and complications related to the metabolic system [1]. It is a heritable disorder which affects women throughout their lifetime and can be transferred to the next generation, although the underlying genetic factors remain unknown [2]. Hyperandrogenism, ovaries with multiple cysts, and impaired ovaries are the key features of PCOS. This disorder affects both developed as well as developing countries. Its prevalence ranges from 4-12% in the general population of women of reproductive age across the world [3].

Throughout puberty, the prevalence of PCOS continuously increases and reaches 26% by the age of 15. Insulin resistance or pre-diabetes and Type 2 diabetes are prevalent in women with PCOS living in Asia. Insulin resistance and high levels of insulin are two common precursors of Type 2 diabetes and have a high prevalence in South Asian women. Type 2 diabetes is inherited in the form of a complex genetic trait that interacts with other factors and contributes to developing PCOS [4]. Symptoms commonly associated with PCOS are irregular or missed periods due to anovulation, ovaries consisting of multiple cysts, non-appearance of ovulation, high level of androgens [5], oligomenorrhea, amenorrhea, prolonged erratic menstrual bleeding [6], infertility [7], hirsutism [8], acne [9], mood swings including depression and anxiety [10], and family history with Type 2 diabetes [11].

Three distinct clinical phenotypes were suggested by the Rotterdam and AE-PCOS Society namely Frank PCOS (oligomenorrhea, higher level of androgens, and PCO), ovulatory PCOS (PCO, higher level of hyperandrogenism and normal menstruation), and non-PCO PCOS (oligomenorrhea, hyperandrogenism, and normal ovary). A fourth phenotype, that is, mild or normoandrogenic PCOS is also recognized by the Rotterdam criteria, which is characterized by oligomenorrhea, PCO, and typical androgen concentrations [12].

In addition to other classical symptoms, stress is highly coexistent with PCOS. Stress in PCOS can be of various types namely psychological distress, mental disorders, anxiety, emotional disarray, and depression [10]. Along with definitive mental stress, ‘metabolic stress’ is also quite common in women with PCOS. Indeed, metabolic stress is the most influencing stress in PCOS. It is often referred to as the stimulant behind all the emotional and anxiety-related consequences in women with PCOS [13].

A characteristic of the ovaries in PCOS is rapid transition from primitive follicles to growing follicles with rising numbers of follicles from 2 mm to 3 mm and then from 3 mm to 4mm [14-16]. Adolescent girls with PCOS features often require the management of their symptoms before the diagnosis of PCOS. The management of adolescents with a confirmed diagnosis of PCOS should include its awareness and lifestyle interventions [17]. The diagnosis of girls with signs and symptoms indicating PCOS includes family history and a complete physical examination. Typically, laboratory examination includes thyroid profile as well as the determination of prolactin, total testosterone, androstenedione, sex hormone-binding globulin (SHBG), and dehydroepiandrosterone (DHEA). Furthermore, adrenal imaging tests can be used for diagnosis depending on clinical examination, physical examination, and initial laboratory results [18].

Mohamed conducted a quasi-experimental study on 300 women that included implementing and designing a helpful instructional guideline about endometriosis. The study shows an important result, indicating an improvement in females' awareness about it. [19]. Belenkaia (2019) showed that polycystic ovarian syndrome (PCOS) is recognized as one of the most common endocrine diseases in women, universally. On the other hand, this term does not capture the variety of medical symbols linked with this syndrome. Menstrual abnormality and medical features of androgen excess, which are common place in women with PCOS, are not included under the definition of PCOS, which is limited to polycystic ovarian morphology (PCOM) [20].

2. METHODOLOGY

2.1. Study Design

A cross-sectional study was conducted focusing on assessment-based questions and the provision of education about PCOS.

2.2. Locality Setting

Data was collected from the various cities of Punjab, Pakistan.

2.3. Duration

This study was completed in October 2021.

2.4. Sample Size

A total of 350 questionnaires were distributed among women.

2.5. Sample Technique

It is a questionnaire-based study.

2.6. Inclusion Criteria

Women between the ages of 16 and 50 years were included in the current study.

2.7. Exclusion Criteria

Women aged less than 16 years or more than 50 years were excluded.

2.8. Data Collection Procedure

Data was collected through a questionnaire developed beforehand. The questionnaire was constructed in parts related to demographics, information sources, understanding of signs and symptoms, risk factors, prevalence, and etiology.

2.9. Data Analysis

Data was tabulated and analyzed through Microsoft Excel and IBM SPSS Statistics (version 25). Chi-square test was used to statistically analyze the comparison between categorical variables, that is, variables that only take a finite number of distinct values. The results were reported in terms of frequencies and percentages calculated for each question in the questionnaire.

3. RESULTS

3.1. Demographic Characteristics

Table 1. Demographic Characteristics

Description	Frequency	Percentage
Age		
15-25 years	196	56
26-35 years	78	22
36-45 years	41	11.7
46-55 years	35	10
Locality		
Urban	250	28.6
Rural	100	71.4

Description	Frequency	Percentage
Education Level		
School	45	12.9
College	162	46.3
University	141	40.3
Other	2	6
Marital Status		
Married	152	43.5
Single	198	56.6
Occupation		
Employee	77	22.5
Household	90	25.5
Student	183	52.3

Demographic characteristics are tabulated in Table 1. The table shows that 196 (56%) women were from the age group of 15-25 years, 78 (22%) were from the age group of 26-35 years, and 41 (11.7%) were from the age group of 36-45 years. It also shows that 100 (28.6%) women belonged to the rural areas of Punjab, while the rest of the 250 (71.4%) women belonged to urban areas. Furthermore, 162 (46.3%) women were enrolled in college and 141 (40.3%) were university going. Whereas, 198 (56.6%) were single.

3.2. Knowledge Regarding PCOS

Knowledge regarding PCOS is tabulated in Table 2. The majority of the women, that is, 56% responded positively to questions regarding PCOS awareness. However, 44% had never heard of PCOS and did not know anything about it.

3.3. Diagnosis of PCOS

The number of women diagnosed with PCOS is tabulated in Table 3. It shows that 82.9% of women had not been diagnosed with PCOS, while 17.1% of them had been diagnosed with the disease.

The results in Table 4 show that there is a significant association between PCOS diagnosis and menstrual problems in women (p-value is less than 0.05 which is significant). According to the above table, 32 women faced skipped periods problem and 16 faced irregular menstrual cycles.

Table 2. Knowledge and Awareness regarding PCOS

Questions	Yes	No	Do not know
Have you ever heard of PCOS?	196 (56%)	154 (44%)	N/A
Do you know the symptoms of PCOS?	116 (33.1%)	234 (66.9%)	N/A
Do you think PCOS is linked with Diabetes Mellitus Type 2?	70 (20%)	81 (23%)	199 (56.9%)
Do you think PCOS has a negative impact on the quality of life in the form of stress, anxiety etc?	85 (24.3%)	83 (23.7%)	182 (52%)
Do you think untreated PCOS can cause infertility in women?	94 (26.9%)	59 (16.9%)	197 (56.3)
Do you think obesity increases the risk of developing PCOS?	119 (34%)	54 (15.4%)	177 (50.6%)
Do you think unpleasant mood is also a risk factor for PCOS?	105 (30%)	62 (17.7%)	183 (52.3%)
Is ultrasound a best way for the detection of PCOS?	97 (27.7%)	59 (16.9%)	194 (55.4%)

Table 3. Diagnosis of PCOS

Description	Yes	No
Have you ever been diagnosed with PCOS?	82.9%	17.1%

Table 4. Association between PCOS Diagnosis and Menstrual Problems in Women

		History of PCOS Diagnosed Patients with Menstrual Problems					
		Yes/No	Irregular menstrual periods	Skipped one or more periods	Excessive bleeding	Clots of blood in periods	*p*
Have you ever been diagnosed with PCOS?	No	290	0	0	0	0	0.00
	Yes	0	16	32	5	7	

Table 5. Association between WHO Obesity Criteria and Number of Diagnosed Patients

		Have you ever been diagnosed with PCOS?		*p*-value
		Yes	No	
WHO Obesity Criteria	Underweight	36	2	0.00
	Normal	199	11	
	Overweight	44	39	
	Obese	11	8	

The results show that there is an association between WHO obesity criteria and the number of diagnosed patients (*p*-value is less than 0.05 which is significant). Following the WHO obesity criteria, 36 underweight, 199 normal, 44 overweight, and 11 obese women were diagnosed with PCOS.

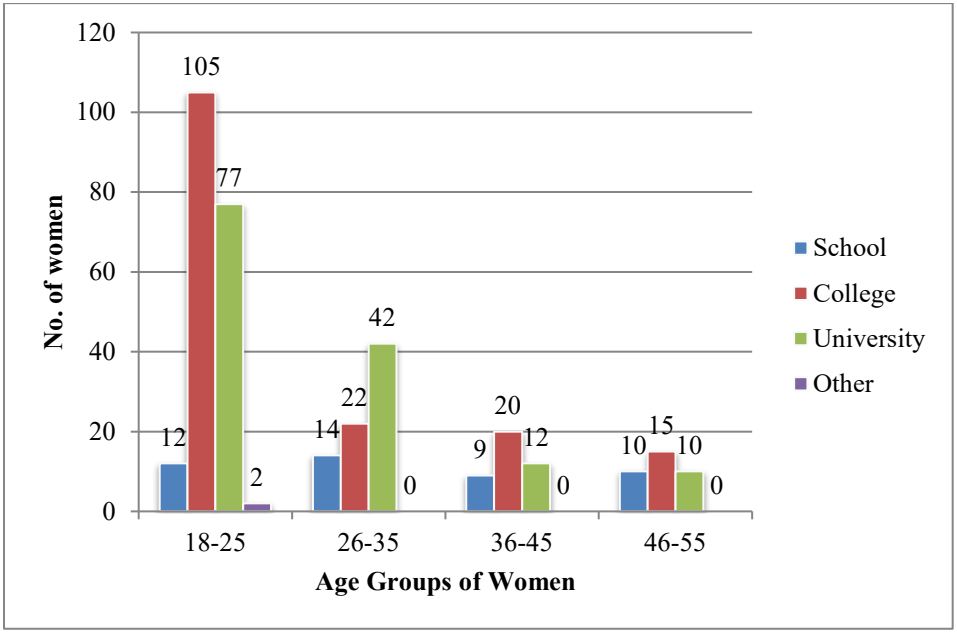

Figure 1. Age Groups of Women and their Education Level

Figure 1 depicts that most women in the age group 18-25 were college educated. While, most women had university education in the age group 26-35. Whereas, most women were college educated in the age group 36-45. Finally, most women in the age group 45-55 were also college educated.

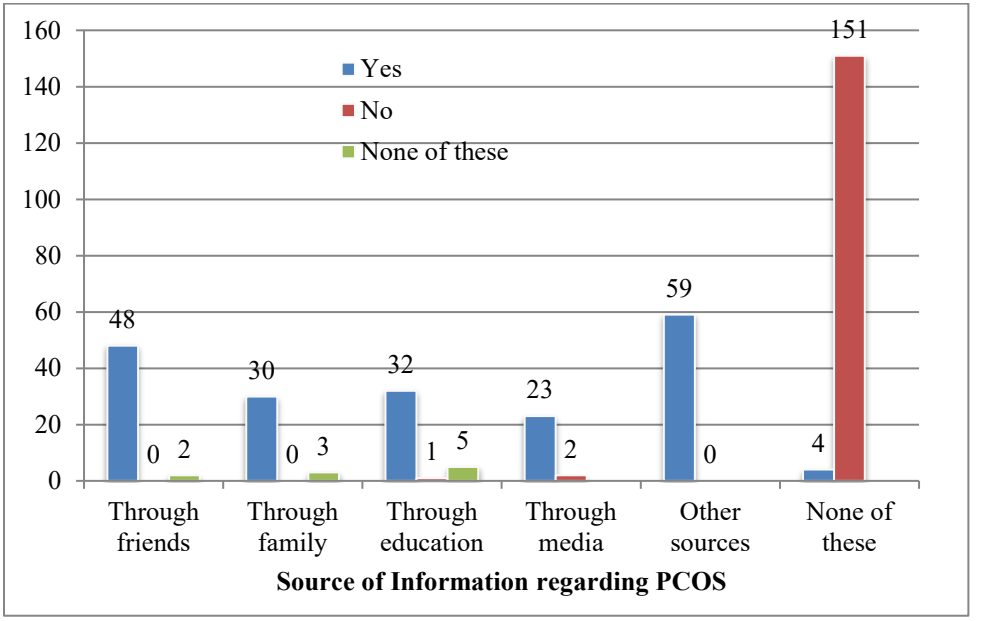

Figure 2. PCOS Awareness in Women and their Source of Information

Figure 2 depicts that out of the 196 women who had heard of PCOS, 48 heard about it through friends, 30 through family, 32 through education, 23 through media, and 59 through other sources.

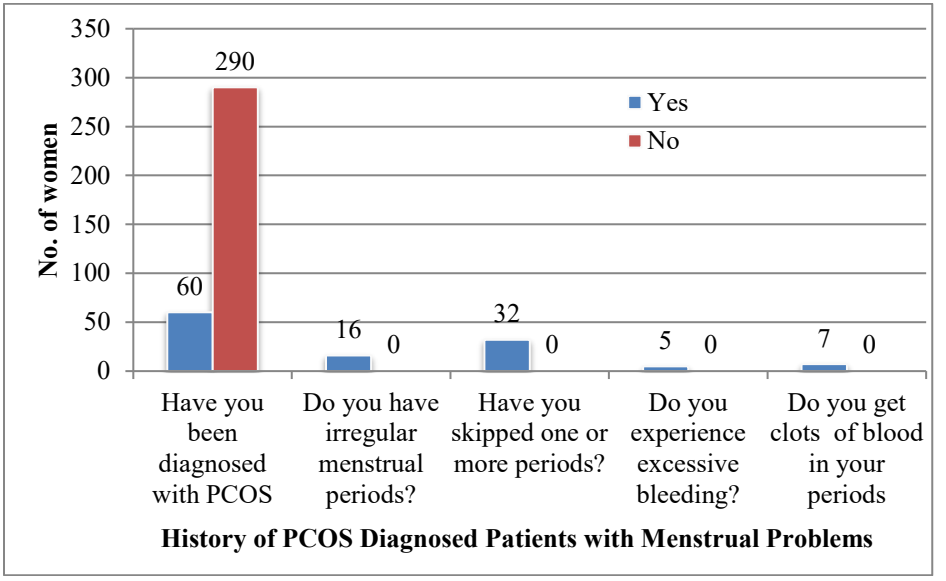

Figure 3. PCOS Diagnosis and Menstrual Problems in Women

Figure 3 depicts that 32 women had faced skipped periods problems and 16 had faced irregular menstrual cycles.

4. DISCUSSION

Sunanda recorded that 85% of women (in their study?) were in the age group of 21-25 years, while 82% of them enjoyed a diet incorporating diverse food groups, and 92% had an orderly menstrual pattern [21]. Sills noticed that more than half (63%) of 657 women involved were in the age range of 26-34 years at the time. Approximately 60% of them were normal according to the WHO criteria of obesity. Nearly 24% were overweight and 6% fell in the obese category. Conversely, 11% of women were underweight [22]. Sanchez noticed that 32% of women were obese in their study [23].

Moreover, about 56% of women under observation had heard of PCOS. On the contrary, 44% of them had never heard of the disease and were unaware of its symptoms, risk factors, treatment options, and severity of consequences. Furthermore, 67% of women, who had heard of PCOS, did not know about its symptoms. Approximately 33% of women were aware of the symptoms of the disease. A survey by Scott estimated that more than 50% of the 657 women involved were fully aware of the syndrome. In this regard, as shown by the analysis, doctors were the primary source of knowledge for 63.5% of women [23].

Out of the 196 women who had heard of PCOS previously, the source was a friend in 14% of cases. Whereas, 10% of them had heard of the syndrome through education, 9% through their family, and 7% through different media including social media, newspaper, and television. Furthermore, 17% of women said that their source of information was their general physician or gynecologist. Sunanda observed poor awareness of PCOS in 76% of women, whereas 10.7% had thorough information of the disease [21]. Sills concluded that over 97% of respondents were acquainted with POCS, while 1.9% had not been briefed about the disease [23]. Sills also noticed that all respondents who were 26 to 34 years of age were comparatively more informed of the condition than those belonging to other age groups [23]. Gul reported that 20 out of 177 participants were conscious of this condition. Of these 20 participants, 11 had qualifications in biological sciences [24].

In the current study, only 14% of women considered irregular menstrual

cycles as something which should not be neglected. Almost 51% didn't know that obese women are at a higher risk of developing PCOS than others, whereas 15% said that obesity has no role in causing the disease. Almost 53% of women didn't know that unpleasant mood is a risk factor for PCOS, while 18% said that it is not related to the disease. Approximately 17% of women didn't know that infertility can be induced because of an untreated PCOS. Only 15% identified hirsutism to be a condition that cannot be ignored and that could lead to PCOS. These problems, that is, menstrual irregularity, hirsutism, and obesity, which are often neglected by women, are associated with elevated testosterone levels and PCO appearance on ultrasound [22]. Joshi concluded that a record of infrequent menstrual periods showed a 93.3% positive probability of the disease and an 86.7% negative probability to identify its potential occurrence [24].

Among 60 women diagnosed with PCOS, 41.7% believed in physical activity. Approximately 31% were aware that physical exercise can improve PCOS related condition. Many women with the disease experience the feelings of hopelessness and insecurity because of their inability to conceive, the size of their bodies, and excessive facial hair. This has a huge effect on the psychological health of women with PCOS. Scott's research suggested distress in 66.5% of women due to PCOS, while this analysis found 32% of women as apprehensive because they were not fully informed about the nature of the disease and if they would be able to control it. About 19% of women feel distressed as the out of form body and the decreased quality of life obstruct their emotional stability, which is also affected by chemical shifts in PCOS [23]. Maiya stated that ranked resistance training helped to reduce the cyst's thickness, improved fertilization, as well as the conceiving rate, as compared to an experimental group [25]. A similar survey by Nidhi found that therapeutic meditation system in PCOS patients minimizes the feelings of depression [26].

In the current study, about 64% of women didn't know that androgen levels are significantly raised during PCOS. Furthermore, approximately 12% chose unaltered androgen, whereas 9% chose low androgen levels as blood test confirmation for the disease. The androgen abundance and PCOS community developed the newest testing manual in 2006. According to this manual, hyper-androgenism and dysfunctional ovaries (oligoavulation or anovulation and/or cysts in ovaries) are the salient features of the disease [27]. Approximately 40% of women were positive that the treatment of

PCOS is possible. Nearly 12.5% declared it as an untreatable disease. About 47.5% didn't know if any treatment for PCOS exists or not.

The treatment of PCOS can be initiated through increased physical activity and regular exercise. Changes in routine are regarded as the first line therapy for women diagnosed with the disease [28]. In a relevant study, Sills found that 99% of women showed interest in other possible treatments of their condition, rather than using fertility medication or contraceptives [23]. Unawareness in women regarding PCOS is a result of the lack of knowledge and poor education about this matter. Illiteracy is also one of the leading causes of the lack of awareness about such a sensitive issue.

4.1. Conclusion

Based on the survey findings, it was concluded that a significant portion of women, approximately 33% of those who claimed to have heard of PCOS, demonstrated an understanding of the syndrome and its associated symptoms. However, it was concerning to note that the majority, constituting 67% of these women, lacked awareness regarding the signs and symptoms of PCOS. Moreover, a substantial number of participants, specifically 152 out of the total 350 women surveyed, acknowledged never having heard of PCOS before.

Healthcare professionals should play a crucial role as primary sources of information about PCOS for women. Targeted educational campaigns can bridge the knowledge gap and enhance awareness, leading to improved understanding, early detection, and management of PCOS.

4.2. Recommendations

Exercise plans that are well-designed for PCOS patients should be introduced. Physicians should promote regular physical activity apart from providing need-based exercise plans. Gynecologists should coordinate with physiotherapists to ensure that PCOS patients are provided with more befitting workout plans. Academicians should educate young students about PCOS, its risk factors, causes, prognosis, symptoms, diagnosis, and available treatment options. These efforts can make early detection of PCOS more likely.

Women who have a BMI above 23 should be informed about its dangers and risks. They should be advised to lose weight in order to maintain a healthy body and mind. Women exhibiting signs of hyper-androgenism or

menstrual irregularities should be checked up to ensure the early detection of the syndrome. Timely identification of the disease combined with immediate therapy enhances the quality of life and helps to avoid health risks. This study can be used to explore the obstructions women face in lifestyle improvements such as regular physical exercise, weight control, following a healthy diet plan, and keeping their menstrual cycle in check. This survey can also be used to observe the effects of these improvements in a test group of women.

REFERENCES

1. Li D, Jiao J, Zhou YM, Wang XX. Epigenetic regulation of traf2-and Nck-interacting kinase (TNIK) in polycystic ovary syndrome. *Am J Transl Res*. 2015;7(6):1152–1160.
2. Li J, Wu Q, Wu XK, et al. Effect of exposure to second-hand smoke from husbands on biochemical hyperandrogenism, metabolic syndrome and conception rates in women with polycystic ovary syndrome undergoing ovulation induction. *Hum Reprod*. 2018;33(4):617–25. https://doi.org/10.1093/humrep/dey027
3. Azziz R, Carmina E, Chen Z, et al. Polycystic ovary syndrome. *Nat Rev Dis Primers*. 2016;2:e16057. https://doi.org/10.1038/nrdp.2016.57
4. Khan IA, Movva S, Shaik NA, et al. Investigation of Calpain 10 gene polymorphism in Asian Indians with gestational diabetes mellitus. *Meta Gene*. 2014;2:299–306. https://doi.org/10.1016/j.mgene.2014.03.001
5. Panda PK, Rane R, Ravichandran R, Singh S, Panchal H. Genetics of PCOS: A systematic bioinformatics approach to unveil the proteins responsible for PCOS. *Genom Data*. 2016;8:52–60. https://doi.org/10.1016/j.gdata.2016.03.008
6. Ingudomnukul E, Baron-Cohen S, Wheelwright S, Knickmeyer R. Elevated rates of testosterone-related disorders in women with autism spectrum conditions. *Horm Behav*. 2007;51(5):597–604. https://doi.org/10.1016/j.yhbeh.2007.02.001
7. Teede H, Deeks A, Moran L. Polycystic ovary syndrome: A complex condition with psychological, reproductive and metabolic manifestations that impacts on health across the lifespan. *BMC Med*. 2010;8:e41. https://doi.org/10.1186/1741-7015-8-41

8. Fauser B, Tarlatzis B, Rebar R, et al. Consensus on women's health aspects of polycystic ovary syndrome (PCOS). *Hum Reprod*. 2011;27(1):14–24. https://doi.org/10.1093/humrep/der396

9. Lowenstein EJ. Diagnosis and management of the dermatologic manifestations of the polycystic ovary syndrome. *Dermatol Ther*. 2006;19(4):210–23. https://doi.org/10.1111/j.1529-8019.2006.00077.x

10. Deeks AA, Gibson-Helm M, Paul E, Teede HJ. Is having polycystic ovary syndrome a predictor of poor psychological function including anxiety and depression? *Hum Reprod*. 2011;26(6):1399–1407. https://doi.org/10.1093/humrep/der071

11. Lujan ME, Jarrett BY, Brooks ED, et al. Updated ultrasound criteria for polycystic ovary syndrome: reliable thresholds for elevated follicle population and ovarian volume. *Hum Reprod*. 2013;28(5):1361–1368. https://doi.org/10.1093/humrep/det062

12. Kim JJ, Hwang KR, Choi YM, et al. Complete phenotypic and metabolic profiles of a large consecutive cohort of untreated Korean women with polycystic ovary syndrome. *Fertil Steril*. 2014;101(5):1424–1430. https://doi.org/10.1016/j.fertnstert.2014.01.049

13. Diamanti- Kandarakis E, Dunaif A. Insulin resistance and the polycystic ovary syndrome revisited: An update on mechanisms and implications. *Endocr Rev*. 2012;33(6):981–1030. https://doi.org/10.1210/er.2011-1034

14. Oróstica L, Rosas C, Plaza-Parrochia F, et al. Altered steroid metabolism and insulin signaling in PCOS endometria: Impact in tissue function. *Curr Pharm Des*. 2016;22(36):5614–5624.

15. Webber L, Stubbs S, Stark J, et al. Formation and early development of follicles in the polycystic ovary. *Lancet*. 2003;362(9389):1017–1021. https://doi.org/10.1016/S0140-6736(03)14410-8

16. Maciel GAR, Baracat EC, Benda JA, et al. Stockpiling of transitional and classic primary follicles in ovaries of women with polycystic ovary syndrome. *J Clin Endocrinol Metab*. 2004;89(11):5321–5327. https://doi.org/10.1210/jc.2004-0643

17. Ibanez L, Oberfield SE, Witchel S, et al. An international consortium

update: Pathophysiology, diagnosis, and treatment of polycystic ovarian syndrome in adolescence. *Horm Res Paediatr.* 2017;88:371–395. https://doi.org/10.1159/000479371

18. Armengaud JB, Charkaluk ML, Trivin C, et al. Precocious pubarche: Distinguishing late-onset congenital adrenal hyperplasia from premature adrenarche. *J Clin Endocrinol Metab.* 2009;94(8):2835–2840. https://doi.org/10.1210/jc.2009-0314

19. Mohamed W, Hassan H. Effect of instructional supportive guideline for improving women's awareness towards endometriosis. *Am J Nurs Res*. 2020;8(1):38–47. https://doi.org/10.12691/ajnr-8-1-5

20. Belenkaia LV, Lazareva LM, Walker W, Lizneva DV, Suturina LV. Criteria, phenotypes and prevalence of polycystic ovary syndrome. *Minerva Ginecol*. 2019;71(3):211–223. https://doi.org/10.23736/s0026-4784.19.04404-6

21. Sunanda B, Nayak S. A study to assess the knowledge regarding PCOS (polycystic ovarian syndrome) among nursing students at NUINS. *J Health Allied Sci NU*. 2016;6(3):24–26. https://doi.org/10.1055/s-0040-1708657

22. Sills ES, Perloe M, Tucker MJ, Kaplan CR, Genton MG, Schattman GL. Diagnostic and treatment characteristics of polycystic ovary syndrome: Descriptive measurements of patient perception and awareness from 657 confidential self-reports. *BMC Women's Health*. 2001;1:e3. https://doi.org/10.1186/1472-6874-1-3

23. Sanchez N. A life course perspective on polycystic ovary syndrome. *Int J Women's Health*. 2014;6:115–122.

24. Joshi B, Mukherjee S, Patil A, Purandare A, Chauhan S, Vaidya R. A cross-sectional study of polycystic ovarian syndrome among adolescent and young girls in Mumbai, India. *Indian J Endocrinol Metab*. 2014;18(3):317–324. https://doi.org/10.4103%2F2230-8210.131162

25. Maiya AG, Sheela R, Kumar P. Exercise-induced weight reduction and fertility outcomes in women with polycystic ovarian syndrome who are obese and infertile: A preliminary report'. *J Exerc Sci Physiother*. 2008;4(1):30–34.

26. Nidhi R, Padmalatha V, Raghuram Nagarathna RA. Effect of holistic

yoga program on anxiety symptoms in adolescent girls with polycystic ovarian syndrome: A randomized control trial. *Int J Yoga*. 2012;5(2):112–117. https://doi.org/10.4103%2F0973-6131.98223

27. Azziz R, Carmina E, Dewailly D, *et al*. The Androgen Excess and PCOS Society criteria for the polycystic ovary syndrome: the complete task force report. *Fertil Steril*. 2009;91(2):456-488. https://doi.org/10.1016/j.fertnstert.2008.06.035

28. Vause TD, Cheung AP, Sierra S, et al. Ovulation induction in polycystic ovary syndrome. *J Obstet Gynaecol Can*. 2010;32(5):495–502. https://doi.org/10.1016/S1701-2163(16)34504-2

Scientific Inquiry and Review (SIR)
Volume 7 Issue 1, 2023
ISSN (P): 2521-2427, ISSN (E): 2521-2435
Homepage: https://journals.umt.edu.pk/index.php/SIR

Article QR

Title:	**Monotone Data Modelling Using Rational Cubic Fractal Interpolation Function**
Author (s):	Tayba Arooj[1], Farheen Ibraheem[2], Malik Zawwar Hussain[3]
Affiliation (s):	[1]Lahore College for Women University, Lahore, Pakistan. [2]Forman Christian College- A Chartered University-FCCU, Lahore, Pakistan. [3]University of the Punjab, Lahore, Pakistan.
DOI:	https://doi.org/10.32350/sir.71.02
History:	Received: October 5, 2022, Revised: December 5, 2022, Accepted: December 5, 2022, Published: March 15, 2023
Citation:	Arooj T, Ibraheem F, Hussain MZ. Monotone data modelling using rational cubic fractal interpolation function. *Sci Inq Rev.* 2023;7(1):17–32. https://doi.org/10.32350/sir.71.02
Copyright:	© The Authors
Licensing:	This article is open access and is distributed under the terms of Creative Commons Attribution 4.0 International License
Conflict of Interest:	Author(s) declared no conflict of interest

A publication of
The School of Science
University of Management and Technology, Lahore, Pakistan

Monotone Data Modelling Using Rational Cubic Fractal Interpolation Function

Tayba Arooj[1], Farheen Ibraheem[2*], and Malik Zawwar Hussain[3]

[1]Department of Mathematics, Lahore College for Women University, Pakistan.
[2]Deparment of Mathematics, Forman Christian College-A Chartered University-FCCU, Lahore, Pakistan.
[3]Deparment of Mathematics, University of the Punjab, Lahore, Pakistan.

ABSTRACT

Geometric modelling of several intricate and complex structures such as trees, mountains, clouds, ferns, geographic topography, and coastlines is challenging in computer graphics. Traditional splines such as trigonometric, polynomial, exponential, and rational fail to simulate this significant class of complex structures, which are highly irregular in nature. For this purpose, this research develops a novel cutting-edge method for synthesizing and modelling structures. The proposed technique; C^1 fractal interpolation function (FIF) builds an iterated function system (IFS) by integrating fractal calculus and rational cubic polynomial functions. Appropriate conditions on scaling and shape parameters are derived to help maintain the inherited shape qualities of the data. Experiments in numerous scientific domains, such as the pharmaceutical and chemical industries have been presented as an example, to confirm the usefulness of the suggested model. Moreover, the graphic results demonstrated that the developed monotone hybrid model (MHM) offers a heterogeneous method for gathering data with a monotone structure.

Keywords: fractal interpolation, hybrid model, monotone interpolation, spline functions

1. INTRODUCTION

Interpolation is an indispensable tool for estimating the unknown function for data modelling. There are numerous interpolation techniques, which use various function families, including polynomial, exponential, rational, trigonometric, and spline. However, these traditional non-recursive approaches resulted in interpolants, which were differentiable several times, with the possible exception of a limited number of points and restricted model smooth structures. Many signals in the real world and in

* Corresponding Author: farheenibraheem@fccollege.edu.pk

experimental data are complex and their composition frequently demonstrates irregularities and hardly ever appears to be smooth. Thereby, interpolants that could picture non-smooth signals, as well as smooth structures, were highly required. The prime purpose of this research is to provide an innovative framework for the approximate representation of non-smooth data from natural (feathers, trees, leaves, clouds, feathers, flowers, glaciers, landscapes, and galaxies), engineering or scientific phenomena together with the collection of smooth data. A novel form of fractal interpolation function is created utilizing the rational spline containing a cubic polynomial in the numerator as well as the denominator.

One of the pivotal characteristics of data generated from countless physical phenomena, scientific problems, and engineering applications is monotonicity where entities only have a meaning when their values are monotone. For instance, in the field of engineering, Tensile Strength, Ultimate Tensile Strength or Ultimate Strength is not an uncommon concept. It refers to the maximum level of stress that a structure or material can tolerate while being pulled or stretched before getting breaking. This phenomenon gave rise to monotone data. The applied forces, commonly called stress and the stretch, referred to as strain, are always in a monotonic relationship where one varies with the change in the value of the other [1]. Certain devices, such as; digital-to-analog (DAC used in audio video devices) and analog-to-digital (ADC used in music recording and digital signal processing), have monotonicity an essential characteristic used in feedback control loops [1]. In CAD and DAC, the digital output code always increases as the analog voltage input increase and vice versa. Monotonicity can be seen in Newton's law of cooling in which the rate of heat loss is directly proportional to the differences in temperature between the bodies [2].

Monotonicity also appears in other phenomena, such as the content of atrazine and nitrate in shallow ground waters, the link between the partial pressure of oxygen, and the percentage dissociation of hemoglobin percentage dissociation and oxygen partial pressure, erythrocyte sedimentation rate in patients with cancer and concentration of uric acid level in a patient affected from gout [3]. It is a fundamental function behind the renowned 'Probability theory' that uses the monotonically increasing function of a random variable in its cumulative distribution.

Natural phenomena can produce monotonic positive data as well. The relationship between a child's height and their intake of food and energy can be considered as an example. For instance, height is a positive quantity and always goes up. There are several other examples in everyday experiences where objects only create meaning when their values are monotonous. Examples are surfaces and the dose-response curve in biochemistry and pharmacology; consumption function that describes the relationship between a household's consumption and its available income in economics, statistical approximations of copulas and quasi-copulas, [4] and empirical option pricing models in finance [4].

Based on different approaches (such as classical spline, spline with knots, and fractal spline) various monotonicity-preserving models for monotone data have been discussed in the previous literature [1-18]. Spline functions have also been used for the solution of partial differential equations [19, 20]. Previously, spline functions have become the main tools for solving monotonicity problems. For instance, Crisp and Hussain [5] solved the issue of monotonicity through Bernstein-Bezier rational cubic functions. Spline functions were also used to provide multiple kinds of monotonicity methods for bivariate functions on triangles [6].

Using different types of spline functions, some other useful techniques and algorithms were supplied to address the problem of monotonicity [1, 3, 7]. Typically, data that comes from experiments (for instance, information drawn from signals in the actual world, including seismic information, financial series, and bioelectric recordings are complex and immensely irregular. As a result, interpolating these data using traditional interpolation techniques became an inappropriate challenge. Barnsley [8] made an attempt by introducing a new interpolation method called Fractal Interpolation using a special type of iterated function system. It provided a powerful framework to deal with highly irregular data. However, consistently, when it is a prerequisite that the interpolant should reflect the inherited shape features (convexity, positivity, monotonicity) of the irregular data set, fractal interpolation functions failed to secure the shape properties of data. Later, Barnsley and Harrington [9] noticed that in case the problem is of shape preservation type, then the parameters of the IFS may be chosen suitably so that the corresponding FIF preserve the inherited properties of the data. This observation initiated a striking relationship

between the classical splines interpolation functions and the fractal interpolation functions.

Recently, with the help of Barnsley and Harrington's results, various spline functions have been generalized in the form of fractal spline functions for instance [4, 10]. Fractal spline [11] though interpolating both regular and irregular data does not guarantee that the model satisfies the monotone trend lies in their data. Non-monotone visual models of the aforementioned experiments misguide us about the actual scenario (which might help scientists to recognize and evaluate various patterns and artifacts in their data) in these experiments. Hence, the visual model must maintain the geometric property of the experimental data in order to achieve precise and proficient results.

The goal of the underlying research is to build a fractal geometry-based function to simulate hidden patterns and future behaviour in many disciplines. A monotone hybrid model (MHM) which is a combination of fractal interpolation function (FIF) and spline interpolation model (SIM) was presented for this purpose. The shape-preserving model is then created with the help of the proposed function to handle the non-linearity problem that the traditional interpolation model was unable to solve. Additionally, the proposed class surpasses its conventional non-recursive counterpart in approximating monotone functions with varied irregularities/fractality in their first derivatives (smooth to nowhere differentiable).

The proposed hybrid model offered a variety of shape control parameters that can be sufficient and highly useful to achieve desired results. To meet the objective, a general piecewise rational cubic fractal interpolation function (GPRC FIF) [11] is used in the construction of MHM.

The proposed model has the following useful features in comparison with the existing models:

- The proposed scheme converts the hybrid model [11] to a monotone hybrid model.
- The proposed hybrid model MHM is the generalization of the model presented in [7].
- Unlike [12], no derivative constraints are imposed in proposed model as MHM works for both data and data with derivatives proficiently.

- Once, the shape parameters are selected, the curve representation becomes unique in its description.
- Existing methods have no degree of freedom [1, 3, 12, 13], whereas the proposed model gives two degrees of freedom.
- The proposed model works for larger as well as smaller data, whereas in [14], constraints are developed on the subinterval lengths for data modelling.

Four shape parameters are used in the proposed model, whereas in [3, 15] one and two shape parameters are used respectively. The remaining sections are structured as follows. Section 2 focuses on a brief introduction to the basic methodology of the hybrid model developed in [11]. In Section 3, a new scheme is developed, which converts the hybrid model to a monotone hybrid model, for solving the problem of monotonicity. Whereas the proposed model is tested on different real data sets to verify their usefulness in Section 4. Comparative analysis has been presented in Section 5 and finally, Section 6 concludes with the significance of the proposed study.

2. METHODOLOGY

In this section, the hybrid model (GPRC FIF) [11] based on the fractal framework and spline function was briefly reviewed. The fractal framework was built on an iterative function system (IFS), which is defined below comprehensively.

2.1. IFS Theory

Let the real interval $I[r_1, r_n]$ be partitioned such that $r_1 < r_2 < \cdots < r_n$. Suppose the data set is given $\{(r_i, \hat{v}_i) \in I \times E : i = 1,2, \dots, n\}$, where E is denoted as a suitable compact set containing all $\hat{v}_i's$. Take $I_i = [r_i, r_{i+1}]$, then the two mappings given below would be contraction homeomorphic so that $\varepsilon_i : I \to I_i$,

with

$$\varepsilon_i(r_1) = r_i, \ \ \varepsilon_i(r_n) = r_{i+1}, \ \ \ i = 1,2, \dots, n-1. \tag{2.1}$$

$$|\varepsilon_i(e_1) - \varepsilon_i(e_2)| \leq l_i |e_1 - e_2|, \ \ \forall\, e_1, e_2 \ \in I, \text{ for some } \ \ 0 < l_i < 1.$$

Suppose, $A = I \times E$ and there is a mapping $\sigma_i : A \to E$, which is continuous if

$\sigma_i(r_1, \hat{v}_1) = \hat{v}_i,\ \sigma_i(r_n, \hat{v}_n) = \hat{v}_{i+1}, i = 1,2, \dots, n-1.$ (2.2)

$|\sigma_i(r, x) - \sigma_i(r, y)| \leq \kappa_i |x - y|, r \in I,\ \forall\ x, y\ \in E,$ for some $-1 < \kappa_i < 1$.

Take $\tau_i: A \to A$, which is defined as:

$$\tau_i(r, \hat{v}) = \big(\varepsilon_i(r), \sigma_i(r, \hat{v})\big), \forall\ (r, \hat{v}) \in A. \quad (2.3)$$

Where

$\varepsilon_i(r) = a_i r + b_i, \sigma_i(r, \hat{v}) = \kappa_i \hat{v} + g_i(r),$

with $a_i = \frac{r_{i+1} - r_i}{r_n - r_1},\ b_i = \frac{r_n r_i - r_1 r_{i+1}}{r_n - r_1}$.

Here, $g_i(r)$ is any suitable continuous function. The set $\{A; \tau_i: i \in (1,2,3, \cdots, n-1)\}$ is termed as an iterative function system.

2.2.Hybrid Model

The hybrid model [11] φ is termed as GPRC FIF corresponding to the iterative function system as:

$$\varphi\big(\varepsilon_i(r)\big) = \kappa_i \varphi(r) + g_i(r), \quad (2.4)$$

with $g_i(r) = \frac{P_i(r)}{Q_i(r)} = \frac{P_i(\hat{\mu})}{Q_i(\hat{\mu})}$,

where

$P_i(\hat{\mu}) = \eta_i(z_i - \kappa_i \hat{v}_1)(1 - \hat{\mu})^3 + (\eta_i h_i d_i - (r_n - r_1)\eta_i \kappa_i d_1 + \delta_i(\hat{v}_i - \kappa_i \hat{v}_1))\hat{\mu}(1 - \hat{\mu})^2 + (-\omega_i h_i d_{i+1} + (r_n - r_1)\omega_i \kappa_i d_n + \rho_i(\hat{v}_{i+1} - \kappa_i \hat{v}_n))\hat{\mu}^2(1 - \hat{\mu}) + \omega_i(\hat{v}_{i+1} - \kappa_i \hat{v}_n)\hat{\mu}^3,$

$Q_i(\mu) = \eta_i(1 - \hat{\mu})^3 + \delta_i \hat{\mu}(1 - \hat{\mu})^2 + \rho_i \hat{\mu}^2(1 - \hat{\mu}) + \omega_i \hat{\mu}^3,\ \ \hat{\mu} = \frac{r - r_1}{r_n - r_1},\ \ \hat{v} \in [r_1, r_n]$.

Here, $\kappa_i < 1$ are the scaling factors, d_i is the derivative value at the knot points and $\eta_i, \delta_i, \rho_i, \omega_i$ are the non-negative shape parameters.

3. A MONOTONE HYBRID MODEL

This section sets up a monotone hybrid model (MHM) to solve the monotonicity problem present in the hybrid model as defined in [11]. In setting up the MHM, certain conditions were imposed to shape the parameters and scaling factors, to acquire the desired model.

Let, the monotone data set $\{(r_i, \hat{v}_i) \in I \times E : i = 1,2, \dots, n\}$ be distributed such that $r_1 \leq r_2 \leq \cdots \leq r_n$ with $\hat{v}_{i+1} \geq \hat{v}_i,\ i = 1,2, \dots, n-1.$

Or alternatively,

$$\xi_i = \frac{\hat{v}_{i+1} - \hat{v}_i}{h_i} \geq 0,\ i = 1,2, \dots, n-1. \tag{3.1}$$

For the function that increases monotonically, the necessary constraints were applied on derivative as:

$$\partial_i \geq 0, i = 1,2, \dots, n. \tag{3.2}$$

For the data set increasing monotonically, there are two possibilities.

Case 1: If $\xi_i = 0$ and $\kappa_i = 0$ particularly for some monotone and collinear data set, the function defined in **Eq.** (**2.4**) is constant in each subinterval. Therefore,

$$\partial_i = \partial_{i+1} = 0, i = 1,2, \dots, n.$$

So that

$$\varphi(r) = \hat{v}_i, \quad \forall\, r \in [r_1, r_n], i = 1,2, \dots, n-1.$$

This demonstrates the process by which a hybrid model automatically transforms into a monotonous hybrid model.

Case 2: If $\xi_i > 0$ and $\xi_i - \kappa_i \xi_n > 0 \Leftrightarrow \kappa_i < \frac{\hat{v}_{i+1} - \hat{v}_i}{\hat{v}_n - \hat{v}_1}$, where $\xi_n = \frac{\hat{v}_n - \hat{v}_1}{h_i}$, for this case, we have the following theorem.

Theorem 3.1: Suppose $\{(r_i, \hat{v}_i) : i = 1,2, \cdots, n\}$ be a monotone data set such that $\hat{v}_i > 0$. Assuming $\eta_i > 0$, $\omega_i > 0$ and ∂_i constitute the derivative at the knot points $\hat{v}_i$. Then the corresponding hybrid function GPRC FIF converts to monotone hybrid model (preserve monotonicity) in each interval if the scaling factors and shape parameters satisfy the following condition:

(i) The scaling factors κ_i, $i = 1,2, \dots, n$, are picked as:

$$0 \leq \kappa_i < min\{a_i, \kappa_{1i}^*, \kappa_{2i}^*, \kappa_{3i}^*\}$$

(ii) The shape parameters δ_i, $\rho_i, i = 1,2, \dots, n,$ are chosen as:

$$\delta_i > \frac{\eta_i\left(\partial_i - \frac{\kappa_i}{a_i}\partial_1\right)}{(\xi_i - \kappa_i\xi_n)},\ \rho_i > max\left\{\frac{\omega_i\left(\partial_{i+1} - \frac{\kappa_i}{a_i}\partial_n\right)}{(\xi_i - \kappa_i\xi_n)}, \left(\frac{3\eta_i\omega_i - \delta_i\omega_i\left(\partial_{i+1} - \frac{\kappa_i}{a_i}\partial_n\right)}{\delta_i(\xi_i - \kappa_i\xi_n) + \eta_i\left(\partial_i - \frac{\kappa_i}{a_i}\partial_1\right)}\right)\right\}.$$

where

$$\kappa_{1i}^* = \frac{a_i\,\partial_{i+1}}{\partial_n}, \quad \kappa_{2i}^* = \frac{a_i\partial_i}{\partial_1}, \kappa_{3i}^* = \frac{\hat{v}_{i+1} - \hat{v}_i}{\hat{v}_n - \hat{v}_1}$$

Proof: Take the monotone data set into consideration without losing generality and

$$\varphi\left(\varepsilon_i(r)\right) = \kappa_i\varphi(\mathrm{r}) + g_i(r)$$

It is clear from single variable calculus that the function, $\varphi\left(\varepsilon_i(r)\right)$ is monotone increasing (decreasing) if and only if $\varphi^{(1)} \geq 0$ ($\varphi^{(1)} \leq 0$).

Here, φ is FIF, so derivative $\varphi^{(1)}$ is also FIF and satisfies functional equation. After careful calculation, we arrived at the following equation by differentiating the above equation with respect to r.

$$\varphi\left(\varepsilon_i(r)\right)^{(1)} = \frac{\kappa_i\,\varphi(r)^{(1)}}{a_i} + g_i{}^{(1)}\,(r) \tag{3.3}$$

The hybrid function defined in (4) becomes monotone hybrid model if $\varphi^{(1)} \geq 0$ and only if $g_i{}^{(1)} \geq 0$ for all $r \in [r_i, r_{i+1}]$.

Taking that $\kappa_i \geq 0\ \forall\ i \in \{1,2,3,\cdots,n\}$, it is evident that $\varphi^{(1)} \geq 0\ ,\forall\ r \in [r_1, r_n]$ if

$$g_i{}^{(1)}\,(r) = \sum_{j=1}^{6} \hat{c}_{ji}\,\frac{\hat{\mu}^{\,6-j}(1-\hat{\mu}\,)^{j-1}}{[q_i(\hat{\mu}\,)]^2} \geq 0\ ,\forall\ \mu \in [0,1]. \tag{3.4}$$

where

$$\hat{c}_{1i} = \omega_i^2(\partial_{i+1} - \frac{\kappa_i}{a_i}\partial_n),$$

$$\hat{c}_{2i} = \hat{c}_{1i} + 2\omega_i(\delta_i(\xi_i - \kappa_i\xi_n) - \eta_i(d_i - \frac{\kappa_i}{a_i}\partial_1)),$$

$$\hat{c}_{3i} = (\hat{c}_{2i} - \hat{c}_{1i}) - \left(3\eta_i\omega_i - \delta_i\rho_i(\xi_i - \kappa_i\xi_n)\right) + (\delta_i\omega_i(\partial_{i+1} - \frac{\kappa_i}{a_i}\partial_n) + \eta_i\rho_i(\partial_i - \frac{\kappa_i}{a_i}\partial_1)),$$

$$\hat{c}_{4i} = (\hat{c}_{5i} - \hat{c}_{6i}) - \left(3\eta_i\omega_i - \delta_i\rho_i(\xi_i - \kappa_i\xi_n)\right) + (\delta_i\omega_i(\partial_{i+1} - \frac{\kappa_i}{a_i}\partial_n) + \eta_i\rho_i(\partial_i - \frac{\kappa_i}{a_i}\partial_1)),$$

$$\hat{c}_{5i} = \hat{c}_{6i} + 2\lambda_i(\rho_i(\xi_i - \kappa_i\xi_n) - \omega_i(\partial_{i+1} - \frac{\kappa_i}{a_i}\partial_n)),$$

$$\hat{c}_{6i} = \eta_i{}^2(\partial_i - \frac{\kappa_i}{a_i}\partial_1).$$

The denominator in **Eq. 3.4** being a squared quantity is always positive. Furthermore, if $\eta_i \geq 0$ and $\omega_i \geq 0$, the sufficient conditions for monotonicity in each subinterval $[r_i, r_{i+1}]$ are:

$$\hat{c}_{ji} \geq 0\,, \quad j = 1, 2, \cdots, 6. \;\; \hat{c}_{1i} \geq 0 \Leftrightarrow \kappa_i \leq \frac{a_i\partial_{i+1}}{d_n}, \tag{3.5}$$

$$\hat{c}_{6i} \geq 0 \;\Leftrightarrow \kappa_i \leq \frac{a_i\partial_i}{\partial_1} \;\; . \tag{3.6}$$

Also from **Eq. (2.1)**, it implies that $\varphi \in \; C^1[r_1, r_n]$,

whenever

$-a_i < \kappa_i < \; a_i$

and

$$\xi_i - \kappa_i\xi_n > 0 \Leftrightarrow \kappa_i < \frac{\hat{v}_{i+1} - \hat{v}_i}{\hat{v}_n - \hat{v}_1}. \tag{3.7}$$

However, $\hat{c}_{2i} > 0 \Leftrightarrow \delta_i > \frac{\eta_i\left(d_i - \frac{\kappa_i}{a_i}\partial_1\right)}{(\xi_i - \kappa_i\xi_n)}$. (3.8)

Similarly, $\hat{c}_{5i} > 0 \Leftrightarrow \rho_i > \frac{\omega_i\left(\partial_{i+1} - \frac{\kappa_i}{a_i}\partial_n\right)}{(\xi_i - \kappa_i\xi_n)}$. (3.9)

Finally, both $\hat{c}_{3i} > 0$ and $\hat{c}_{4i} > 0$ iff

$$\rho_i > \left(\frac{3\eta_i\omega_i - \delta_i\omega_i(\partial_{i+1} - \frac{\kappa_i}{a_i}\partial_n)}{\delta_i(\xi_i - \xi_n) + \eta_i(d_i - \frac{\kappa_i}{a_i}\partial_1)}\right), \tag{3.10}$$

provided

$$\delta_i > \frac{\eta_i\left(\partial_i - \frac{\kappa_i}{a_i}\partial_1\right)}{(\xi_i - \kappa_i\xi_n)}.$$

Hence, the results of **Eq. 3.5-3.10**, proved the theorem.

Corollary 1: If $\kappa_i = 0, i = 1,2, \ldots, n-1$ in above **Theorem 3.1**, the sufficient condition convert to

$\delta_i > \frac{\eta_i \partial_i}{\xi_i}$, $\rho_i > max\left\{\frac{\omega_i \partial_{i+1}}{\xi_i}, \left(\frac{3\eta_i\omega_i - \delta_i\omega_i\partial_{i+1}}{\delta_i\xi_i + \eta_i\partial_i}\right)\right\}$.

This is sufficient condition of monotonicity for classical GPRC.

4. RESULTS AND DISCUSSION

This section presents two experiments, which demonstrated the validity and adaptability of the proposed MHM. In these experiments, the derivatives values were calculated through geometric mean method. The monotone data set taken in Table 1 presents the experimental result concerning the watering the great northern beans. Distilled water with pH of 8.5 and Potassium Hydroxide was combined in the chemical solution, which was later used to watering the beans. After 40 days, the beans plant was taken out from vat to weight for the effect of chemical solution. It can be easily noticed that resulting data is monotone. The r-values represented the days and the v-values showed the height of beans.

Table 1. Height of Great Northern Beans

i	1	2	3	4	5	6	7	8
$\boldsymbol{r_i}$	1	2	12	18	24	30	36	40
$\hat{v}_i$	0	0	0.42	2.08	3.43	3.78	4.12	4.37

The data demonstrated in Table 1 is monotone; therefore, the resulting curve must be monotone. However, from Figure 1, which is constructed through hybrid model [11] it can be observed that the arbitrary value (η_i=7, δ_i=4, ρ_i=8.2, ω_i=99, κ_i=0.9) does not preserve the inherited monotonicity of the curve. On the other hand, Figure 2 displays multiple curves, which are produced through the proposed MHM. In Figure 2, it is found that the curve at different iterations preserve the essential characteristic of the data, which is monotonicity, proficiently. Figures 3 and Figure 4 highlighted the effect of diverse values of λ_i and ω_i ,rescpectively. The data presented in these figures showed that with different choices of parameter values through MHM, monotone curve of any particular requirement may be easily gained.

The monotone data set in Table 2 reports the varying degree of saturation of hemoglobin with partial pressure of oxygen. It was observed that saturation of hemoglobin was directly proportional to the partial pressure of oxygen. The r-values represented the partial pressure of oxygen and z-values indicated the percentage of saturation.

Table 2. The varying ability of hemoglobin

i	1	2	3	4	5
r_i	0	2	8	10	18
$\hat{v}_i$	0	70	91	91	110

The data demonstrated in Table 2 shows the monotone relationship, therefore, the curve must exhibit the same characteristic. Figure 5 is generated through the random values to the shape parameters and scaling factors (η_i=2.9, δ_i=3, ρ_i=7, ω_i=15, κ_i=0.7) in the description of hybrid model as defined in **Eq.** (**2.4**). Figure 5 depicts non-monotone hemoglobin dissociation curve (HDC) which does not make any sense, as the behaviour of the curve should retain monotonicity. This flaw is removed in Figure 6 by using the proposed method presented in Section 3. It can easily be observed that Figure 6 conserve monotonicity at each level of iterations. Figures 6 and 7 showed the profile of HDC with diverse values of η_i and ω_i. It is worth noticing that although various parameters may lead to different results but all conserve monotonicity.

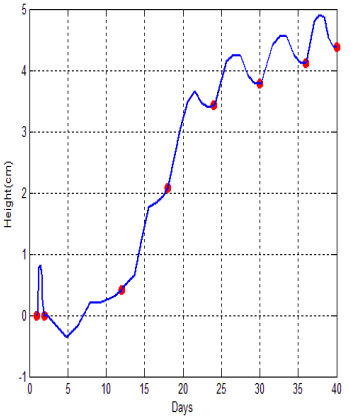

Figure 1. Hybrid model **[1]**

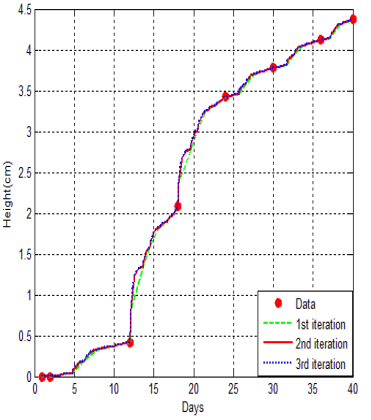

Figure 2. MHM using $\eta_i = 0.5$, $\omega_i = 70$

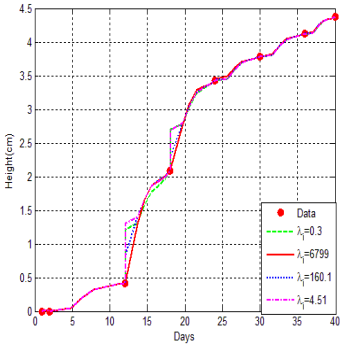

Figure 3. Effect of $\boldsymbol{\eta_i}$ using $\boldsymbol{\omega_i = 9981}$

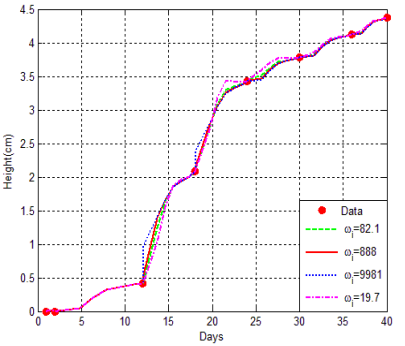

Figure 4. Effect of ω_i using $\eta_i = 87.65$

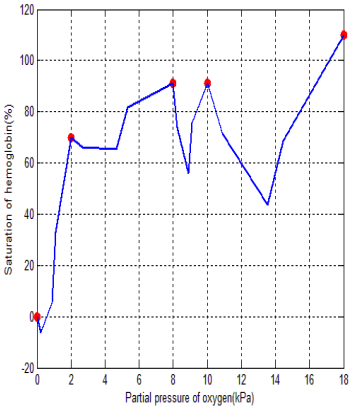

Figure 5. Hybrid model[1]

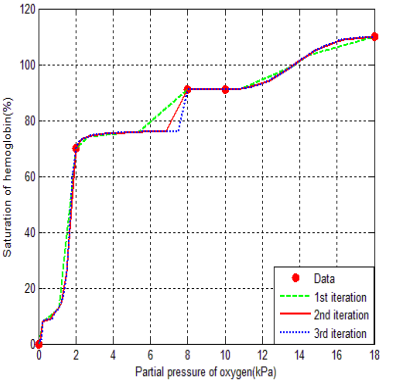

Figure 6. MHM using $\eta_i = 73665$, $\omega_i = 115$

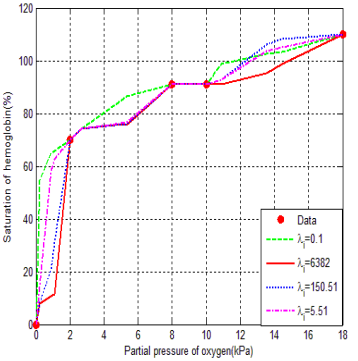

Figure 7. Effect of η_i using $\omega_i = 3.8$

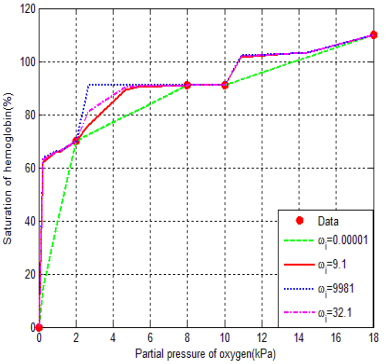

Figure 8. Effect of ω_i using $\eta_i = 0.00001$

4.1. Comparative Analysis

The proposed method guarantees to produce monotone model as compared to the hybrid model [11], which does not ensure to exhibit monotone model when data is monotone. All the existing models [3, 12, 13], failed to provide even a single degree of freedom, so MHM was a noteworthy addition as it offered two degree of freedom to modify and enhance the model. Unlike, [14] and [12], it is easy in the applicability, as it does not constrain the interval length or impose any conditions on derivatives, respectively. The scheme developed in [7] only works for regular data but the proposed approach, which is generalization of [7] is applicable for both regular and irregular datasets.

4.2. Conclusion

General Piecewise Rational Cubic Fractal Interpolation Function (GPRCFIF) was developed to provide a deeper understanding of the data, which displays rough, irregular, and fragmented configuration. Generally, it originates from complex functions or experiments. The GPRCFIF offers the family of four parameters and one scaling factor to modify, upgrade, and change the visual images. One of the most prominent characteristics of the GPRCFIF is its capacity to visualize data with smooth curves by setting all scaling factors to zero. The current study, in particular addressed the problem of monotonicity through the novel proposed model MHM. The experimental results illustrated that the performance of the proposed MHM was very efficient and heterogeneous as it contains the ability (due to recursive nature) to produce multiple monotone curves for the same monotone data according to the user's desire.

REFERENCES

1. Hussain MZ, Hussain M. Visualization of data preserving monotonicity. *Appl Math Comput*. 2007;190(2):1353–1364. https://doi.org/10.1016/j.amc.2007.02.022

2. Sarfraz M, Hussain MZ, Hussain M. Modeling rational spline for visualization of shaped data. *J Numer Math*. 2013;21(1):63–87. https://doi.org/10.1515/jnum-2013-0003

3. Hussain MZ, Sarfraz M, Hussain M. Scientific data visualization with shape preserving C^1 rational cubic interpolation. *Eur J Pure Appl Math*. 2010;2:194–212.

4. Chand AKB, Vijender N, Navescues MA. Shape preserving of scientific data through rational fractal splines. *Calcolo*. 2014;51: 329–362. https://doi.org/10.1007/s10092-013-0088-2

5. Cripps RJ, Hussain MZ. C^1 Monotone cubic Hermite interpolant. *Appl Math Lett*. 2012;25(8):1161–1165. https://doi.org/10.1016/j.aml.2012.02.050

6. Floater MS, Pena JM. Monotonicity preserving on triangles. *Math Comput*. 2000;69(232):1505–1519. https://doi.org/10.1090/S0025-5718-99-01176-X

7. Hussain MZ, Sarfraz M. Monotone piecewise rational cubic interpolation. *Int J Comp Math*. 2009;86(3):423–430. https://doi.org/10.1080/00207160701595145

8. Barnsley MF. Fractal functions and interpolation. *Constr Approx*. 1986;2:303–329. https://doi.org/10.1007/BF01893434

9. Barnsley MF, Harrington AN. The calculus of fractal interpolation functions. *J Approx Theory*. 1989;57:14–34. https://doi.org/10.1016/0021-9045(89)90080-4

10. Balasubramani N. Shape preserving rational cubic fractal interpolation function. *J Comput Appl Math*. 2017;319:277–295. https://doi.org/10.1016/j.cam.2017.01.014

11. Arooj T, Hussain MZ, Hussain F. Scientific Data Visualization via Hybrid Model based on Fractal Spline Interpolation. *Punjab Univ J Math*. 2019;51(9):123–136.

12. Sarfraz M. A rational cubic spline for visualization of monotonic data. *Comput Graph*. 2000;24:509–516. https://doi.org/10.1016/S0097-8493(00)00053-4

13. Sarfraz M. A rational cubic spline for visualization of monotonic data: an alternative approach. *Comput Graph*. 2003;27:107–121. https://doi.org/10.1016/S0097-8493(02)00249-2

14. Lamberti P, Manni C. Shape preserving functional interpolation via parametric cubics. *Numer Algor*. 2001;28:229–254.

15. Sarfraz M, Hussain MZ, Hussain M. Modeling rational spline for visualization of shaped data. *J Numer Math*. 2013;21(1):63–87. https://doi.org/10.1515/jnum-2013-0003

16. Beliakov G. Monotonicity preserving approximation of multivariate scattered data. *BIT Numer Math*. 2005;45(4):653–677. https://doi.org/10.1007/s10543-005-0028-x

17. Sarfraz M, Hussain MZ, Hussain F. Shape preserving curves using quadratic trigonometric splines. *Appl Math Comput*. 2015; 265:1126–1144. https://doi.org/10.1016/j.amc.2015.05.131

18. Hussain MZ, Hussain F, Sarfraz M. Shape preserving positive trigonometry spline curves. *Iran J Sci Technol Trans Sci*. 2018; 42:763–775. https://doi.org/10.1007/s40995-016-0056-1

19. Ahmad B, Perviaz A, Ahmad O, Dayan F. Numerical solution of fourth order homogeneous parabolic partial differential equations using non-polynomial cubic spline method (NPCSM). *Sci Inquiry Rev*. 2021;5(4):19–37. https://doi.org/10.32350/sir/54.02

20. Ahmad B, Perviaz A, Ahmad MO, Dayan F. Solution of parabolic partial differential equations via non-polynomial cubic spline technique. *Sci Inquiry Rev*. 2021;5(3):60–76. https://doi.org/10.32350/sir/53.05

Scientific Inquiry and Review (SIR)
Volume 7 Issue 1, 2023
ISSN (P): 2521-2427, ISSN (E): 2521-2435
Homepage: https://journals.umt.edu.pk/index.php/SIR

Article QR

Title:	**TOPSIS Technique of MCDM under Cubic Intuitionistic Fuzzy Soft Set Environment**
Author (s):	Muhammad Saqlain[1], Raiha Imran[2], Sabahat Hassan[3]
Affiliation (s):	[1]King Mongkut's University of Technology, Thonburi, Thailand [2]Riphah International University, Lahore Campus, Pakistan [3]Lahore Garrison University, Pakistan.
DOI:	https://doi.org/10.32350/sir.71.03
History:	Received: October 8, 2022, Revised: December 12, 2022, Accepted: December 13, 2022, Published: March 15, 2023
Citation:	Saqlain M, Imran R, Hussan S. TOPSIS technique of MCDM under cubic intuitionistic fuzzy soft set environment. *Sci Inq Rev.* 2023;7(1):33–52. https://doi.org/10.32350/sir.71.03
Copyright:	© The Authors
Licensing:	This article is open access and is distributed under the terms of Creative Commons Attribution 4.0 International License
Conflict of Interest:	Author(s) declared no conflict of interest

A publication of
The School of Science
University of Management and Technology, Lahore, Pakistan

TOPSIS Technique of MCDM under Cubic Intuitionistic Fuzzy Soft Set Environment

Muhammad Saqlain[1*], Raiha Imran[2], and Sabahat Hassan[3]

[1]Department of Mathematics, King Mongkut's University of Technology, Thonburi, Thailand.
[2]Department of Mathematics, Riphah International University, Lahore Campus, Pakistan.
[3]Department of Mathematics, Lahore Garrison University, Pakistan.

ABSTRACT

A powerful tool for dealing with ambiguity, attributive values, fuzziness, and inconsistency is the cubic intuitionistic fuzzy soft set. In this paper, multi-criteria group decision-making (MCGDM) technique called extended TOPSIS based on distance and similarity measures is presented. Furthermore, a real-world problem is resolved by applying CIFS-set to support the theoretical visualization. Arguably, the proposed technique works well and has practical uses.

Keywords: cubic set, intuitionistic fuzzy set, intuitionistic fuzzy soft set, multi-criteria group decision-making (MCGDM), TOPSIS technique

1. INTRODUCTION

Taking the best decision requires taking into account a range of factors due to increasing complexities in business, engineering, scientific, and technological environments. The most effective way to select the ideal alternative among all possible options is decision-making. Since generalized variants are frequently used in decision-making, nearly every other problem has a considerable range of requirements. Such requirements frequently come into conflict with each other and no solution may ever be able to fully satisfy all of them. To address such challenges, decision-makers need to overcome the MCGDM problem. For this purpose, many mathematical theories have been expounded such as the fuzzy set theory, intuitionistic set theory, and interval-valued intuitionistic set theory. In 1965, fuzzy set theory was introduced by Zadeh [1]. This theory deals with membership value over closed interval [0,1] and overcomes the vague and ambiguous environment. However, due to the increased complexities in the environment, a decision-maker faces difficulties to express their idea in the

* Corresponding Author: msgondal0@gmail.com

form of a single membership value. To deal with such a situation, the intuitionistic fuzzy set (IFS) [2] theory was introduced. This theory not only deals with the membership value but also with the non-membership value and hence gives a more precise result which helps in decision-making. In this context, many researchers have presented different theories based on distance and similarities measures [3–5].

The technique known as the order of preference by similarity to ideal solution (TOPSIS) was introduced by Lai et al. [6] and remains a widely known method. The purpose of this method is to identify the longest path from the negative ideal alternative (NIA) as well as the shortest path from the positive ideal alternative (PIA).

Since this technique has been introduced, various researchers have used the TOPSIS method to resolve decision-making problems in an ambiguous environment. Interval-valued intuitionistic fuzzy set and its fundamental properties was proposed by [7]. Jahanshahloo et al. [8] presented the TOPSIS method for DM under a fuzzy environment, Chu *et al.* [9] suggested the TOPSIS method for robot selection, and Zulqarnain *et al.* [10] generalized the fuzzy TOPSIS for MCGDM. Saqlain et al. [11] discussed the use of the TOPSIS method for the selection of a smartphone. Shen et al. [12] extended the application of this technique under intuitionistic fuzzy environment, Chang et al. [13] discussed the distance approaches using the TOPSIS method, Li et al. [14] suggested the Pythagorean fuzzy TOPSIS based on similarity measures, and Gupta et al. [15] discussed the extended TOPSIS under interval-valued intuitionistic fuzzy environment.

All these theories involve uncertainty to some extent as they do not deal with the membership and non-membership values simultaneously along with fuzziness. To deal with such kind of situations, Garg [16] proposed the TOPSIS method for MCGDM under a cubic environment which deals with both the intuitionistic value and fuzziness, simultaneously. Pramanik et al. [17] defined the TOPSIS method for neutrosophic cubic information, Jun et al. [18] suggested the cubic fuzzy set (CFS), while Garg [19] discussed the cubic intuitionistic fuzzy set (CIFS) and its fundamental properties. The soft set theory with its fundamentals was proposed by Maji et al. [20]. The theory of soft set was merged with cubic set and is known as cubic intuitionistic fuzzy soft set (CIFSS). It was proposed by Saqlain et al. [21].

Cubic intuitionistic fuzzy set (CIFS) is considered highly effective for decision-making problems as it involves interval-valued intuitionistic fuzzy number (IVIFS) and intuitionistic fuzzy number (IFS) over the interval. Still, this theory does not deal with multi-attributive values. Considering the soft set, this paper attempts to define the multi-attributive decision-making problem under the cubic intuitionistic fuzzy soft environment, where each element is defined by the CIF-number (CIFN). A methodology which utilizes the extended TOPSIS method is also proposed. Furthermore, some distance and similarity measure formulas have been defined which evaluate the positive ideal alternative (PIA) and negative ideal alternative (NIA).

2. PRELIMINARY SECTION

In this section, some basic concepts of intuitionistic fuzzy set (IF-set), interval-valued intuitionistic fuzzy set (IVIF-set), soft set, intuitionistic fuzzy soft set (IFS-set), CF-set, CIF-set, and CIFS-set are defined.

Definition 2.1 [2]. An intuitionistic fuzzy set (IF-set) $\mathfrak{k}$ over a crisp set U is defined by a function $\mathfrak{u}_{\mathfrak{U}}$ represented by the mapping

$$\mathfrak{u}_{\mathfrak{U}} = \mathrm{U} \to [0,1] \times [0,1],$$

where $\mathfrak{u}_{\mathfrak{U}}$ is the membership function which deals with truthiness and falsity and U be a universal discourse. Thus, an intuitionistic fuzzy set (IF-set) over set U can be represented as

$$\mathfrak{k} = \left\{\left\langle \mathfrak{z}, \left(\mathfrak{t}_{\mathfrak{k}}(\mathfrak{z}), \mathfrak{f}_{\mathfrak{k}}(\mathfrak{z})\right)\right\rangle \middle| \mathfrak{z} \epsilon \mathrm{U}\right\} \; such\ that \;\; 0 \leq \mathfrak{t}_{\mathfrak{k}}(\mathfrak{z}) + \mathfrak{f}_{\mathfrak{k}}(\mathfrak{z}) \leq 1; \; \forall \mathfrak{z} \epsilon \mathrm{U}.$$

Definition 2.2 [20]. Let U be a universal discourse. An interval-valued intuitionistic fuzzy set (IVIF-set) $\mathfrak{k}$ over a crisp set U is defined by a function $\mathfrak{u}_{\mathfrak{U}}$ represented by the mapping

$$\mathfrak{u}_{\mathfrak{U}} = \mathrm{U} \to \mathrm{P}([0,1] \times [0,1]),$$

where $\mathfrak{u}_{\mathfrak{U}}$ is the membership function which represents the degree of belongingness and the non-belongingness value. Thus, an interval-valued intuitionistic fuzzy set (IVIF-set) over set U can be represented as

$$\mathfrak{k} = \{\langle \mathfrak{z}, ([\mathfrak{t}_{\mathfrak{k}}(\mathfrak{z})^{-}, \mathfrak{t}_{\mathfrak{k}}(\mathfrak{z})^{+}], [\mathfrak{f}_{\mathfrak{k}}(\mathfrak{z})^{-}, \mathfrak{f}_{\mathfrak{k}}(\mathfrak{z})^{+}])\rangle | \mathfrak{z} \epsilon \mathrm{U}\} \; such\ that \;\; 0 \leq \mathfrak{t}_{\mathfrak{k}}(\mathfrak{z}) + \mathfrak{f}_{\mathfrak{k}}(\mathfrak{z}) \leq 1; \; \forall \mathfrak{z} \epsilon \mathrm{U}.$$

Definition 2.3 [19]. Consider U to be a universal set and $\mathfrak{c} = \{\mathfrak{c}_1, \mathfrak{c}_2, \mathfrak{c}_3, \ldots, \mathfrak{c}_n\}$ be the set of attributive values. Then, a soft set $\mathfrak{S}$ over a crisp set U is defined by a function $\varphi_{\mathfrak{S}}$ represented by the mapping

$\varphi_{\mathcal{S}}: \mathcal{C} \to P(U)$,

where $\varphi_{\mathcal{S}}$ is an approximate function and its value $\varphi_{\mathcal{S}}(\mathcal{C}_i)$ can be represented as

$$\mathcal{S} = \left\{\left(\mathcal{C}_i, \varphi_{\mathcal{S}}(\mathcal{C}_i)\right) : \mathcal{C}_i \in \mathcal{C}, \varphi_{\mathcal{S}}(\mathcal{C}_i) \in P(U)\right\}.$$

Definition 2.4 [17]. Let U be the set of universal discourse and $\mathfrak{Z}$ be a cubic fuzzy set (CF-set) over U and defined as

$$\mathfrak{Z} = \{\langle \mathcal{C}, \mathfrak{U}_{\mathfrak{k}}(\mathfrak{Z}), \mathrm{v}\rangle | \mathfrak{Z} \epsilon U\},$$

where $\mathfrak{U}_{\mathfrak{k}}(\mathfrak{Z}) = [\mathfrak{U}_{\mathfrak{k}}(\mathfrak{Z})^{-}, \mathfrak{U}_{\mathfrak{k}}(v)^{+}]$ and v represents the interval-valued fuzzy set and FN in $\mathfrak{Z}\epsilon U$, respectively.

This pair is denoted as $\mathfrak{Z} = (\mathfrak{U}_{\mathfrak{k}}, \mathrm{v})$, which is known as a cubic fuzzy set.

Definition 2.5 [18]. The term cubic intuitionistic fuzzy set (CIF-set) $\mathfrak{Z}$ defined over U is defined as

$$\mathfrak{Z} = \{\langle \mathcal{C}, \mathfrak{U}_{\mathfrak{k}}(\mathfrak{Z}), \mathrm{v}\rangle | \mathfrak{Z} \epsilon U\},$$

where $\mathfrak{U}_{\mathfrak{k}}(\mathfrak{Z}) = \{\langle \mathcal{C}, \langle [\mathfrak{t}_{\mathfrak{k}}(\mathfrak{Z})^{-}, \mathfrak{t}_{\mathfrak{k}}(\mathfrak{Z})^{+}], [\mathfrak{f}_{\mathfrak{k}}(\mathfrak{Z})^{-}, \mathfrak{f}_{\mathfrak{k}}(\mathfrak{Z})^{+}]\rangle\}$, and $\mathrm{v} = [\mathfrak{t}_{\mathfrak{k}}(\mathfrak{Z}), \mathfrak{f}_{\mathfrak{k}}(\mathfrak{Z})]$ represent the interval-valued IFS-set and intuitionistic set (IS) respectively such that $0 \leq \mathfrak{t}_{\mathfrak{k}}(\mathfrak{Z}) + \mathfrak{f}_{\mathfrak{k}}(\mathfrak{Z}) \leq 1$. Also, $0 \leq \mathfrak{t}_{\mathfrak{k}}(\mathfrak{Z}), \mathfrak{f}_{\mathfrak{k}}(\mathfrak{Z}) \leq 1$.

This pair is denoted as $\mathfrak{Z} = (\mathfrak{U}, \mathrm{v})$ and termed as a cubic intuitionistic fuzzy set.

Definition 2.6 [18]. The term cubic intuitionistic fuzzy soft set (CIFS-set) $\mathfrak{Z}$ defined over U is given as

$$\mathfrak{Z} = \{\langle \mathcal{C}_i, \mathfrak{U}(\mathfrak{Z}_i), \mathrm{v}_i\rangle | \mathfrak{Z}_i \epsilon U\},$$

where $\mathfrak{U}(\mathfrak{Z}_i) = \{\langle \mathcal{C}_i, \langle [\mathfrak{t}_{\mathfrak{k}}(\mathfrak{Z}_i)^{-}, \mathfrak{t}_{\mathfrak{k}}(\mathfrak{Z}_i)^{+}], [\mathfrak{f}_{\mathfrak{k}}(\mathfrak{Z}_i)^{-}, \mathfrak{f}_{\mathfrak{k}}(\mathfrak{Z}_i)^{+}]\rangle\}$, and $\mathrm{v}_i = [\mathfrak{t}_{\mathfrak{k}}(\mathfrak{Z}_i), \mathfrak{f}_{\mathfrak{k}}(\mathfrak{Z}_i)]$ represents the interval-valued IFS-set and intuitionistic set (IS) respectively such that $0 \leq \mathfrak{t}_{\mathfrak{k}}(\mathfrak{Z}_i) + \mathfrak{f}_{\tilde{A}}(\mathfrak{Z}_i) \leq 1$. Also, $0 \leq \mathfrak{t}_{\mathfrak{k}}(\mathfrak{Z}_i), \mathfrak{f}_{\mathfrak{k}}(\mathfrak{Z}_i) \leq 1$.

This pair is denoted as $\mathfrak{Z} = (\mathfrak{U}_i, \mathrm{v}_i)$ and termed as cubic intuitionistic fuzzy soft set.

Definition2.7 [18]. Consider

$$\mathfrak{B} = \begin{Bmatrix} \langle \mathcal{C}_i, \langle [\mathfrak{t}_{\mathfrak{B}}(\mathfrak{Z}_i)^{-}, \mathfrak{t}_{\mathfrak{B}}(\mathfrak{Z}_i)^{+}], [\mathfrak{f}_{\mathfrak{B}}(\mathfrak{Z}_i)^{-}, \mathfrak{f}_{\mathfrak{B}}(\mathfrak{Z}_i)^{+}]\rangle, \\ \langle [\mathfrak{t}_{\mathfrak{B}}(\mathfrak{Z}_i), \mathfrak{f}_{\mathfrak{B}}(\mathfrak{Z}_i)]\rangle \end{Bmatrix},$$

$\mathcal{Y} = \left\{\left\langle \begin{matrix} c_j, \langle [\mathfrak{t}_{\mathcal{Y}}(\mathfrak{Z}_i)^-, \mathfrak{t}_{\mathcal{Y}}(\mathfrak{Z}_i)^+], [\mathfrak{f}_{\mathcal{Y}}(\mathfrak{Z}_i)^-, \mathfrak{f}_{\mathcal{Y}}(\mathfrak{Z}_i)^+], \\ \langle \mathfrak{t}_{\mathcal{Y}}(\mathfrak{Z}_i), \mathfrak{f}_{\mathcal{Y}}(\mathfrak{Z}_i) \rangle \end{matrix} \right\rangle\right\}$ be the two CIFS-sets. Then, for $q \geq 1$, the distance measures are defined as

- Distance measures

$$\mathrm{d}_q(\mathcal{B}, \mathcal{Y}) = \left(\langle \frac{1}{6} \sum_{i=1}^{n} \{|\mathfrak{t}_{\mathcal{B}}(\mathfrak{Z}_i)^- - \mathfrak{t}_{\mathcal{Y}}(\mathfrak{Z}_i)^-|^q + |\mathfrak{t}_{\mathcal{B}}(\mathfrak{Z}_i)^+ - \mathfrak{t}_{\mathcal{Y}}(\mathfrak{Z}_i)^+|^q + |\mathfrak{f}_{\mathcal{B}}(\mathfrak{Z}_i)^- - \mathfrak{f}_{\mathcal{Y}}(\mathfrak{Z}_i)^-|^q + |\mathfrak{f}_{\mathcal{B}}(\mathfrak{Z}_i)^+ - \mathfrak{f}_{\mathcal{Y}}(\mathfrak{Z}_i)^+|^q + |\mathfrak{t}_{\mathcal{B}}(\mathfrak{Z}_i) - \mathfrak{t}_{\mathcal{Y}}(\mathfrak{Z}_i)|^q + |\mathfrak{f}_{\mathcal{B}}(\mathfrak{Z}_i) - \mathfrak{f}_{\mathcal{Y}}(\mathfrak{Z}_i)|^q\} \rangle\right)^{\frac{1}{q}}.$$

- Normalized distance measures

$$\mathrm{d}_q'(\mathcal{B}, \mathcal{Y}) = \left(\langle \frac{1}{6n} \sum_{i=1}^{n} \{|\mathfrak{t}_{\mathcal{B}}(\mathfrak{Z}_i)^- - \mathfrak{t}_{\mathcal{Y}}(\mathfrak{Z}_i)^-|^q + |\mathfrak{t}_{\mathcal{B}}(\mathfrak{Z}_i)^+ - \mathfrak{t}_{\mathcal{Y}}(\mathfrak{Z}_i)^+|^q + |\mathfrak{f}_{\mathcal{B}}(\mathfrak{Z}_i)^- - \mathfrak{f}_{\mathcal{Y}}(\mathfrak{Z}_i)^-|^q + |\mathfrak{f}_{\mathcal{B}}(\mathfrak{Z}_i)^+ - \mathfrak{f}_{\mathcal{Y}}(\mathfrak{Z}_i)^+|^q + |\mathfrak{t}_{\mathcal{B}}(\mathfrak{Z}_i) - \mathfrak{t}_{\mathcal{Y}}(\mathfrak{Z}_i)|^q + |\mathfrak{f}_{\mathcal{B}}(\mathfrak{Z}_i) - \mathfrak{f}_{\mathcal{Y}}(\mathfrak{Z}_i)|^q\} \rangle\right)^{\frac{1}{q}},$$

where n represents the mean of attributive values.

3. EXTENDED TOPSIS TECHNIQUE

In this section, based on the suggested distance measure, a TOPSIS (technique for order of preference by similarity to ideal solution) technique for tackling MAGDM problems in the form of CIFS sets is proposed.

3.1 Description of the Problem

A recently opened restaurant is hiring a new head chef to take charge of the kitchen. For hiring a head chief, they have published the advertisement in the newspaper and different applicants have applied in response. Assume that there is a set of m applicants (alternative) $\mathfrak{Z}_i = \{\mathfrak{Z}_1, \mathfrak{Z}_2, \mathfrak{Z}_3, \dots, \mathfrak{Z}_m\}$ chosen for the interview. The restaurant has gathered decision-makers $\{T^1, T^2, T^3, T^4\}$ and assigned them the duty to identify the best head chef for the restaurant. The selection committee has decided to assess the applicants $\mathfrak{Z} = \{\mathfrak{Z}_1, \mathfrak{Z}_2, \mathfrak{Z}_3, \dots, \mathfrak{Z}_m\}$ based on n different criteria $\mathfrak{C} = \{\mathfrak{C}_1, \mathfrak{C}_2, \mathfrak{C}_3, \dots, \mathfrak{C}_n\}$. All applicants participated in group talk for this purpose and a panel then developed results for each applicant in the form of CIFS-set criteria $\mathfrak{X}_{ij} = (\mu_{ij}, \mathrm{v}_{ij})$, where

$\mu_{ij}(\mathfrak{Z}_i) = \langle [\mathfrak{t}_{ij}(\mathfrak{Z}_i)^-, \mathfrak{t}_{ij}(\mathfrak{Z}_i)^+], [\mathfrak{f}_{ij}(\mathfrak{Z}_i)^-, \mathfrak{f}_{ij}(\mathfrak{Z}_i)^+] \rangle$ and $\mathrm{v}_{ij} = [\mathfrak{t}_{ij}(\mathfrak{Z}_i), \mathfrak{f}_{ij}(\mathfrak{Z}_i)]$ represent the interval-valued IFS-set and intuitionistic set

(IS), respectively. Here, the components $[\mathfrak{t}_{ij}(\mathfrak{z}_i)^-, \mathfrak{t}_{ij}(\mathfrak{z}_i)^+]$ and $\mathfrak{t}_{ij}(\mathfrak{z}_i)$ show that satisfaction degree corresponds to a given alternative H_i which satisfies the criterion C_j, whereas the components $[\mathfrak{f}_{ij}(\mathfrak{z}_i)^-, \mathfrak{f}_{ij}(\mathfrak{z}_i)^+]$ and $\mathfrak{f}_{ij}(\mathfrak{z}_i)$ represent the degree of dissatisfaction with the given alternative $\mathfrak{z}_i$ regarding the criterion $\mathfrak{c}_j$. Thus, overall results are recorded in the form of a CIFS-set environment and defined in matrix form which is represented as $D = (\mathfrak{X})_{m\times n}$.

3.1.1. Computing CIFS-PIA and CIFS-NIA. The CIFS-positive ideal alternative (CIFS-PIA) and CIFS-negative ideal alternative (CIFS-NIA) regarding the alternative $\mathfrak{z}_i (i = 1,2, \dots, m)$ may be selected as 1 and 0, respectively. It shows the ranking values of each alternative. Thus, the ranking values of CIFS-PIA and CIFS-NIA can be represented as

$$\mathfrak{X}^+ = (\langle [1,1], [0,0] \rangle, \langle 0,1 \rangle)_{1\times n} \; and \; \mathfrak{X}^- = (\langle [0,0], [1,1] \rangle, \langle 1,0 \rangle)_{1\times n}.$$

So, $\mathfrak{X}^+$ and $\mathfrak{X}^-$ complement each other.

If the decision-maker wants to define the other reference points as

$$\mathfrak{X}^+{}_j = \left(\langle \left[t_j^{L+}, t_j^{U+}\right], [f_j^{L+}, f_j^{U+}] \rangle, \langle p_j^+, q_j^+ \rangle\right), \tag{3.1}$$

and

$$\mathfrak{X}^-{}_j = \left(\langle \left[t_j^{L-}, t_j^{U-}\right], [f_j^{L-}, f_j^{U-}] \rangle, \langle p_j^-, q_j^- \rangle\right), \tag{3.2}$$

where

$$t_j^{L+} = \max_j(\mathfrak{t}_{ij}(\mathfrak{z}_i)^-), t_j^{U+} = \max_j(\mathfrak{t}_{ij}(\mathfrak{z}_i)^+), f_j^{L+} = \min_j(\mathfrak{f}_{ij}(\mathfrak{z}_i)^-), f_j^{U+} = \min_j(\mathfrak{f}_{ij}(\mathfrak{z}_i)^+),$$
$$p_j^+ = \min_j(\mathfrak{t}_{ij}(\mathfrak{z}_i)), \; q_j^+ = \max_j(\mathfrak{f}_{ij}(\mathfrak{z}_i)) \; \forall i$$

and $t_j^{L-} = \min_j(\mathfrak{t}_{ij}(\mathfrak{z}_i)^-), t_j^{U-} = \min_j(\mathfrak{t}_{ij}(\mathfrak{z}_i)^+), f_j^{L-} = \max_j(\mathfrak{f}_{ij}(\mathfrak{z}_i)^-), f_j^{U-} = \max_j(\mathfrak{f}_{ij}(\mathfrak{z}_i)^+), p_j^- = \max_j\left(\mathfrak{t}_{ij}(\mathfrak{z}_i)\right), q_j^- = \min_j\left(\mathfrak{f}_{ij}(\mathfrak{z}_i)\right) \; \forall i.$

3.1.2. Computing Distance Measures Between Alternatives. Consider the criteria in terms of the weight vector $w_i = (w_1, w_2, \dots, w_n)$ along with CIFS-PIA($\mathfrak{X}^+$) and CIFS-NIA($\mathfrak{X}^-$). We evaluate the weighted distances between the alternatives $\mathfrak{z}_i$ and its $\mathfrak{X}^+$ as well as $\mathfrak{X}^-$ defined as

$$\mathrm{d}_q''(\mathfrak{Z}_i, \mathfrak{X}^+) = \left[\frac{1}{6}\sum_{j=1}^{n} w_j\left\{\left|t_j^{L+} - \mathfrak{t}_{ij}(\mathfrak{Z}_i)^-\right|^q + \left|t_j^{U+} - \mathfrak{t}_{ij}(\mathfrak{Z}_i)^+\right|^q + \left|\mathfrak{f}_{ij}(\mathfrak{Z}_i)^- - f_j^{L+}\right|^q + \left|\mathfrak{f}_{ij}(\mathfrak{Z}_i)^+ - f_j^{U+}\right|^q + \left|\mathfrak{t}_{ij}(\mathfrak{Z}_i) - p_j^+\right|^q + \left|q_j^+ - \mathfrak{f}_{ij}(\mathfrak{Z}_i)\right|^q\right\}\right]^{1/q}, \tag{3.3}$$

and

$$\mathrm{d}_q''(\mathfrak{Z}_i, \mathfrak{X}^-) = \left[\frac{1}{6}\sum_{j=1}^{n} w_j\left\{\left|\mathfrak{t}_{ij}(\mathfrak{Z}_i)^- - t_j^{L-}\right|^q + \left|\mathfrak{t}_{ij}(\mathfrak{Z}_i)^+ - t_j^{U-}\right|^q + \left|f_j^{L-} - \mathfrak{f}_{ij}(\mathfrak{Z}_i)^-\right|^q + \left|f_j^{U-} - \mathfrak{f}_{ij}(\mathfrak{Z}_i)^+\right|^q + \left|p_j^- - \mathfrak{t}_{ij}(\mathfrak{Z}_i)\right|^q + \left|\mathfrak{f}_{ij}(\mathfrak{Z}_i) - q_j^-\right|^q\right\}\right]^{1/q}, \tag{3.4}$$

where $q \geq 1 \in$ R".

The relative closeness coefficient of alternative $\mathfrak{Z}_i (i = 1,2, \dots, m)$ with respect to CIFS-PIA$(\mathfrak{X}^+)$ (which is based on weighted distances) is defined as

$$\mathbb{C}_i = \frac{\mathrm{d}_q''(\mathfrak{Z}_i, \mathfrak{X}^-)}{\mathrm{d}_q''(\mathfrak{Z}_i, \mathfrak{X}^-) + \mathrm{d}_q''(\mathfrak{Z}_i, \mathfrak{X}^+)}; \mathrm{d}_q''(\mathfrak{Z}_i, \mathfrak{X}^+) \neq 0\,. \tag{3.5}$$

Further,

$0 \leq \mathrm{d}_q''(\mathfrak{Z}_i, \mathfrak{X}^-) \leq \mathrm{d}_q''(\mathfrak{Z}_i, \mathfrak{X}^-) + \mathrm{d}_q''(\mathfrak{Z}_i, \mathfrak{X}^+)$ *and* $0 \leq \mathbb{C}_i \leq 1$.

3.1.3. Group Decision-making TOPSIS Approach. Using the above analysis, an approach is presented to solve the group decision-making problem under the CIFS-set environment. For this purpose, consider there are $'T'$ decision-makers $\{T^1, T^2, \dots, T^k\}$ which evaluate the set of 'm' alternatives $\mathfrak{Z}_i (i = 1,2, \dots, m)$ under the set of 'n' different criteria $\mathfrak{d} = \{\mathfrak{d}_1, \mathfrak{d}_2, \mathfrak{d}_3, \dots, \mathfrak{d}_n\}$.

These decision-makers give the results in the form of CIFS-set $\left(\mathfrak{X}_{ij}\right)^k = \left(\left(\mu_{ij}\right)^k, \left(\mathrm{v}_{ij}\right)^k\right)$,

where $(\mu_{ij}(\mathfrak{Z}_i))^k$
$= \left\langle[(\mathfrak{t}_{ij}(\mathfrak{Z}_i)^-)^k, (\mathfrak{t}_{ij}(\mathfrak{Z}_i)^+)^k], [(\mathfrak{f}_{ij}(\mathfrak{Z}_i)^-)^k, (\mathfrak{f}_{ij}(\mathfrak{Z}_i)^+)^k]\right\rangle$ and $(\mathrm{v}_{ij})^k$
$= [\left(\mathfrak{t}_{ij}(\mathfrak{Z}_i)\right)^k, (\mathfrak{f}_{ij}(\mathfrak{Z}_i)])^k$, where $K = 1,2, \dots, k$.

Further, suppose that the criteria of the weight vector $(w_i)^k = ((w_1)^k, (w_2)^k, \dots, (w_n)^k)^T$ such that each $(w_i)^k > 0$ and $\sum_{i=1}^{n}(w_i)^k = 1$.

Moreover, to overcome the diverse judgments by different decision-makers, their decision is prioritized according to weight vector $\gamma = (\gamma_1, \gamma_2, \dots, \gamma_K)$, such that $\gamma_k > 0$ and $\sum_{k=1}^{K} \gamma_k = 1$.

The stepwise algorithm of TOPSIS is presented below.

Step 1: Arrange the ranking values of the alternative given by each decision-maker in the form of a matrix

$$T^{(k)} = \begin{matrix} \\ \mathfrak{Z}_1 \\ \mathfrak{Z}_2 \\ \vdots \\ \mathfrak{Z}_m \end{matrix} \begin{bmatrix} \mathfrak{d}_1 & \mathfrak{d}_2 & \dots & \mathfrak{d}_n \\ \mathfrak{X}_{11}{}^{(k)} & \mathfrak{X}_{12}{}^{(k)} & \dots & \mathfrak{X}_{1n}{}^{(k)} \\ \mathfrak{X}_{21}{}^{(k)} & \mathfrak{X}_{22}{}^{(k)} & \dots & \mathfrak{X}_{2n}{}^{(k)} \\ \vdots & \vdots & \ddots & \vdots \\ \mathfrak{X}_{m1}{}^{(k)} & \mathfrak{X}_{m2}{}^{(k)} & \dots & \mathfrak{X}_{mn}{}^{(k)} \end{bmatrix}$$

Step 2: For each decision-maker $T^k = \{T^1, T^2, \dots, T^K\}$, compute CIFS-PIA and CIFS-NIA corresponding to the applicants $\mathfrak{Z}_i (i = 1,2, \dots, m)$ using the **Eq. (3.4)** and **(3.5)** respectively and defined as

$$(\mathfrak{X}^+{}_j)^k = \left(\langle\left[(t_j^{L+})^k, (t_j^{U+})^k\right], \left[(f_j^{L+})^k, (f_j^{U+})^k\right]\rangle, \langle(p_j^+)^k, (q_j^+)^k\rangle\right) \quad (3.6)$$

and

$$(\mathfrak{X}^-{}_j)^k = \left(\langle\left[(t_j^{L-})^k, (t_j^{U-})^k\right], \left[(f_j^{L-})^k, (f_j^{U-})^k\right]\rangle, \langle(p_j^-)^k, (q_j^-)^k\rangle\right), \quad (3.7)$$

where

$$\begin{aligned}(t_j^{L+})^k = \min_j\left\{(\mathfrak{t}_{ij}(\mathfrak{Z}_i)^-)^{(k)}\right\}, (t_j^{U+})^k = \min_j\left\{(\mathfrak{t}_{ij}(\mathfrak{Z}_i)^+)^{(k)}\right\}, (f_j^{L+})^k \\ = \min_j\left\{(\mathfrak{f}_{ij}(\mathfrak{Z}_i)^-)^{(k)}\right\}, (f_j^{U+})^k = \min_j\left\{(\mathfrak{f}_{ij}(\mathfrak{Z}_i)^+)^{(k)}\right\}, \\ (p_j^+)^k = \min_j\left\{(\mathfrak{t}_{ij}(\mathfrak{Z}_i))^{(k)}\right\}, (q_j^+)^k = \max_j\left\{(\mathfrak{f}_{ij}(\mathfrak{Z}_i))^{(k)}\right\} \forall i\end{aligned}$$

and

$$\begin{aligned}(t_j^{L-})^k = \min_j\left\{(\mathfrak{t}_{ij}(\mathfrak{Z}_i)^-)^{(k)}\right\}, (t_j^{U-})^k = \min_j\left\{(\mathfrak{t}_{ij}(\mathfrak{Z}_i)^+)^{(k)}\right\}, (f_j^{L-})^k \\ = \max_j\left\{(\mathfrak{f}_{ij}(\mathfrak{Z}_i)^-)^{(k)}\right\}, (f_j^{U-})^k = \max_j\left\{(\mathfrak{f}_{ij}(\mathfrak{Z}_i)^+)^{(k)}\right\}, \\ (p_j^-)^k = \max_j\left\{\left(\mathfrak{t}_{ij}(\mathfrak{Z}_i)\right)^{(k)}\right\}, (q_j^-)^k \\ = \min_j\left\{\left(\mathfrak{f}_{ij}(\mathfrak{Z}_i)\right)^{(k)}\right\} \forall i.\end{aligned}$$

***Step 3*:** For each decision-maker, compute the separation measures between the alternatives $\mathfrak{Z}_i$ from its CIFS-PIA$(\mathfrak{Y}^+)$ and CIFS-NIA$(\mathfrak{Y}^-)$ which are denoted by $\mathfrak{d}_q''((\mathfrak{Z}_i)^k, (\mathfrak{Y}^+)^k)$ and $\mathfrak{d}_q''((\mathfrak{Z}_i)^k, (\mathfrak{Y}^-)^k)$, respectively.

***Step 4*:** For each decision-maker, the relative closeness coefficient is determined as

$$\mathbb{C}_i^{(k)} = \frac{\mathfrak{d}_q''((\mathfrak{Z}_i)^k, (\mathfrak{Y}^-)^k)}{\mathfrak{d}_q''((\mathfrak{Z}_i)^k, (\mathfrak{Y}^+)^k) + \mathfrak{d}_q''((\mathfrak{Z}_i)^k, (\mathfrak{Y}^-)^k)}; \quad k = 1,2, \dots, K \tag{3.8}$$

where $\mathfrak{d}_q''((\mathfrak{Z}_i)^k, (\mathfrak{Y}^+)^k) \neq 0$.

***Step 5*:** Rank the alternatives based on the descending values of $\mathbb{C}_i$s

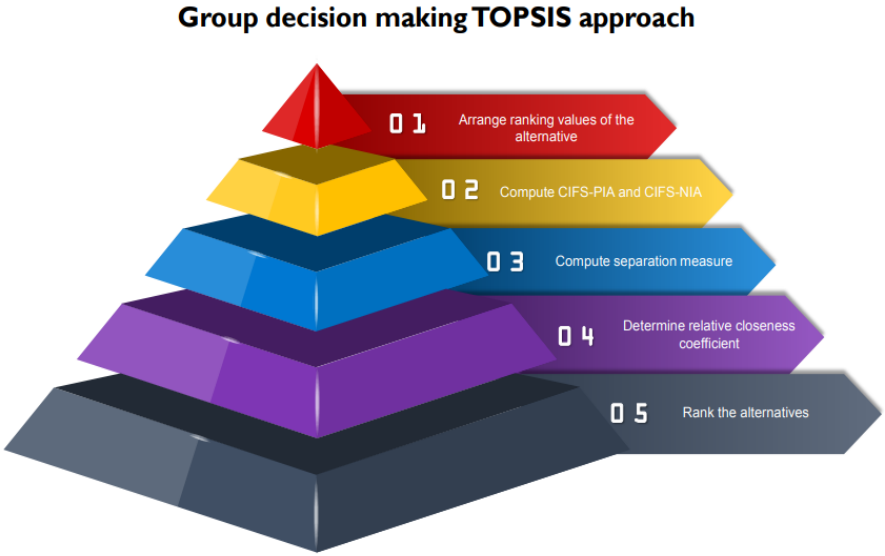

Figure 1. TOPSIS Algorithm

Example: To demonstrate the above-mentioned approach depicted in Figure 1, an example is discussed below.

4. RESULTS

4.1 Case Study

A recently opened restaurant is hiring a new head chef to take charge of the kitchen. For hiring a head chef, they have published the advertisement in the newspaper and different applicants have applied in response. A total

of four individuals $\mathfrak{z}_i; i = 1,2,3,4$ have been chosen for the interview. The restaurant has gathered decision-makers $\{T^1, T^2, T^3, T^4\}$ and given them the responsibility to identify the best head chef for the restaurant. The selection committee has decided to assess the applicants $\mathfrak{z}_i; i = 1,2,3,4$ based on four criteria $\mathfrak{d} = \{\mathfrak{d}_1, \mathfrak{d}_2, \mathfrak{d}_3, \mathfrak{d}_4\}$ defined as $\mathfrak{d}_1$: *cooking experience* $\mathfrak{d}_2$: *time management*, $\mathfrak{d}_3$: *presentable*, $\mathfrak{d}_4$: *team handling*. For the assessment, they conducted group discussion with all the applicants and the results are formulated by a panel in the form of an IVIFS set. From lots of applicants appearing for group discussion, only four applicants are shortlisted for the interview. At this stage, the results are recorded in the form of an IFS set. Then, the following steps of the proposed approach are executed to find the best head chef for the kitchen.

4.1.1. Step 1: Ranking Values of Alternatives Corresponding to Each Decision-maker

Table 1. Ranking Values of Alternatives Corresponding to $T^{(1)}$ Decision-maker

Decision maker	Applicants and Weighs	$\mathfrak{d}_1$	$\mathfrak{d}_2$	$\mathfrak{d}_3$	$\mathfrak{d}_4$
$T^{(1)}$	$\mathfrak{Z}_1$	$\left(\langle[0.30,0.50],[0.20,0.40]\rangle, \langle 0.35,0.29\rangle\right)$	$\left(\langle[0.25,0.35],[0.10,0.30]\rangle, \langle 0.19,0.27\rangle\right)$	$\left(\langle[0.32,0.40],[0.38,0.49]\rangle, \langle 0.35,0.49\rangle\right)$	$\left(\langle[0.40,0.44],[0.50,0.52]\rangle, \langle 0.55,0.35\rangle\right)$
	$\mathfrak{Z}_2$	$\left(\langle[0.15,0.30],[0.35,0.40]\rangle, \langle 0.17,0.40\rangle\right)$	$\left(\langle[0.15,0.18],[0.20,0.30]\rangle, \langle 0.29,0.63\rangle\right)$	$\left(\langle[0.30,0.40],[0.35,0.42]\rangle, \langle 0.40,0.40\rangle\right)$	$\left(\langle[0.55,0.59],[0.18,0.33]\rangle, \langle 0.16,0.20\rangle\right)$
	$\mathfrak{Z}_3$	$\left(\langle[0.39,0.48],[0.10,0.18]\rangle, \langle 0.20,0.15\rangle\right)$	$\left(\langle[0.23,0.32],[0.47,0.50]\rangle, \langle 0.30,0.60\rangle\right)$	$\left(\langle[0.40,0.45],[0.20,0.25]\rangle, \langle 0.29,0.19\rangle\right)$	$\left(\langle[0.37,0.42],[0.40,0.50]\rangle, \langle 0.30,0.70\rangle\right)$
	$\mathfrak{Z}_4$	$\left(\langle[0.42,0.55],[0.30,0.45]\rangle, \langle 0.15,0.30\rangle\right)$	$\left(\langle[0.44,0.50],[0.19,0.25]\rangle, \langle 0.42,0.20\rangle\right)$	$\left(\langle[0.16,0.32],[0.18,0.22]\rangle, \langle 0.17,0.34\rangle\right)$	$\left(\langle[0.20,0.55],[0.38,0.49]\rangle, \langle 0.80,0.17\rangle\right)$
	weights	0.40	0.20	0.25	0.15

Table 2. Ranking Values of Alternatives Corresponding to $\boldsymbol{T^{(2)}}$ Decision-maker

Decision maker	Applicants and Weighs	$\mathfrak{d}_1$	$\mathfrak{d}_2$	$\mathfrak{d}_3$	$\mathfrak{d}_4$
$T^{(2)}$	$\mathfrak{Z}_1$	$\left(\langle[0.35,0.45],[0.48,0.54]\rangle, \langle 0.60,0.27\rangle\right)$	$\left(\langle[0.40,0.60],[0.15,0.20]\rangle, \langle 0.35,0.19\rangle\right)$	$\left(\langle[0.16,0.35],[0.24,0.32]\rangle, \langle 0.32,0.20\rangle\right)$	$\left(\langle[0.11,0.20],[0.16,0.35]\rangle, \langle 0.40,0.17\rangle\right)$
	$\mathfrak{Z}_2$	$\left(\langle[0.15,0.30],[0.35,0.40]\rangle, \langle 0.20,0.70\rangle\right)$	$\left(\langle[0.60,0.70],[0.19,0.25]\rangle, \langle 0.60.0.10\rangle\right)$	$\left(\langle[0.30,0.45],[0.21,0.35]\rangle, \langle 0.50,0.30\rangle\right)$	$\left(\langle[0.40,0.50],[0.10,0.20]\rangle, \langle 0.40,0.30\rangle\right)$
	$\mathfrak{Z}_3$	$\left(\langle[0.19,0.39],[0.10,0.29]\rangle, \langle 0.11,0.20\rangle\right)$	$\left(\langle[0.20,0.35],[0.17,0.36]\rangle, \langle 0.10,0.40\rangle\right)$	$\left(\langle[0.10,0.18],[0.12,0.15]\rangle, \langle 0.20,0.35\rangle\right)$	$\left(\langle[0.19,0.27],[0.25,0.32]\rangle, \langle 0.20,0.70\rangle\right)$
	$\mathfrak{Z}_4$	$\left(\langle[0.10,0.29],[0.18,0.36]\rangle, \langle 0.30,0.42\rangle\right)$	$\left(\langle[0.15,0.40],[0.16,0.32]\rangle, \langle 0.30,0.63\rangle\right)$	$\left(\langle[0.47,0.50],[0.32,0.42]\rangle, \langle 0.15,0.29\rangle\right)$	$\left(\langle[0.25,0.29],[0.40,0.44]\rangle, \langle 0.66,0.18\rangle\right)$
	weights	0.35	0.30	0.15	0.20

Table 3. Ranking Values of Alternatives Corresponding to $T^{(3)}$ Decision-maker

Decision maker	Applicants & Weighs	$\mathfrak{d}_1$	$\mathfrak{d}_2$	$\mathfrak{d}_3$	$\mathfrak{d}_4$
$T^{(1)}$	$\mathfrak{Z}_1$	$\left(\langle[0.30,0.50],[0.20,0.40]\rangle, \langle 0.35,0.29\rangle\right)$	$\left(\langle[0.25,0.35],[0.10,0.30]\rangle, \langle 0.19,0.27\rangle\right)$	$\left(\langle[0.32,0.40],[0.38,0.49]\rangle, \langle 0.35,0.49\rangle\right)$	$\left(\langle[0.40,0.44],[0.50,0.52]\rangle, \langle 0.55,0.35\rangle\right)$
	$\mathfrak{Z}_2$	$\left(\langle[0.15,0.30],[0.35,0.40]\rangle, \langle 0.17,0.40\rangle\right)$	$\left(\langle[0.15,0.18],[0.20,0.30]\rangle, \langle 0.29,0.63\rangle\right)$	$\left(\langle[0.30,0.40],[0.35,0.42]\rangle, \langle 0.40,0.40\rangle\right)$	$\left(\langle[0.55,0.59],[0.18,0.33]\rangle, \langle 0.16,0.20\rangle\right)$
	$\mathfrak{Z}_3$	$\left(\langle[0.39,0.48],[0.10,0.18]\rangle, \langle 0.20,0.15\rangle\right)$	$\left(\langle[0.23,0.32],[0.47,0.50]\rangle, \langle 0.30,0.60\rangle\right)$	$\left(\langle[0.40,0.45],[0.20,0.25]\rangle, \langle 0.29,0.19\rangle\right)$	$\left(\langle[0.37,0.42],[0.40,0.50]\rangle, \langle 0.30,0.70\rangle\right)$
	$\mathfrak{Z}_4$	$\left(\langle[0.42,0.55],[0.30,0.45]\rangle, \langle 0.15,0.30\rangle\right)$	$\left(\langle[0.44,0.50],[0.19,0.25]\rangle, \langle 0.42,0.20\rangle\right)$	$\left(\langle[0.16,0.32],[0.18,0.22]\rangle, \langle 0.17,0.34\rangle\right)$	$\left(\langle[0.20,0.55],[0.38,0.49]\rangle, \langle 0.80,0.17\rangle\right)$
	weights	0.40	0.20	0.25	0.15

Table 4. Ranking Values of Alternatives Corresponding to $T^{(4)}$ Decision-maker

Decision maker	Applicants & Weighs	$\mathfrak{d}_1$	$\mathfrak{d}_2$	$\mathfrak{d}_3$	$\mathfrak{d}_4$
$T^{(4)}$	$\mathfrak{Z}_1$	$\left(\langle[0.20,0.35],[0.48,0.54]\rangle, \langle 0.30,0.45\rangle\right)$	$\left(\langle[0.36,0.40],[0.11,0.50]\rangle, \langle 0.45,0.20\rangle\right)$	$\left(\langle[0.30,0.55],[0.24,0.32]\rangle, \langle 0.10,0.30\rangle\right)$	$\left(\langle[0.11,0.20],[0.16,0.29]\rangle, \langle 0.35,0.19\rangle\right)$
	$\mathfrak{Z}_2$	$\left(\langle[0.18,0.30],[0.25,0.40]\rangle, \langle 0.20,0.70\rangle\right)$	$\left(\langle[0.18,0.30],[0.19,0.34]\rangle, \langle 0.40,0.20\rangle\right)$	$\left(\langle[0.15,0.35],[0.20,0.60]\rangle, \langle 0.25,0.40\rangle\right)$	$\left(\langle[0.40,0.20],[0.10,0.50]\rangle, \langle 0.50,0.20\rangle\right)$
	$\mathfrak{Z}_3$	$\left(\langle[0.10,0.29],[0.15,0.35]\rangle, \langle 0.11,0.30\rangle\right)$	$\left(\langle[0.20,0.30],[0.11,0.60]\rangle, \langle 0.30,0.50\rangle\right)$	$\left(\langle[0.10,0.29],[0.40,0.50]\rangle, \langle 0.30,0.40\rangle\right)$	$\left(\langle[0.29,0.37],[0.25,0.35]\rangle, \langle 0.25,0.60\rangle\right)$
	$\mathfrak{Z}_4$	$\left(\langle[0.25,0.32],[0.40,0.45]\rangle, \langle 0.20,0.32\rangle\right)$	$\left(\langle[0.16,0.20],[0.25,0.32]\rangle, \langle 0.10,0.63\rangle\right)$	$\left(\langle[0.45,0.60],[0.20,0.25]\rangle, \langle 0.29,0.63\rangle\right)$	$\left(\langle[0.21,0.39],[0.20,0.49]\rangle, \langle 0.66,0.28\rangle\right)$
	weights	0.45	0.19	0.25	0.11

4.1.2. Step 2: Computing CIFS-PIA and CIFS-NIA for Each Decision-maker. Computing the CIFS-PIA and CIFS-NIA for each decision-maker is depicted below in Table 5.

Using the **Eq.** (**3.1**) and **(3.2**), CIFS-PIA and CIFS-NIA are computed respectively as follows:

$$(\mathfrak{X}^{+}{}_{j})^{k} = \left(\langle\left[(t_j^{L+})^k, (t_j^{U+})^k\right], \left[(f_j^{L+})^k, (f_j^{U+})^k\right]\rangle, \langle(p_j^{+})^k, (q_j^{+})^k\rangle\right)$$

and

$$(\mathfrak{X}^{-}{}_{j})^{k} = \left(\langle\left[(t_j^{L-})^k, (t_j^{U-})^k\right], \left[(f_j^{L-})^k, (f_j^{U-})^k\right]\rangle, \langle(p_j^{-})^k, (q_j^{-})^k\rangle\right),$$

where

$$(t_j^{L+})^k = \max_j\left\{(\mathfrak{t}_{ij}(\mathfrak{z}_i)^{-})^{(k)}\right\}, (t_j^{U+})^k = \max_j\left\{(\mathfrak{t}_{ij}(\mathfrak{z}_i)^{+})^{(k)}\right\}, (f_j^{L+})^k = \min_j\left\{(\mathfrak{f}_{ij}(\mathfrak{z}_i)^{-})^{(k)}\right\}, (f_j^{U+})^k = \min_j\left\{(\mathfrak{f}_{ij}(\mathfrak{z}_i)^{+})^{(k)}\right\},$$
$$(p_j^{+})^k = \min_j\left\{(\mathfrak{t}_{ij}(\mathfrak{z}_i))^{(k)}\right\}, (q_j^{+})^k = \max_j\left\{(\mathfrak{f}_{ij}(\mathfrak{z}_i))^{(k)}\right\} \forall i$$

and

$$(t_j^{L-})^k = \min_j\left\{(\mathfrak{t}_{ij}(\mathfrak{z}_i)^{-})^{(k)}\right\}, (t_j^{U-})^k = \min_j\left\{(\mathfrak{t}_{ij}(\mathfrak{z}_i)^{+})^{(k)}\right\}, (f_j^{L-})^k = \max_j\left\{(\mathfrak{f}_{ij}(\mathfrak{z}_i)^{-})^{(k)}\right\}, (f_j^{U-})^k = \max_j\left\{(\mathfrak{f}_{ij}(\mathfrak{z}_i)^{+})^{(k)}\right\},$$
$$(p_j^{-})^k = \max_j\left\{\left(\mathfrak{t}_{ij}(\mathfrak{z}_i)\right)^{(k)}\right\}, (q_j^{-})^k = \min_j\left\{\left(\mathfrak{f}_{ij}(\mathfrak{z}_i)\right)^{(k)}\right\} \forall i.$$

Table 5. Positive and Negative Ideal for Each Decision-maker

DM	PIA / NIA	$\mathfrak{d}_1$	$\mathfrak{d}_2$	$\mathfrak{d}_3$	$\mathfrak{d}_4$
$\mathcal{T}^{(1)}$	$\mathfrak{X}^{+}{}_1$	$\left(\langle\begin{matrix}[0.42,0.50],\\ [0.10,0.18]\end{matrix}\rangle, \begin{matrix}\\ \langle 0.17,0.40\rangle\end{matrix}\right)$	$\left(\langle\begin{matrix}[0.44,0.50],\\ [0.10,0.25]\end{matrix}\rangle, \begin{matrix}\\ \langle 0.19,0.63\rangle\end{matrix}\right)$	$\left(\langle\begin{matrix}[0.40,0.45],\\ [0.18,0.22]\end{matrix}\rangle, \begin{matrix}\\ \langle 0.17,0.49\rangle\end{matrix}\right)$	$\left(\langle\begin{matrix}[0.55,0.59],\\ [0.18,0.33]\end{matrix}\rangle, \begin{matrix}\\ \langle 0.16,0.70\rangle\end{matrix}\right)$
	$\mathfrak{X}^{-}{}_1$	$\left(\langle\begin{matrix}[0.15,0.30],\\ [0.35,0.45]\end{matrix}\rangle, \begin{matrix}\\ \langle 0.35,0.15\rangle\end{matrix}\right)$	$\left(\langle\begin{matrix}[0.15,0.18],\\ [0.47,0.50]\end{matrix}\rangle, \begin{matrix}\\ \langle 0.42,0.20\rangle\end{matrix}\right)$	$\left(\langle\begin{matrix}[0.16,0.32],\\ [0.38,0.49]\end{matrix}\rangle, \begin{matrix}\\ \langle 0.40,0.19\rangle\end{matrix}\right)$	$\left(\langle\begin{matrix}[0.20,0.42],\\ [0.50,0.52]\end{matrix}\rangle, \begin{matrix}\\ \langle 0.80,0.17\rangle\end{matrix}\right)$

DM	PIA NIA	$\mathfrak{d}_1$	$\mathfrak{d}_2$	$\mathfrak{d}_3$	$\mathfrak{d}_4$
$\mathcal{T}^{(2)}$	$\mathfrak{Z}^{+}{}_2$	$\left(\left\langle \begin{matrix}[0.35,0.45],\\ [0.10,0.29]\end{matrix}\right\rangle, \langle 0.11,0.70\rangle\right)$	$\left(\left\langle \begin{matrix}[0.60,0.70],\\ [0.15,0.20]\end{matrix}\right\rangle, \langle 0.10,0.63\rangle\right)$	$\left(\left\langle \begin{matrix}[0.47,0.50],\\ [0.12,0.15]\end{matrix}\right\rangle, \langle 0.15,0.35\rangle\right)$	$\left(\left\langle \begin{matrix}[0.40,0.50],\\ [0.10,0.20]\end{matrix}\right\rangle, \langle 0.20,0.70\rangle\right)$
	$\mathfrak{Z}^{-}{}_2$	$\left(\left\langle \begin{matrix}[0.10,0.29],\\ [0.48,0.54]\end{matrix}\right\rangle, \langle 0.60,0.20\rangle\right)$	$\left(\left\langle \begin{matrix}[0.15,0.35],\\ [0.19,0.36]\end{matrix}\right\rangle, \langle 0.60,0.10\rangle\right)$	$\left(\left\langle \begin{matrix}[0.10,0.18],\\ [0.32,0.42]\end{matrix}\right\rangle, \langle 0.50,0.20\rangle\right)$	$\left(\left\langle \begin{matrix}[0.11,0.20],\\ [0.40,0.44]\end{matrix}\right\rangle, \langle 0.66,0.17\rangle\right)$
$\mathcal{T}^{(3)}$	$\mathfrak{Z}^{+}{}_3$	$\left(\left\langle \begin{matrix}[0.30,0.50],\\ [0.10,0.30]\end{matrix}\right\rangle, \langle 0.20,0.35\rangle\right)$	$\left(\left\langle \begin{matrix}[0.30,0.38],\\ [0.20,0.30]\end{matrix}\right\rangle, \langle 0.11,0.40\rangle\right)$	$\left(\left\langle \begin{matrix}[0.32,0.60],\\ [0.30,0.30]\end{matrix}\right\rangle, \langle 0.11,0.70\rangle\right)$	$\left(\left\langle \begin{matrix}[0.32,0.45],\\ [0.10,0.20]\end{matrix}\right\rangle, \langle 0.30,0.40\rangle\right)$
	$\mathfrak{Z}^{-}{}_3$	$\left(\left\langle \begin{matrix}[0.10,0.35],\\ [0.40,0.45]\end{matrix}\right\rangle, \langle 0.45,0.10\rangle\right)$	$\left(\left\langle \begin{matrix}[0.10,0.15],\\ [0.40,0.45]\end{matrix}\right\rangle, \langle 0.60,0.10\rangle\right)$	$\left(\left\langle \begin{matrix}[0.10,0.40],\\ [0.50,0.50]\end{matrix}\right\rangle, \langle 0.25,0.32\rangle\right)$	$\left(\left\langle \begin{matrix}[0.10,0.29],\\ [0.50,0.50]\end{matrix}\right\rangle, \langle 0.45,0.20\rangle\right)$
$\mathcal{T}^{(4)}$	$\mathfrak{Z}^{+}{}_4$	$\left(\left\langle \begin{matrix}[0.25,0.35],\\ [0.15,0.35]\end{matrix}\right\rangle, \langle 0.11,0.70\rangle\right)$	$\left(\left\langle \begin{matrix}[0.36,0.40],\\ [0.11,0.32]\end{matrix}\right\rangle, \langle 0.10,0.63\rangle\right)$	$\left(\left\langle \begin{matrix}[0.30,0.55],\\ [0.20,0.25]\end{matrix}\right\rangle, \langle 0.10,0.63\rangle\right)$	$\left(\left\langle \begin{matrix}[0.40,0.39],\\ [0.10,0.29]\end{matrix}\right\rangle, \langle 0.25,0.60\rangle\right)$
	$\mathfrak{Z}^{-}{}_4$	$\left(\left\langle \begin{matrix}[0.10,0.29],\\ [0.40,0.54]\end{matrix}\right\rangle, \langle 0.30,0.30\rangle\right)$	$\left(\left\langle \begin{matrix}[0.16,0.20],\\ [0.25,0.60]\end{matrix}\right\rangle, \langle 0.45,0.20\rangle\right)$	$\left(\left\langle \begin{matrix}[0.10,0.29],\\ [0.40,0.60]\end{matrix}\right\rangle, \langle 0.30,0.30\rangle\right)$	$\left(\left\langle \begin{matrix}[0.11,0.20],\\ [0.25,0.50]\end{matrix}\right\rangle, \langle 0.66,0.19\rangle\right)$

4.1.3. Step 3: Evaluation of Separation Measures. Without the loss of generality, assuming q=2 separation measures are calculated between the applicants from their CIFS-PIA and CIFS-NIA corresponding to each decision-maker and denoted by $\mathfrak{d}_{\boldsymbol{q}}''\left((\mathfrak{Z}_{\boldsymbol{i}})^{\boldsymbol{k}}, (\mathfrak{Z}^{+})^{\boldsymbol{k}}\right)$ **and** $\mathfrak{d}_{\boldsymbol{q}}''\left((\mathfrak{Z}_{\boldsymbol{i}})^{\boldsymbol{k}}, (\mathfrak{Z}^{-})^{\boldsymbol{k}}\right)$ respectively, as depicted in Table 6.

Using **Eqs.** (**3.6**) and (**3.7**)

$$\mathfrak{d}_q''(\mathfrak{Z}_i, \mathfrak{Z}^{+}) = \left[\frac{1}{6}\sum_{j=1}^{n} w_j\left\{\left|t_j^{L+} - \mathfrak{t}_{ij}(\mathfrak{Z}_i)^{-}\right|^q + \left|t_j^{U+} - \mathfrak{t}_{ij}(\mathfrak{Z}_i)^{+}\right|^q + \left|\mathfrak{f}_{ij}(\mathfrak{Z}_i)^{-} - f_j^{L+}\right|^q + \left|\mathfrak{f}_{ij}(\mathfrak{Z}_i)^{+} - f_j^{U+}\right|^q + \left|\mathfrak{t}_{ij}(\mathfrak{Z}_i) - p_j^{+}\right|^q + \left|q_j^{+} - \mathfrak{f}_{ij}(\mathfrak{Z}_i)\right|^q\right\}\right]^{1/q}$$

and

$$\mathfrak{d}_q''(\mathfrak{Z}_i, \mathfrak{Z}^{-}) = \left[\frac{1}{6}\sum_{j=1}^{n} w_j\left\{\left|\mathfrak{t}_{ij}(\mathfrak{Z}_i)^{-} - t_j^{L-}\right|^q + \left|\mathfrak{t}_{ij}(\mathfrak{Z}_i)^{+} - t_j^{U-}\right|^q + \left|f_j^{L-} - \mathfrak{f}_{ij}(\mathfrak{Z}_i)^{-}\right|^q + \left|f_j^{U-} - \mathfrak{f}_{ij}(\mathfrak{Z}_i)^{+}\right|^q + \left|p_j^{-} - \mathfrak{t}_{ij}(\mathfrak{Z}_i)\right|^q + \left|\mathfrak{f}_{ij}(\mathfrak{Z}_i) - q_j^{-}\right|^q\right\}\right]^{1/q}.$$

Solving these separation measures corresponding to each decision-maker, we get

Table 6. Evaluation of Separation Measures

Applicants	$T^{(1)}$		$T^{(2)}$		$T^{(3)}$		$T^{(4)}$	
	$T_i^{(1+)}$	$T_i^{(1-)}$	$T_i^{(2+)}$	$T_i^{(2-)}$	$T_i^{(3+)}$	$T_i^{(3-)}$	$T_i^{(4+)}$	$T_i^{(4-)}$
$\mathfrak{Z}_1$	0.3553	0.3102	0.4961	0.3927	0.2703	0.2501	0.3651	0.2461
$\mathfrak{Z}_2$	0.3927	0.4116	0.4087	0.4672	0.2180	0.2151	0.2583	0.2076
$\mathfrak{Z}_3$	0.3784	0.3478	0.2645	0.4783	0.2158	0.2426	0.2764	0.2123
$\mathfrak{Z}_4$	0.4067	0.3600	0.3538	0.3330	0.2058	0.2037	0.1947	0.1582

4.1.4. Step 4: Computing the Relative Closeness Coefficient. Using Eq. (3.8), the relative closeness coefficient and the ranking order of the applicants corresponding to each decision-maker is computed as

$$\mathbb{C}_i^{(k)} = \frac{\mathrm{d}_q''((\mathfrak{Z}_i)^k, (\mathfrak{X}^-)^k)}{\mathrm{d}_q''((\mathfrak{Z}_i)^k, (\mathfrak{X}^+)^k) + \mathrm{d}_q''((\mathfrak{Z}_i)^k, (\mathfrak{X}^-)^k)}; \quad k = 1,2, \dots, K$$

where $\mathrm{d}_q''((\mathfrak{Z}_i)^k, (\mathfrak{X}^+)^k) \neq 0$.

The outcome is manifested in Table 7.

Table 7. Relative Closeness

Applicants	$T^{(1)}$	$T^{(2)}$	$T^{(3)}$	$T^{(4)}$
	$\mathbb{C}_i^{(1)}$	$\mathbb{C}_i^{(2)}$	$\mathbb{C}_i^{(3)}$	$\mathbb{C}_i^{(4)}$
$\mathfrak{Z}_1$	0.4661	0.4418	0.4806	0.4027
$\mathfrak{Z}_2$	0.5117	0.5334	0.4967	0.4456
$\mathfrak{Z}_3$	0.4789	0.6439	0.5292	0.4344
$\mathfrak{Z}_4$	0.4695	0.4849	0.4974	0.4483

4.1.5. Step 5: Ranking of Alternatives. Using the relative closeness coefficient, the ranking of alternatives corresponding to each decision-maker is manifested in Table 8.

Table 8. Ranking of Alternatives

Applicants	$T^{(1)}$		$T^{(2)}$		$T^{(3)}$		$T^{(4)}$	
	$\mathbb{C}_i^{(1)}$	Ranking	$\mathbb{C}_i^{(2)}$	Ranking	$\mathbb{C}_i^{(3)}$	Ranking	$\mathbb{C}_i^{(4)}$	Ranking
$\mathfrak{Z}_1$	0.4661	4	0.4418	4	0.4806	4	0.4027	4
$\mathfrak{Z}_2$	0.5117	1	0.5334	2	0.4967	3	0.4456	2

Applicants	$T^{(1)}$		$T^{(2)}$		$T^{(3)}$		$T^{(4)}$	
	$\mathbb{C}_i^{(1)}$	Ranking	$\mathbb{C}_i^{(2)}$	Ranking	$\mathbb{C}_i^{(3)}$	Ranking	$\mathbb{C}_i^{(4)}$	Ranking
$\mathfrak{Z}_3$	0.4789	2	0.6439	1	0.5292	1	0.4344	3
$\mathfrak{Z}_4$	0.4695	3	0.4849	3	0.4974	2	0.4483	1

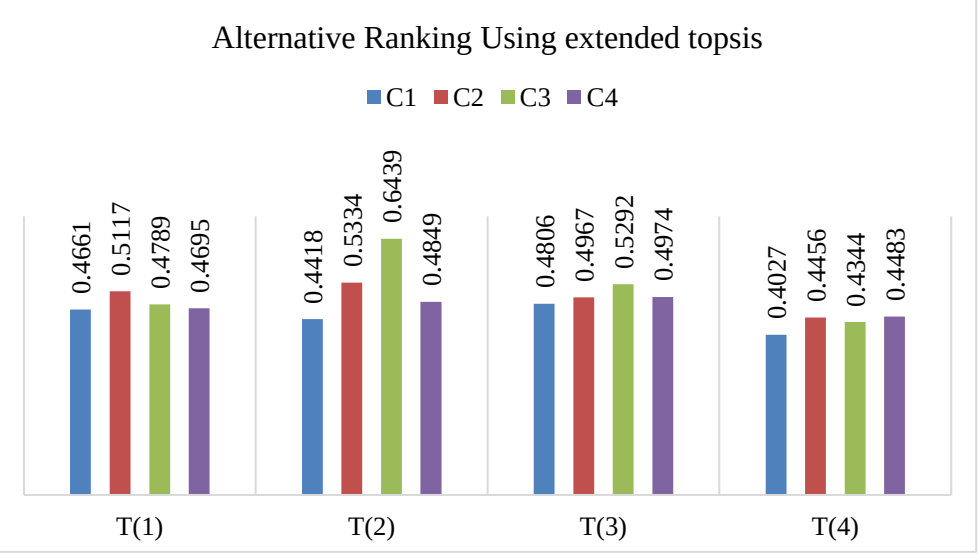

Figure 2. Alternative Ranking using Extended TOPSIS Method

Table 9. Final Scores of Alternatives

	$T^{(1)}$	$T^{(2)}$	$T^{(3)}$	$T^{(4)}$
$\mathbb{C}_i^{(1)}$	0.4661	0.4418	0.4806	0.4027
$\mathbb{C}_i^{(2)}$	0.5117	0.5334	0.4967	0.4456
$\mathbb{C}_i^{(3)}$	0.4789	0.6439	0.5292	0.4344
$\mathbb{C}_i^{(4)}$	0.4695	0.4849	0.4974	0.4483

5. DISCUSSION

The problem of the selection of the head chef at a famous restaurant has been solved by applying the extended TOPSIS method based on the suggested distance and similarities measure. Based on the proposed method, four decision-makers were selected to select the best head chef to take charge of the kitchen. Each decision-maker assigned the rating values that corresponded to each attribute and alternative, as shown in tables 1-4. Using CIF-PIA and CIF-NIA, the separation measure between the alternatives was

computed, as shown in tables 5-6. Then, the last relative closeness coefficient was calculated, as shown in Table 7. Each value of the relative closeness coefficient was arranged in descending order and all alternatives were ranked corresponding to each decision-maker, as shown in Table 8 and Figure 2. According to $\mathsf{T}^{(1)}$ decision-maker, $\mathfrak{Z}_2$ remains the PIA for the selection of head chef. According to $\mathsf{T}^{(2)}$ decision-maker, $\mathfrak{Z}_3$ is the PIA for the selection of head chef. According to $\mathsf{T}^{(3)}$ decision-maker, $\mathfrak{Z}_3$ is the PIA for the selection of head chef and according to $\mathsf{T}^{(4)}$ decision-maker, $\mathfrak{Z}_4$ is the PIA for the selection of head chef. However, if only one head chef needs to be selected, then the highest ranking PIA should be arranged in descending order and the best head chef should be chosen to take charge of the kitchen.

5.1.Conclusion

In this project, the issue of MCGDM under the CIFS-set environment has been discussed. An adaptation of the TOPSIS method has been illustrated to show the effectiveness of the proposed operators. According to the findings, these decision-making techniques can represent uncertainty more effectively than the current approaches and provide us with a comprehensive understanding of real-life scenarios. The problem of the selection of head chef for the newly opened restaurant has been dealt with in this research. The proposed approach of TOPSIS yields the best head chef. The findings of this research can be applied in the future to hypersoft set, interval-valued soft set, bi-polar soft set, and other ambiguous environments.

REFERENCES

1. Zadeh LA. Fuzzy sets. *Inf Control*. 1965;8(3):338–353. https://doi.org/10.1016/S0019-9958(65)90241-X
2. Atanassov KT. Intuitionistic fuzzy sets. *Fuzzy Sets Syst*. 1986;20(1):87–96. https://doi.org/10.1016/S0165-0114(86)80034-3
3. Szmidt E, Kacprzyk, J. Distances between intuitionistic fuzzy sets. *Fuzzy Sets Syst.* 2000;114(3):505–518. https://doi.org/10.1016/S0165-0114(98)00244-9
4. Wang W, Xin X. Distance measure between intuitionistic fuzzy sets. *Pattern Recognit Lett*. 2005;26(13):2063–2069. https://doi.org/10.1016/j.patrec.2005.03.018

5. Hung WL, Yang MS. Similarity measures of intuitionistic fuzzy sets based on Hausdorff distance. *Pattern Recognit Lett*. 2004;25(14):1603–1611. https://doi.org/10.1016/j.patrec.2004.06.006
6. Lai YJ, Liu TY, Hwang CL. TOPSIS for MODM. *Eur J Oper Res*. 1994;76(3):486–500. https://doi.org/10.1016/0377-2217(94)90282-8
7. Atanassov K, Gargov G. Interval valued intuitionistic fuzzy sets. *Fuzzy Sets Syst*. 1989;31(3):343–349. https://doi.org/10.1016/0165-0114(89)90205-4
8. Jahanshahloo GR, Lotfi FH, Izadikhah M. Extension of the TOPSIS method for decision-making problems with fuzzy data. *Appl Math Comput*. 2006;181(2):1544–1551. https://doi.org/10.1016/j.amc.2006.02.057
9. Chu TC, Lin YC. A fuzzy TOPSIS method for robot selection. *Int J Adv Manuf Technol*. 2003;21(4):284–290. https://doi.org/10.1007/s001700300033
10. Zulqarnain RM, Xin XL, Saeed M, Smarandache F, Ahmad N. Generalized fuzzy TOPSIS to solve multi-criteria decision-making problems. *J New Theory*. 2020;32:40–50.
11. Saqlain M, Jafar MN, Riaz M. A new approach of neutrosophic soft set with generalized fuzzy TOPSIS in application of smart phone selection. *Neutrosophic Sets Syst*. 2020;32:307–316.
12. Shen F, Ma X, Li Z, Xu Z, Cai D. An extended intuitionistic fuzzy TOPSIS method based on a new distance measure with an application to credit risk evaluation. *Inf Sci*. 2018;428:105–119. https://doi.org/10.1016/j.ins.2017.10.045
13. Chang CH, Lin JJ, Lin JH, Chiang MC, Ho WR. Domestic open-end equity mutual fund performance evaluation using extended TOPSIS method with different distance approaches. *Expert Syst Appl*. 2010;37(6):4642–4649. https://doi.org/10.1016/j.eswa.2009.12.044
14. Li H, Su L, Cao Y, Lv L. A pythagorean fuzzy TOPSIS method based on similarity measure and its application to project delivery system selection. *J Intell Fuzzy Syst*. 2019;37(5):7059–7071. https://doi.org/10.3233/JIFS-181690
15. Gupta P, Mehlawat MK, Grover N, Pedrycz W. Multi-attribute group decision making based on extended TOPSIS method under interval-

valued intuitionistic fuzzy environment. *Appl Soft Comput*. 2018;69:554–567. https://doi.org/10.1016/j.asoc.2018.04.032
16. Garg H, Kaur G. Extended TOPSIS method for multi-criteria group decision-making problems under cubic intuitionistic fuzzy environment. *Sci Iran*. 2020;27(1):396–410. https://doi.org/10.24200/sci.2018.5307.1194
17. Pramanik S, Dey PP, Giri BC, Smarandache F. An extended TOPSIS for multi-attribute decision making problems with neutrosophic cubic information. *Neutrosophic Sets Syst*. 2017;17(1):20–28.
18. Jun YB, Kim CS, Yang KO. Cubic sets. *Ann Fuzzy Math Inform*. 2012;4(1):83-98.
19. Garg H, Kaur G. Cubic intuitionistic fuzzy sets and its fundamental properties. *J Mul Valued Log Soft Comput*. 2019;33(6):507–537.
20. Maji PK, Biswas R, Roy AR. Soft set theory. *Comput Math Appl*. 2003;45(4-5):555–562. https://doi.org/10.1016/S0898-1221(03)00016-6
21. Saqlain M, Imran R, Hassan S. Cubic Intuitionistic fuzzy soft set and its distance measures. *Sci Inquiry Rev*. 2022;6(2):59–75. https://doi.org/10.32350/sir.62.04

Scientific Inquiry and Review (SIR)
Volume 7 Issue 1, 2023
ISSN (P): 2521-2427, ISSN (E): 2521-2435
Homepage: https://journals.umt.edu.pk/index.php/SIR

Article QR

Title:	**Transmission Analysis of Hepatitis B Epidemic Model using Standard and Non-standard Schemes**
Author (s):	Ihsan Ullah Khan[1], Muhammad Irfan[1], Azhar Iqbal[2], Amjid Hussain[1]
Affiliation (s):	[1]Gomal University, Dera Ismail Khan, KPK, Pakistan [2] Dawood University of Engineering and Technology, Karachi, Pakistan
DOI:	https://doi.org/10.32350/sir.71.04
History:	Received: December 8, 2022, Revised: January 10, 2023, Accepted: January 10, 2023, Published: March 15, 2023
Citation:	Khan IU, Irfan M, Iqbal A, Hussain A. Transmission analysis of Hepatitis B epidemic model using standard and non-standard schemes. *Sci Inq Rev.* 2023;7(1):53–70. https://doi.org/10.32350/sir.71.04
Copyright:	© The Authors
Licensing:	This article is open access and is distributed under the terms of Creative Commons Attribution 4.0 International License
Conflict of Interest:	Author(s) declared no conflict of interest

A publication of
The School of Science
University of Management and Technology, Lahore, Pakistan

Transmission Analysis of Hepatitis B Epidemic Model using Standard and Non-standard Schemes

Ihsan Ullah Khan[1*], Muhammad Irfan[1], Azhar Iqbal [2], and Amjid Hussain[1]

[1]Department of Mathematics, Institute of Numerical Sciences, Gomal University, Dera Ismail Khan, Pakistan

[2] Department of Mathematics, Dawood University of Engineering and Technology, Karachi, Pakistan

ABSTRACT

Mathematical modeling is a vast field that has interdisciplinary implications for research. These models help to investigate the basic dynamics and quantitative behavior of infectious diseases that affect human beings, such as COVID-19, hepatitis B virus (HBV), and human immunodeficiency virus (HIV). The current study investigates the spread of HBV by using the basic virus model. In order to determine the stability of disease-free and endemic equilibria, the basic reproduction number is determined. The convergence and divergence of disease-free and endemic equilibria are demonstrated by using standard finite difference (SFD) and non-standard finite difference (NSFD) schemes. Arguably, SFD schemes, namely Euler and Runge-Kutta order four (RK-4) schemes, converge for lower step sizes, while the NSFD scheme converges for all step sizes. The latter is a strong, efficient, and reliable method that shows a clear picture of the continuous model. All the results are validated using numerical simulations in order to better comprehend the dynamics of the disease. The theoretical and numerical findings in this work can be applied as a useful tool for tracking the prevalence of HBV infectious disease.

Keywords: convergence, divergence, HBV model, local and global stability, numerical schemes

1. INTRODUCTION

HBV is a devastating liver infection and an epidemic that poses a considerable health hazard, specifically in developing nations [1, 2]. HBV damages the liver and causes numerous shocking disorders. Almost 360 million people worldwide are affected by this infectious disease and among them are more than 150 million HBV transporters (who transmit the disease to healthy people) [3, 4]. Also, more than 150 million of them have chronic

* Corresponding Author: ihsanmrwt@gu.edu.pk

hepatitis C virus (HCV) infection and another 150–200 million are HBV chronic liver infection carriers [5]. HBV is transmitted by exposed sex, blood transfusion, and spreads into the recently born infant during pregnancy from the infected mother.

Mathematical models [6-19] are very useful for analyzing the dynamics of real-world problems. Researchers utilize ordinary differential equations [6-11] as well as partial differential equations [12-15] to investigate different characteristics of physical objects. Fractional order [16-19] mathematical models are also among the most investigated topics in the world in this regard. Mathematical modeling also helps in the analysis of experimental results, as well as understanding the fundamental biological mechanisms of disease transmission. Many mathematical models have been suggested to improve the understanding and knowledge of HBV disease. Zeuzem et al. [6] and Nowak et al. [7] recommended simple virus infection models in which clear immune responses are not required. These models are mostly applied in the analysis of virus infection dynamics. In [8], the author proposed and examined the stochastic SACR model for the transmission of HBV disease. In [9, 10], the authors focused on population characteristics, infectious diseases, infection characteristics, and related social factors of HBV. Aja et al. [11] constructed a model based on statistical data which is not only useful for forecasting disease transmission but also helps to identify the key factors that affect the disease spread.

In early 1980s, mathematical modelling was used to investigate the dynamics of HBV and the efficiency of disease control. To date, several systematic methods have been applied for the prevention of HBV transmission [20-22]. The most attractive and effective way of reducing the prevalence of HBV in newborns is vaccination. In case of vaccination, the emphasis shifts towards the use of a mathematical model to forecast the long-term consequences of immunization on hepatitis B regulation. Many scientists have analyzed the transmission mechanism of HBV and evaluated the effect of various vaccine policies [23, 24]. Recently, in [25], the author proposed and analyzed a non-linear basic adaptation system for HBV spread. The stability of disease-free and endemic equilibria was discussed for the continuous model. The author used a mathematical framework for the continuous model to study the stability of equilibria which strictly depend on the basic reproduction number.

The aim of the current study is to prevent the spread of HBV and explore its threats to the health of general people. Multiple numerical schemes, such as Euler, RK-4, and the NSFD scheme have been deployed to assess the various properties of the model and demonstrate their ecological feasibility and accuracy. The findings demonstrate that the aforementioned schemes give a thorough description of the continuous model.

The structure of the current paper is organized as follows. The HBV disease model and corresponding parameters are described in Section 2. In Section 3, the expression for R_0, the equilibria of the system, and their stability are explored for the continuous model. SFD schemes, including Euler, RK-4, and the NSFD scheme are produced for the continuous model in Section 4. The fundamental dynamic properties of the continuous model containing the positivity of solutions cannot be preserved by Euler and RK-4 schemes for higher step sizes, leading to numerical solutions that are different from the solutions of the original system. However, the NSFD scheme gives positive solutions for all finite step sizes and basically overcomes the shortcomings of the SFD schemes. The analysis also demonstrates that the NSFD scheme is unconditionally convergent and provides better results in all aspects than Euler and RK-4 schemes. The theoretical findings are strengthened by numerical simulations at each stage. In Section 5, brief conclusions are offered to sum up the whole work.

2. INTRODUCTION OF HEPATITIS B DISEASE MODEL

Figure 1 depicts the non-linear basic HBV epidemic model [25].

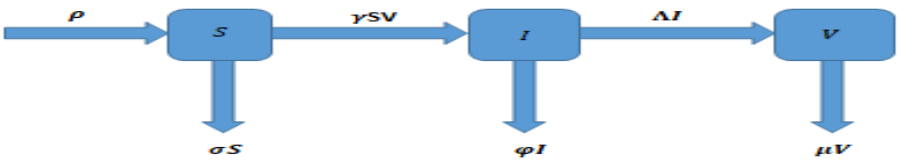

Figure 1. Illustration of Hepatitis B Disease Model

$$\frac{dS}{dt} = \rho - \sigma S - \gamma SV,$$
$$\frac{dI}{dt} = \gamma SV - \varphi I, \qquad (2.1)$$
$$\frac{dV}{dt} = \Lambda I - \mu V.$$

2.1. Parameters

The parameters used in system (**2.1**) are described as follows:

S shows the number of uninfected cells in the population

I shows the number of infected cells in the population

V shows the number of free virus particles in the population

γ shows the constant rate that explains the process reliability

ρ shows the constant rate

Λ shows the rate at which the virus leaves infected cells

σ shows the die rate of uninfected cells

φ shows how fast infected cells are dying

μ shows a free virus

The parameters $\rho, \gamma, \sigma, \varphi, \Lambda, \mu$ are all positive constants.

3. STABILITY ANALYSIS OF CONTINUOUS MODEL (1) EQUILIBRIA

The following subsection gives the equilibria of model (1).

3.1. Equilibria of Model

If all other classes are equal to zero aside from the susceptible class, the above described system (**2.1**) has the disease-free equilibrium (DFE) point $E_0 = \left(\frac{\rho}{\sigma}, 0, 0\right)$. If the system (**2.1**) is solved simultaneously, then the endemic equilibrium (EE) point occurs which is $E^* = (S^*, I^*, V^*) = \left(\frac{\varphi\mu}{\gamma\Lambda}, \frac{\sigma\mu(R_0-1)}{\gamma\Lambda}, \frac{\sigma(R_0-1)}{\gamma}\right)$. In the following, R_0 is provided which is crucial for the stability of the equilibria of model (1).

3.2. Basic Reproductive Number (R_0)

The most essential threshold quantity for any infectious disease is R_0. It helps to assess whether a contagious disease will spread among the people or not. R_0 is a significant biological quantity that may be determined using the modified technique known as the "next generation matrix" [26]. The transmission matrix $F(x)$ and translation matrix $V(x)$ for system (**2.1**) can be described as follows:

$$F(x) = \begin{bmatrix} \gamma SV \\ 0 \end{bmatrix} \text{ and } V(x) = \begin{bmatrix} \varphi I \\ -\Lambda I + \mu V \end{bmatrix}.$$

From the above, we can easily get

$$F = \begin{bmatrix} 0 & \frac{\gamma\rho}{\sigma} \\ 0 & 0 \end{bmatrix} \text{ and } V = \begin{bmatrix} \varphi & 0 \\ -\Lambda & \mu \end{bmatrix}.$$

As $R_0 = \rho(FV^{-1})$, so using the above information, R_0 becomes

$$R_0 = \frac{\gamma\rho\Lambda}{\mu\varphi\sigma}.$$

3.3. Stability of Equilibria

Theorem 3.1 [25]**:** The DFE point of system (**2.1**) is locally asymptotically stable (LAS) whenever $R_0 < 1$, as displayed in Figure 2(a).

Theorem 3.2 [25]**:** The EE point of system (1) is LAS whenever $R_0 > 1$, as displayed in Figure 2(b).

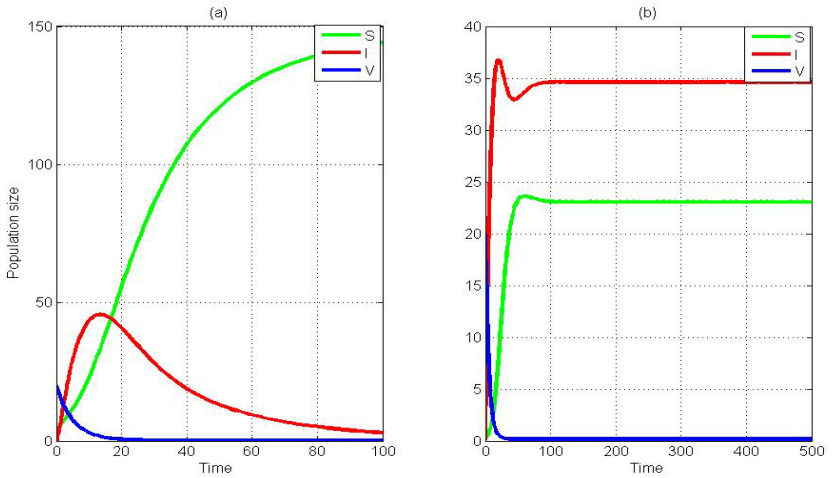

Figure 2. Numerical simulations for HBV model (1) with (a) $\gamma = .085$, (b) $\gamma = .85$. The remaining values of the parameters are offered as $\mu = .196, \sigma = .0667, \Lambda = .001, \varphi = .1, \rho = 10$.

According to the numerical simulations depicted in Figure 2(a), the DFE point of the continuous system (**2.1**) is stable if $R_0 < 1$. On the other hand, as illustrated in Figure 2(b), the EE point exists and becomes stable if R_0 >1. It is evident from Figure 2 and the preceding discussion that the EE

point emerges and remains stable when the DFE point becomes unstable, that is, when R_0 passes the critical value $R_0 = 1$, the system exhibits transcritical bifurcation and stability exchange from one equilibrium point to another. It shows that R_0=1 is the saddle point for system (**2.1**). More details can be found in [25].

4. NUMERICAL ANALYSIS OF SYSTEM (1)

In the current section, different discrete schemes for the continuous model (1) are constructed. The main aim is to better understand the dynamics of HBV disease transmission. Three schemes, namely Euler, RK-4, and NSFD schemes [27, 28] are constructed. It is demonstrated that the NSFD scheme is not only independent of step size but also more preferable as compared to the other defined schemes in every aspect.

4.1. Euler Scheme

Subsequent steps can be employed to construct the Euler scheme for system (**2.1**).

$$\frac{S^{p+1} - S^p}{h} = \rho - \sigma S^p - \gamma S^p V^p$$

$$S^{p+1} - S^p = h[\rho - \sigma S^p - \gamma S^p V^p]$$

$$S^{p+1} = S^p + h[\rho - \sigma S^p - \gamma S^p V^p].$$

Similarly

$$\frac{I^{p+1} - I^p}{h} = \gamma S^p V^p - \varphi I^p$$

$$I^{p+1} = I^p + h[\gamma S^p V^p - \varphi I^p],$$

and

$$\frac{V^{p+1} - V^p}{h} = \Lambda I^p - \mu V^p ,$$

$$V^{p+1} = V^p + h[\Lambda I^p - \mu V^p].$$

Therefore, the Euler scheme becomes

$$\begin{aligned} S^{p+1} &= S^p + h[\rho - \sigma S^p - \gamma S^p V^p] \\ I^{p+1} &= I^p + h[\gamma S^p V^p - \varphi I^p] \\ V^{p+1} &= V^p + h[\Lambda I^p - \mu V^p]. \end{aligned} \tag{4.1}$$

Once the step size is small, then the numerical solutions offered by the Euler scheme are positive, as illustrated in Figure 3(a-c). According to Figure 3(d), stability is disrupted as the step size increases. Therefore, the stability and positivity of Euler scheme does not maintain for all finite step sizes.

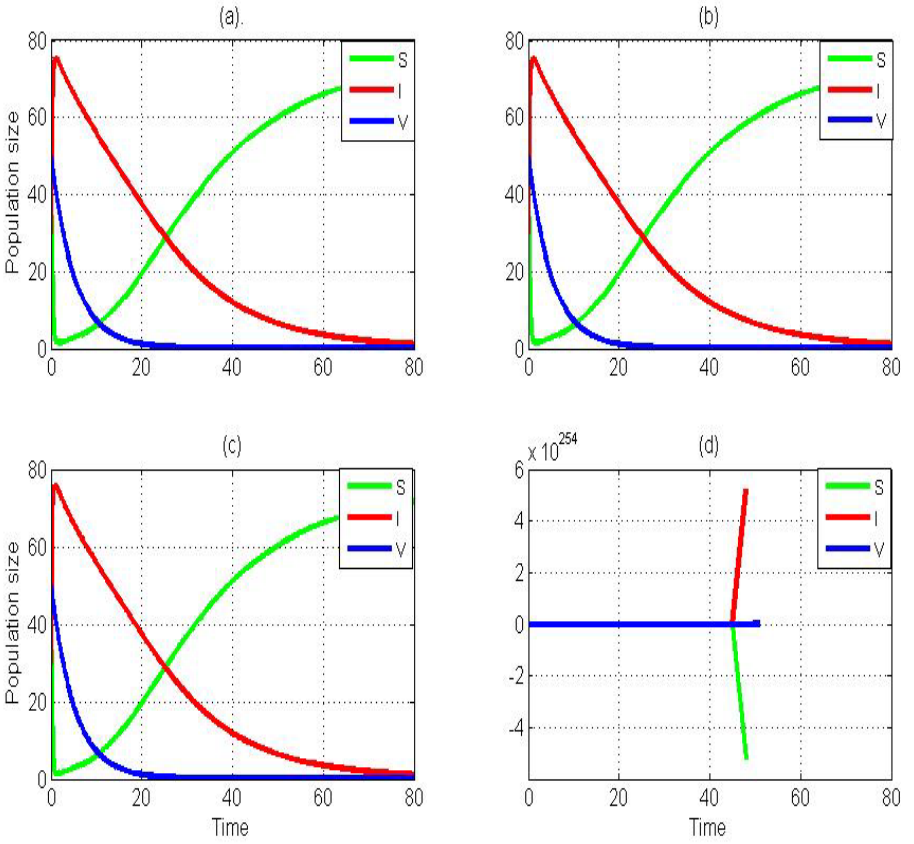

Figure 3. Graphs generated by Euler scheme (**4.1**) with (a) h=0.001, (b) h=0.01, (c) h=0.1 and (d) h=3. The remaining values of the parameters are offered as $\gamma = 0.085, \mu = 0.196, \sigma = 0.0667, \Lambda = 0.001, \varphi = 0.1, \rho = 10$.

4.2. Fourth-order Runge-Kutta Scheme (RK-4)

To develop the RK-4 scheme, it is assumed that $S = p_1, I = q_1$ and $V = r_1$. Then, the RK-4 scheme is described as follows:

Stage 1

$p_1 = h[\rho - (d + \gamma V^p)S^p],$
$q_1 = h[\gamma S^p V^p - \varphi I^p],$
$r_1 = h[\Lambda I^p - \mu V^p].$

Stage 2

$$p_2 = h\left[\rho - \left(\sigma + \gamma\left(V^p + \frac{r_1}{2}\right)\left(S^p + \frac{p_1}{2}\right)\right)\right],$$

$$q_2 = h\left[\gamma\left(V^p + \frac{r_1}{2}\right)\left(S^p + \frac{p_1}{2}\right) - \varphi\left(I^p + \frac{q_1}{2}\right)\right],$$

$$r_2 = h\left[\Lambda\left(I^p + \frac{q_1}{2}\right) - \mu\left(V^p + \frac{r_1}{2}\right)\right].$$

Stage 3

$$p_3 = h\left[\rho - \left(\sigma + \gamma\left(V^p + \frac{r_2}{2}\right)\left(S^p + \frac{p_2}{2}\right)\right)\right],$$

$$q_3 = h\left[\gamma\left(V^p + \frac{r_2}{2}\right)\left(S^p + \frac{p_2}{2}\right) - \varphi\left(I^p + \frac{q_2}{2}\right)\right],$$

$$r_3 = h\left[\Lambda\left(I^p + \frac{q_2}{2}\right) - \mu\left(V^p + \frac{r_2}{2}\right)\right].$$

Stage 4

$p_4 = h[\rho - (\sigma + \gamma(V^p + r_3)(S^p + p_3))],$
$q_4 = h[\gamma(V^p + r_3)(S^p + p_3) - \varphi(I^p + q_3)],$
$r_4 = h[\Lambda(I^p + q_3) - \mu(V^p + r_3)].$

Finally, we get

$$S^{p+1} = S^p + \frac{1}{6}[p_1 + 2p_2 + 2p_3 + p_4],$$
$$I^{p+1} = \frac{1}{6}[q_1 + 2q_2 + 2q_3 + q_4], \qquad (4.2)$$
$$V^{p+1} = \frac{1}{6}[r_1 + 2r_2 + 2r_3 + r_4].$$

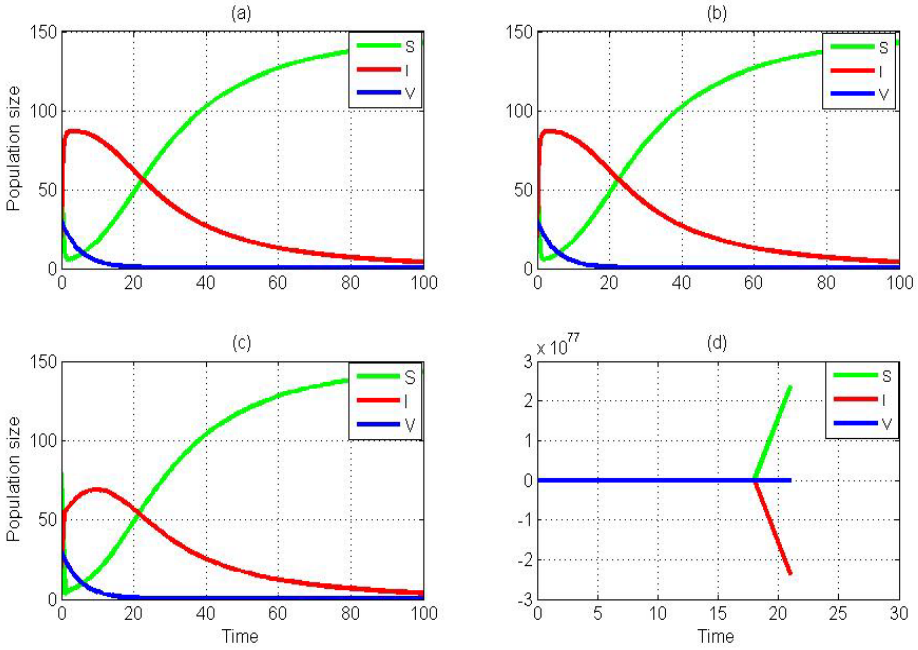

Figure 4. Graphs generated by RK-4 scheme (**4.2**) with (a) h=0.01, (b) h=0.1, (c) h=1 and (d) h=3. The remaining values of the parameters are offered as $\gamma = 0.085, \mu = .196, \sigma = .0667,\ \Lambda = .001, \varphi = 0.1, \rho = 10$.

Figure 4(a-d) provides a graphic representation of RK-4 scheme (**4.2**). The graphs produced by the RK-4 scheme are positive and convergent for small step sizes, as seen in Figure. 4(a-c). Figure 4(d) illustrates that the stability of model (1) is destroyed as the step size increases, that is, the RK-4 scheme diverges for large values of h.

4.3. Non-standard Finite Difference (NSFD) Scheme

Mickens [29] propagated the NSFD scheme which approximates the solutions of ordinary and partial differential equations. According to Shokri et al. [30], there are two factors that affect the study of the NSFD scheme. The first is how to discretize the derivative and the second constitutes the best way to approximate the nonlinear terms. The forward finite difference approximation is one of the general methods of first order derivative discretization. The first order derivative $\frac{dy}{dx}$ is written in standard form as $\frac{y(x+h)-y(x)}{h}$, where h stands for the step size. According to Mickens, this can

be expressed as $\frac{y(x+h)-y(x)}{\varphi(h)}$, where $\varphi(h)$ is referred to as the denominator function. There are various formulas for $\varphi(h)$ that can be viewed in [30]. In the current paper $\varphi(h) = h$. The following steps can be taken to construct the NSFD scheme for system (**2.1**).

$$\frac{S^{p+1}-S^{p}}{h} = \rho - \sigma S^{p+1} - \gamma S^{p+1}V^{p},$$
$$\frac{I^{p+1}-I^{p}}{h} = \gamma S^{p}V^{p} - \varphi I^{p+1},$$
$$\frac{V^{p+1}-V^{p}}{h} = \Lambda I^{p} - \mu V^{p+1}.$$

The above equations can be rewritten as

$$S^{p+1} = \frac{h\rho+S^{p}}{1+h\sigma+h\gamma V^{p}},$$
$$I^{p+1} = \frac{I^{p}+h\gamma S^{p}V^{p}}{1+h\varphi} \tag{4.3}$$
$$V^{p+1} = \frac{V^{p}+h\Lambda I^{p}}{1+h\mu}.$$

4.3.1. Investigating the Stability of Equilibria for the NSFD Scheme. In order to discuss the local stability, suppose

$$F = S^{p+1} = \frac{h\rho + S^{p}}{1 + h\alpha + h\epsilon V^{p}},$$
$$G = I^{p+1} = \frac{I^{p}+h\gamma S^{p}V^{p}}{1+h\varphi}, \tag{4.4}$$
$$H = V^{p+1} = \frac{V^{p}+h\Lambda I^{p}}{1+h\mu}.$$

Theorem 4.1: The DFE point E_0 for the discrete NSFD scheme (**4.3**) is LAS if $R_0 < 1$.

Proof: Consider the Jacobean matrix

$$J = \begin{bmatrix} \frac{\partial F}{\partial S} & \frac{\partial F}{\partial I} & \frac{\partial F}{\partial V} \\ \frac{\partial G}{\partial S} & \frac{\partial G}{\partial I} & \frac{\partial G}{\partial V} \\ \frac{\partial H}{\partial S} & \frac{\partial H}{\partial I} & \frac{\partial H}{\partial V} \end{bmatrix}. \tag{4.5}$$

From (4.4), the following derivatives can be easily obtained

$\frac{\partial F}{\partial S}=\frac{1}{(1+h\sigma+h\gamma V)},\frac{\partial F}{\partial I}=0,\frac{\partial F}{\partial V}=\frac{(h\rho+S)h\gamma}{[(1+h\sigma+h\gamma V)]^2},\frac{\partial G}{\partial S}=\frac{\gamma hV}{(1+h\varphi)},\frac{\partial G}{\partial I}=\frac{1}{(1+h\varphi)},\frac{\partial G}{\partial V}=\frac{h\gamma S}{(1+h\omega)},\frac{\partial H}{\partial S}=0,\frac{\partial H}{\partial I}=\frac{h\Lambda}{1+h\mu},\frac{\partial H}{\partial V}=\frac{1}{1+h\mu}.$

By replacing all the above derivatives in (**4.5**), we obtain

$$J=\begin{bmatrix}\frac{1}{1+h\sigma+h\gamma V} & 0 & 0\\ 0 & \frac{1}{1+h\varphi} & 0\\ 0 & \frac{h\Lambda}{1+h\mu} & \frac{1}{1+h\mu}\end{bmatrix}.$$

Putting $E_0=\left(\frac{\rho}{\sigma},0,0\right)$, we obtain

$$J=\begin{bmatrix}\frac{1}{1+h\sigma} & 0 & 0\\ 0 & \frac{1}{1+h\gamma} & 0\\ 0 & \frac{h\Lambda}{1+h\mu} & \frac{1}{1+h\mu}\end{bmatrix}.$$

To verify the eigenvalues, we consider

$|J(E_0)-\lambda I|=0,$

that is,

$$\begin{vmatrix}\frac{1}{1+h\sigma}-\lambda & 0 & 0\\ 0 & \frac{1}{1+h\gamma}-\lambda & 0\\ 0 & \frac{h\Lambda}{1+h\mu} & \frac{1}{1+h\mu}-\lambda\end{vmatrix}=0. \quad (4.6)$$

System (**4.6**) has the following characteristic equation

$$\left(\frac{1}{1+h\sigma}-\lambda\right)\left(\lambda^2+\left(\frac{1}{1+h\gamma}+\frac{1}{1+h\mu}\right)\lambda+(1-R_0)\left(\frac{1}{(1+h\mu)(1+h\gamma)}\right)\right)=0. \quad (4.7)$$

Using one of the eigenvalues from (4.7), $\lambda_1=\frac{1}{1+h\sigma}<1$ is obtained. The other two eigenvalues can be obtained from

$$\lambda^2 + \left(\frac{1}{1+h\gamma} + \frac{1}{1+h\mu}\right)\lambda + (1 - R_0)\left(\frac{1}{(1+h\mu)(1+h\gamma)}\right) = 0.$$

According to Routh Hurwitz criterion [31, 32], the roots of the above equation are less than one if $R_0 < 1$. As a result, the DFE point for the NSFD scheme is LAS.

Theorem 4.2: The EE point E^* for the discrete NSFD scheme (**4.3**) is LAS, if $R_0 > 1$.

Proof: In a manner analogous to **Theorem 4.1**, the Jacobian matrix is obtained as

$$J = \begin{bmatrix} \frac{\partial F}{\partial S} & \frac{\partial F}{\partial I} & \frac{\partial F}{\partial V} \\ \frac{\partial G}{\partial S} & \frac{\partial G}{\partial I} & \frac{\partial G}{\partial V} \\ \frac{\partial H}{\partial S} & \frac{\partial H}{\partial I} & \frac{\partial H}{\partial V} \end{bmatrix}. \tag{4.8}$$

By putting all the derivatives from **Theorem** (**4.1**), the Jacobian matrix (**4.8**) becomes

$$J = \begin{bmatrix} \frac{1}{(1+h\sigma+h\gamma V)} & 0 & \frac{(h\rho+S)h\gamma}{[(1+h\sigma+h\gamma V)]^2} \\ \frac{\gamma h V}{(1+h\varphi)} & \frac{1}{(1+h\varphi)} & \frac{h\gamma S}{(1+h\varphi)} \\ 0 & \frac{h\Lambda}{1+h\mu} & \frac{1}{1+h\mu} \end{bmatrix} \tag{4.9}$$

Furthermore, by replacing EE point E^* in matrix (**4.9**), we obtain

$$J(E^*) = \begin{bmatrix} \frac{1}{(1+h\sigma+h\gamma V^*)} & 0 & \frac{(h\rho+S^*)h\gamma}{[(1+h\sigma+h\gamma V^*)]^2} \\ \frac{\gamma h V^*}{(1+h\varphi)} & \frac{1}{(1+h\varphi)} & \frac{h\epsilon S^*}{(1+h\varphi)} \\ 0 & \frac{h\Lambda}{1+h\mu} & \frac{1}{1+h\mu} \end{bmatrix}.$$

To check the eigenvalues, we take

$$|J(E^*) - \lambda I| = 0,$$

that is,

$$\begin{vmatrix} \frac{1}{(1+h\sigma+h\gamma V^*)} - \lambda & 0 & \frac{(h\rho+S^*)h\gamma}{[(1+h\sigma+h\gamma V^*)]^2} \\ \frac{\gamma h V^*}{(1+h\varphi)} & \frac{1}{(1+h\varphi)} - \lambda & \frac{h\gamma S^*}{(1+h\varphi)} \\ 0 & \frac{h\Lambda}{1+h\mu} & \frac{1}{1+h\mu} - \lambda \end{vmatrix} = 0. \quad (4.10)$$

From (**4.10**), $\lambda_1 = \frac{1}{(1+h\sigma+h\gamma V^*)}$ is obtained. The other two eigenvalues can be obtained from

$$\lambda^2 - \lambda\left(\frac{1}{(1+h\varphi)} + \frac{1}{1+h\mu}\right) - \left(\left(\frac{(h\rho+S^*)h\gamma}{(1+h\sigma+h\gamma V^*)^2} \times \frac{h\Lambda}{1+h\mu} \times \frac{\gamma h V^*}{(1+h\varphi)}\right) + \left(\frac{h\Lambda}{1+h\mu} \times \frac{\gamma h V^*}{(1+h\varphi)}\right)\right)(R_0 - 1) = 0. \quad (4.11)$$

The Routh Hurwitz criterion [31, 32] demonstrates that the roots of equation (**4.11**) are smaller than one if $R_0 > 1$. This demonstrates that E^* for the discrete NSFD scheme (4.3) is LAS whenever $R_0 > 1$.

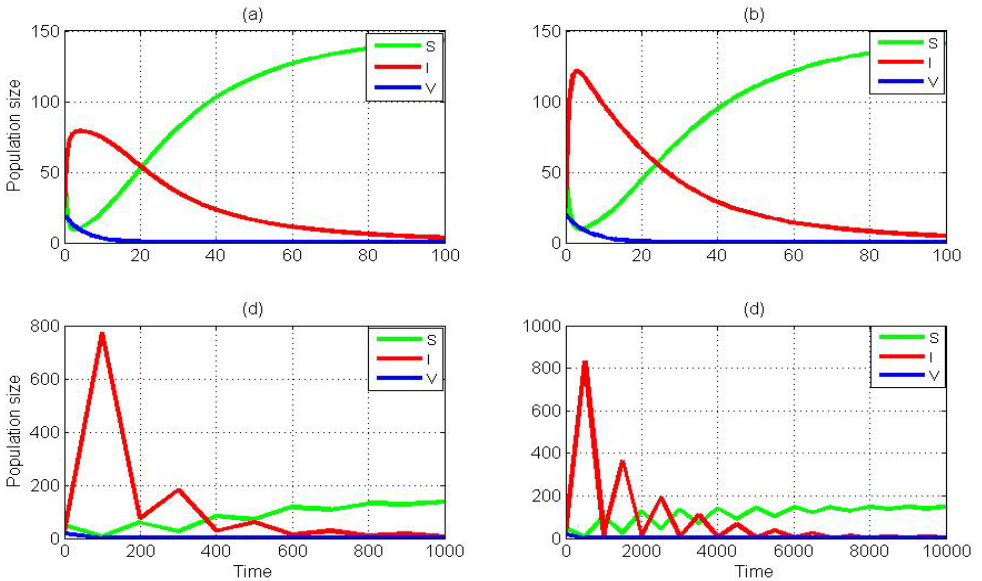

Figure 5. Graphs generated by the NSFD scheme (**4.3**) with (a) h=0.1, (b) h=1, (c) h=100 and (d) h=500. The remaining values of the parameters are offered as $\gamma = .085, \mu = 0.196, \sigma = .0667, \Lambda = .001, \varphi = 0.1$ ρ=10.

Figure 5(a-d) depicts that the NSFD scheme (**4.3**) remains stable for each step size. The SFD scheme, however, shows convergence for lower step sizes. This demonstrates that for each step size the NSFD scheme is positive forever and unconditionally convergent.

5. CONCLUSION

The basic disease model for HBV has been proposed and examined in the current paper. For the proposed epidemic system, the equilibria and threshold quantity R_0 have been determined. In order to verify the convergence and divergence of the DFE and EE points, various numerical approaches have been employed. It has been demonstrated that RK-4 and Euler schemes depend on step sizes and are conditionally convergent which makes them ineffective. On the other hand, the NSFD approach developed for the current model is not step size dependent. This shows that the NSFD scheme is incredibly effective in comparison to the notable Euler and RK-4 numerical schemes. This scheme is a simple technique that demonstrates how discrete and continuous models behave appropriately and provide mathematically accurate results. By employing it, the spread of HBV epidemic diseases can be monitored effectively. The findings presented in this paper are beneficial to humanity in the field of medicine and can be applied also as a useful tool to predict the appearance of HBV epidemic disease. Each section includes numerical simulations to validate the theoretical findings.

REFERENCES

1. Kamyad AV, Akbari R, Heydari AA, Heydari A. Mathematical modeling of transmission dynamics and optimal control of vaccination and treatment for Hepatitis B virus. *Comput Math Methods Med*. 2014;2014:e475451. https://doi.org /10.1155/2014/475451
2. Gentile I, Borgia G. Vertical transmission of Hepatitis B virus: Challenges and solutions. *Int J Women's Health*. 2014;6:605–611. http://dx.doi.org/10.2147/IJWH.S51138
3. Sirilert S, Traisrisilp K, Sirivatanapa P, Tongsong T. Pregnancy outcomes among chronic carriers of Hepatitis B virus. *Int J Gynaecol Obstet*. 2014;126(2):106–110. https://doi.org/10.1016/j.ijgo.2014.02.019
4. World Health Organization. Prevention and control of viral hepatitis infection: Framework for global action. No. WHO/HSE/PED/HIP/GHP

2012.1. World Health Organization. https://apps.who.int/iris/handle/10665/130012. 2012.
5. Zou L, Zhang W, Ruan S. (2010). Modeling the transmission dynamics and control of Hepatitis B virus in China. *J Theor Biol*. 2010;262(2):330–338. https://doi.org/10.1016/j.jtbi.2009.09.035
6. Zeuzem S, Schmidt JM, Lee J, Ruster B, Roth WK. Effect of interferon alfa on the dynamics of Hepatitis C virus turnover in vivo. *Hepatology*. 1996;23(2):366–371. https://doi.org/10.1002/hep.51023025
7. Nowak MA, Bangham CR. Population dynamics of immune responses to persistent viruses. *Science*. 1996;272(5258):74–79. https://doi.org/10.1126/science.272.5258.74
8. Khan A, Hussain G, Zahri M, Zaman G, Humphries UW. A stochastic SACR epidemic model for HBV transmission. *J Biol Dyn*. 2020;14(1):788–801. https://doi.org/10.1080/17513758.2020.1833993
9. Nakata Y, Kuniya T. Global dynamics of a class of SEIRS epidemic models in a periodic environment. *J Math Anal Appl*. 2010;363(1):230–237. https://doi.org/10.1016/j.jmaa.2009. 08.027
10. Hethcote HW. The mathematics of infectious diseases. *SIAM Rev Soc Ind Appl Math*. 2000;42(4):599–653. https://doi.org/10.1137/S0036144500371907.
11. Aja RO, Omale D. Stability analysis of the transmission dynamics of Hepatitis B virus infection with controls in a population. *Int J Adv Math*. 2018;2018(6):52–63.
12. Iqbal MS, Yasin MW, Ahmed N, Akgül A, Rafiq M, Raza A. Numerical simulations of nonlinear stochastic Newell-Whitehead-Segel equation and its measurable properties. *J Comput Appl Math*. 2023;418:e114618. https://doi.org/10.1016/j.cam.2022.114618
13. Bilal S, Shah IA, Akgül A, Tekin MT, Botmart T, Yahia IS. A comprehensive mathematical structuring of magnetically effected Sutterby fluid flow immersed in dually stratified medium under boundary layer approximations over a linearly stretched surface. *Alexandria Eng J.* 2022;61(12):11889–11898. https://doi.org/10.1016/j.aej.2022.05.044
14. Qureshi ZA, Bilal S, Khan U, et al. Mathematical analysis about influence of Lorentz force and interfacial nano layers on nanofluids flow through orthogonal porous surfaces with injection of SWCNTs. *Alexandria Eng J*. 2022;61(12):12925–12941. https://doi.org/10.1016/j.aej.2022.07.010

15. Shah IA, Bilal S, Akgül A, et al. On analysis of magnetized viscous fluid flow in permeable channel with single wall carbon nano tubes dispersion by executing nano-layer approach. *Alexandria Eng J*. 2022;61(12):11737–11751. https://doi.org/10.1016/j.aej.2022.05.037
16. Modanli M, Göktepe E, Akgül A, Alsallami SA, Khalil EM. Two approximation methods for fractional order Pseudo-Parabolic differential equations. *Alexandria Eng J*. 2022;61(12):10333–10339. https://doi.org/10.1016/j.aej.2022. 03.061
17. Farman M, Akgül A, Tekin MT, et al. Fractal fractional-order derivative for HIV/AIDS model with Mittag-Leffler kernel. *Alexandria Eng J*. 2022;61(12):10965–10980. https://doi.org/ 10.1016/j.aej.2022.04.030
18. Attia N, Akgül A, Seba D, Nour A, Asad J. A novel method for fractal-fractional differential equations. *Alexandria Eng J*. 2022;61(12):9733–9748. https://doi.org/10.1016/j.aej.2022.02.004
19. Xu C, Farman M, Hasan A, et al. Lyapunov stability and wave analysis of Covid-19 omicron variant of real data with fractional operator. *Alexandria Eng J*. 2022;61(12):11787–11802. https://doi.org/10.1016/ j.aej.2022.05.025
20. Zhao S, Xu Z, Lu Y. A mathematical model of Hepatitis B virus transmission and its application for vaccination strategy in China. *Int J Epidemiol*. 2000;29(4):744–752. https://doi.org/10.1093/ije/29.4.744
21. Gupta E, Bajpai M, Sharma P, Shah A, Sarin SK. Unsafe injection practices: A potential weapon for the outbreak of blood borne viruses in the community. *Ann Med Health Sci Res*. 2013;3(2):177–181. https://doi.org/10.4103/2141-9248.113657
22. Kabir KA, Kuga K, Tanimoto J. Analysis of SIR epidemic model with information spreading of awareness. *Chaos Solitons Fractals*. 2019;119:118–125. https://doi.org/10.1016/j.chaos.2018.12.017
23. Blumberg BS. *Hepatitis B: The Hunt for a Killer Virus*. United States of America: Princeton University Press; 2002. https://doi.org/10.1086/376070
24. McLean AR, Blumberg BS. Modelling the impact of mass vaccination against hepatitis B. I. Model formulation and parameter estimation. *Biol Sci.* 1994;256(1345):7–15. https://doi.org/10.1098/rspb.1994.0042
25. Khatun Z, Islam MS, Ghosh U. Mathematical modeling of Hepatitis B virus infection incorporating immune responses. *Sensors Int*. 2020;1:e100017. https://doi.org/10.1016/j.sintl.2020.100017

26. Van den Driessche P, Watmough J. Reproduction numbers and sub-threshold endemic equilibria for compartmental models of disease transmission. *Math Biosci*. 2002;180(1-2):29–48. https://doi.org/10.1016/S0025-5564(02)00108-6
27. Mickens RE. Calculation of denominator functions for nonstandard finite difference schemes for differential equations satisfying a positivity condition. *Numer Methods Partial Differ Equ*. 2007;23(3):672–691. https://doi.org/10.1002/num.20198
28. Lambert JD. *Numerical methods for ordinary differential systems: The initial value problem*. New York: John Wiley & Sons, Inc; 1991.
29. Mickens RE. *Nonstandard finite difference models of differential equations*. World Scientific Publishing; 1993.
30. Shokri A, Khalsaraei MM, Molayi M. Nonstandard dynamically consistent numerical methods for MSEIR Model. *J Appl Comput Mech*. 2022;8(1):196–205. https://doi.org/10.22055/jacm.2021.36545.2863
31. Ucakan Y, Gulen S, Koklu K. Analysing of tuberculosis in Turkey through SIR, SEIR and BSEIR Mathematical Models. *Math Comput Model Dyn Syst*. 2021;27(1):179–202. https://doi.org/10.1080/13873954.2021. 1881560
32. Khan MA, Badshah Q, Islam S, Khan I, Shafie S, Khan SA. Global dynamics of SEIRS epidemic model with non-linear generalized incidences and preventive vaccination. *Adv Differ Equ*. 2015:e88. https://doi.org/10. 1186/s13662-015-0429-3

Scientific Inquiry and Review (SIR)
Volume 7 Issue 1, 2023
ISSN (P): 2521-2427, ISSN (E): 2521-2435
Homepage: https://journals.umt.edu.pk/index.php/SIR

Article QR

Title:	**Image Registration using the Rigid Group**
Author (s):	Muhammad Yousuf Tufail, Saima Gul
Affiliation (s):	NED University of Engineering & Technology, Karachi, Pakistan
DOI:	https://doi.org/10.32350/sir.71.05
History:	Received: November 22, 2022, Revised: February 7, 2023, Accepted: February 7, 2023, Published: March 15, 2023
Citation:	Tufail MY, Gul S. Image registration using the rigid group. *Sci Inq Rev.* 2023;7(1):71–86. https://doi.org/10.32350/sir.71.05
Copyright:	© The Authors
Licensing:	This article is open access and is distributed under the terms of Creative Commons Attribution 4.0 International License
Conflict of Interest:	Author(s) declared no conflict of interest

A publication of
The School of Science
University of Management and Technology, Lahore, Pakistan

Image Registration using the Rigid Group

Muhammad Yousuf Tufail*, and Saima Gul

NED University of Engineering and Technology, Karachi, Pakistan

Abstract

Image registration is the process of approximate matching of the source image to the target so that they resemble each other. In this study, two-dimensional image registration is presented using the rigid group. This group is a finite dimensional group (four-dimensional in this case) under composition. The dimensions of the rigid group are scaling, rotation, and translations along the axes. In this paper, an algorithm for the construction of rigid transformation is presented using the discretized objective function. This objective function is based on SSD (sum of the squares of the distances between the pixels intensities) and calculates the discrepancy between the images. The coarse search and the gradient descent approaches have been used for the optimization. The proposed algorithm is implemented on variety of images. The numerical examples illustrate the ability of the proposed algorithm.

Keywords: algorithms, coarse search, image registration, optimization, rigid group.

1. INTRODUCTION

Image registration is the process of the approximate matching of the source image to the target so that their appearances resemble each other. The pioneer work of D'Arcy Thompson remains the original inspiration in the field of image registration. In his famous book *On Growth and form* [1, 2], which was first published in 1917 and then re-published in 1942, he presented the idea of image transformation between species. Some of the images and their relative transformations that he referred in his book motivated the current authors to further explore finite dimensional group, which is the scope of this paper. Although there have been many developments in image registration since 1942, still the most remarkable and influential approach is to find a diffeomorphism between the two images using a method known as "Large Deformation Diffeomorphic Metric Mapping (LDDMM)" [3–7].

* Corresponding Author: tufail@neduet.edu.pk

Lisa Gottesfeld Brown published the first comprehensive review of image registration in 1992 [8]. Brown highlighted the various requirements of image registration namely (i) a feature space (contains information about the images), (ii) a search space (consists of a set of transformations), (iii) a search strategy (selection of transformations to get an optimal solution), and (iv) a similarity metric (to measure the discrepancy between the images). Brown suggested only three lists of transformations (all were finite) including (a) affine transformation (shearing, aspect ratio, and rigid), (b) perspective transformation (a transformation that maps 3D to 2D), and (c) polynomial transformation (suitable when minor information regarding camera geometry is available [2, 9]). The basic steps in image registration still remain the same. However, the choice of transformations has evolved drastically. The full set of diffeomorphisms, that is, non-rigid registration using infinite dimensional group is an integral part of image registration and widely applied in medical imaging [6–7, 10].

Several methods for image deformation have been developed and applied to the distinct fields of mathematics and computer science since 1992. These methods include artificial intelligence[11], image encryption [12], graph theory, [13] and many more [14–26]. The adoption of diffeomorphic image registration has caused a revolutionary and significant change in the field. Diffeomorphisms refer to those smooth functions whose inverse are also smooth [2, 9, 27].

In this paper, image registration is presented using the group of rigid diffeomorphisms. Two-dimensional grey scale images [2, 9] have been used to conduct the experiments. Image registration is subject to the optimal solution of the current study's objective function which is defined in **Eq. (2.2)**. This equation demonstrates how close the images are. This objective function is based on **SSD** (sum of the squares of the distances between the pixels intensities). For more details, see equation (2.9) in Section 2.2 in [2]).

2. RIGID GROUP AND IMAGE REGISTRATION

The rigid group of diffeomorphisms is one of the most common group which is extensively used in image registration. It has been studied extensively over the past several decades, both for medical and non-medical applications [28–33]. This group consists of uniform scaling, rotations, and arbitrary translations along the axes [8, 19, 34–36]. Let us first present each of these separately.

2.1. Rotation

Suppose an arbitrary point $\begin{pmatrix} X \\ Y \end{pmatrix}$ in $\mathbb{R}^2$. Let $\zeta \in [0,2\pi[$ be the angle of rotation, then the rotation transformation ψ_1 to generate a new point $\begin{pmatrix} X' \\ Y' \end{pmatrix}$ in $\mathbb{R}^2$ is defined as

$$\begin{pmatrix} X' \\ Y' \end{pmatrix} = \psi_1 \begin{pmatrix} X \\ Y \end{pmatrix} = \begin{pmatrix} \cos\zeta & -\sin\zeta \\ \sin\zeta & \cos\zeta \end{pmatrix} \begin{pmatrix} X \\ Y \end{pmatrix}.$$

2.2. Scaling

Suppose $\gamma \in \mathbb{R}^+$, then the scaling transformation ψ_2 over $\begin{pmatrix} X \\ Y \end{pmatrix}$ is represented below as

$$\begin{pmatrix} X' \\ Y' \end{pmatrix} = \psi_2 \begin{pmatrix} X \\ Y \end{pmatrix} = \gamma \begin{pmatrix} X \\ Y \end{pmatrix}.$$

2.3. Translation along the Axes

Suppose $tr_x, tr_y \in \mathbb{R}$ are the translations along the x-axis and y-axis respectively. The translation transformation ψ_3 over $\begin{pmatrix} X \\ Y \end{pmatrix}$ is defined below as

$$\begin{pmatrix} X' \\ Y' \end{pmatrix} = \psi_3 \begin{pmatrix} X \\ Y \end{pmatrix} = \begin{pmatrix} X + tr_x \\ Y + tr_y \end{pmatrix}.$$

The diffeomorphims group generated by the composition of scaling, rotation, and translations along the axes is termed as the rigid group. See **Proposition 2.1** for more details. The composition of individual transformations yields $\begin{pmatrix} X' \\ Y' \end{pmatrix} = \psi\left(\begin{pmatrix} X \\ Y \end{pmatrix}\right)$, where $\psi = \psi_3 \circ \psi_2 \circ \psi_1$

$$\begin{pmatrix} X' \\ Y' \end{pmatrix} = \gamma \begin{pmatrix} \cos\zeta & -\sin\zeta \\ \sin\zeta & \cos\zeta \end{pmatrix} \begin{pmatrix} X \\ Y \end{pmatrix} + \begin{pmatrix} tr_x \\ tr_y \end{pmatrix}, \zeta \in [0,2\pi[, 0 \neq \gamma \in \mathbb{R}^+.$$

The formula to represent the inverse rigid diffeomorphism is defined as

$$\begin{pmatrix} X \\ Y \end{pmatrix} = \frac{1}{\gamma}\begin{pmatrix} \cos\zeta & -\sin\zeta \\ \sin\zeta & \cos\zeta \end{pmatrix}^{-1}\left\{\begin{pmatrix} X' \\ Y' \end{pmatrix} - \begin{pmatrix} tr_x \\ tr_y \end{pmatrix}\right\}, \zeta \in [0,2\pi[, 0 \neq \gamma \in \mathbb{R}^+$$

$$= \frac{1}{\gamma}\begin{pmatrix} \cos\zeta & \sin\zeta \\ -\sin\zeta & \cos\zeta \end{pmatrix}\left\{\begin{pmatrix} X' \\ Y' \end{pmatrix} - \begin{pmatrix} tr_x \\ tr_y \end{pmatrix}\right\}, \zeta \in [0,2\pi[, 0 \neq \gamma \in \mathbb{R}^+.$$

Proposition 2.1. The existence of the composition of rigid diffeomorphisms in the domain $\Omega \subset \mathbb{R}^2$ implies the following fact:

$$(\psi_1 \circ \psi_2) \cdot \big(I(\boldsymbol{x})\big) = \psi_1 \cdot \big(\psi_2 . I(\boldsymbol{x})\big), \forall \psi_1, \psi_2 \in \mathrm{rig}(\Omega, \mathbb{R}^2).$$

Here, '.' denotes the action of ψ over the image I, $\circ$ indicates the composition, see Section 1.2.4 in [2], and the set of rigid diffeomorphisms is represented with rig $(\Omega, \mathbb{R}^2)$.

Proof: Suppose ψ_1 and ψ_2 are rigid diffeomorphisms in Ω such that their composition $\psi_1 \circ \psi_2$ is also a diffeomorphism in Ω, then

$$\begin{aligned}
(\psi_1 \circ \psi_2) \cdot I(\mathbf{x}) &= I((\psi_1 \circ \psi_2)^{-1}(\mathbf{x})) \\
&= I\big((\psi_2^{-1} \circ \psi_1^{-1})(\mathbf{x})\big) \\
&= I(\psi_2^{-1}(\mathbf{x}) \circ \psi_1^{-1}(\mathbf{x})) \\
&= I \circ \psi_2^{-1}(\mathbf{x}) \circ \psi_1^{-1}(\mathbf{x}) \\
&= (I \circ \psi_2^{-1}(\mathbf{x})) \circ \psi_1^{-1}(\mathbf{x}) \\
&= (\psi_2 \cdot I(\mathbf{x})) \circ \psi_1^{-1}(\mathbf{x}) \\
&= \psi_1 \cdot \big(\psi_2 \cdot I(\mathbf{x})\big)
\end{aligned}$$

Definition 2.1. Suppose I_1 and I_2 are two greyscale images. The discrepancy between the images is computed with the following matching functional or objective function

$$M(\psi) = \int_\Omega \{(I_1 \circ \psi^{-1})(\boldsymbol{x}) - I_2(\boldsymbol{x})\}^2 dxdy, \boldsymbol{x} = (X, Y)^T \in \Omega \subset \mathbb{R}^2 \quad (2.1)$$

where ψ represents an element from the rigid group (See Section 2). Then, the process of finding an optimal ψ that minimizes **Eq. (2.1)** is termed as a rigid registration. It is clear that **Eq. (2.1)** is the continuous version of the objective function. As far as numerical computation is concerned, the continuous form is discretized. Suppose we define our discrete domain $\mathbb{D}$. This domain serves as the discrete domain for all the images presented in this paper. Suppose M is a positive integer and $\mathbb{D} = \{([0, M - \alpha]/(M -$

$\alpha) - 0.5) \times ([0, M - \alpha]/(M - \alpha) - 0.5); \alpha = 1\}$ is a uniform square grid that contains M^2 grid points, a simple example by setting $M = 100$ is shown in Figure 1. Consider $M = 100$ for all the numerical examples in this paper. The discrete form of the objective function (defined in **Eq. (2.1)**) is

$$M(\psi) = \sum_{i=1}^{M} \sum_{j=1}^{M} \left((I_1 \circ \psi^{-1})(y_{ij}) - I_2(y_{ij}) \right)^2. \qquad (2.2)$$

Here, y_{ij} indicates the value of the image at position (i, j) in the image matrix.

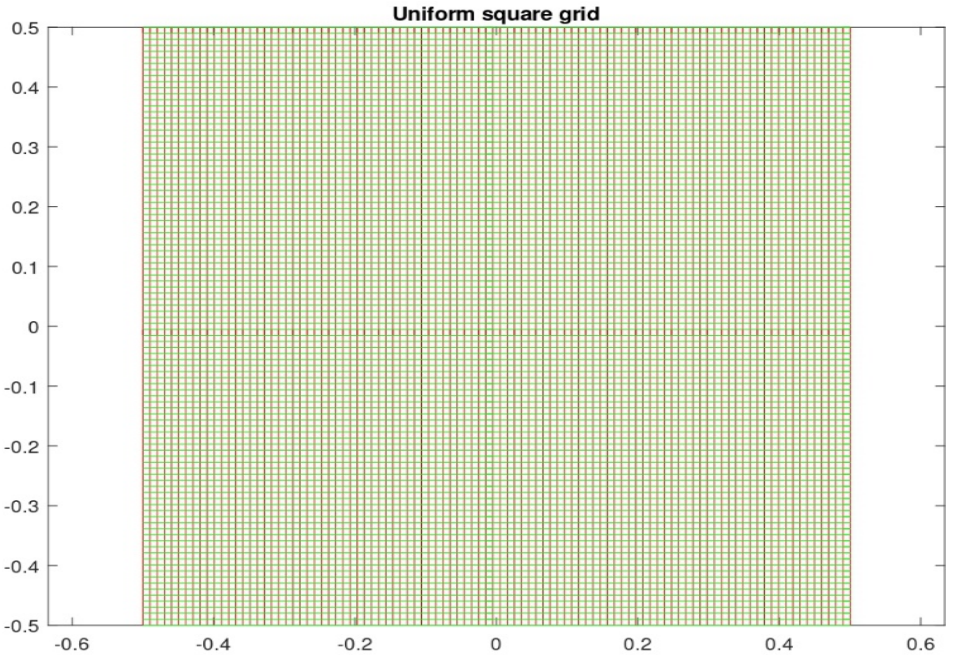

Figure 1. A Total of 10,000 Points for a Square Grid are Given. The range for Data Points is $\left\{[-\beta, \eta] \times [-\beta, \eta]; \beta = \eta = \frac{1}{2}\right\}$, with 100 Grid Points per Side, i.e., $M = 100$.

Moreover, the values of I_1 are defined over the uniform grid points, i.e., at y_{ij} and not at $\psi^{-1}(y_{ij})$. Furthermore, it must be noticed that the domain of $I_1 \circ \psi^{-1}$ is not Ω, instead it is $\psi(\Omega)$ at the continuous level. It is highly likely (for some points) that $I_1 \circ \psi^{-1}$ move outside Ω in the registration. Thus, Ω is a restricted subset of R^2. As far as computation is concerned, the

following values for $I_1 \circ \psi^{-1}(y_{ij})$ are used.

1. If $\psi^{-1}(y_{ij}) \in \Omega$, bilinear interpolation (Section 2.1.2 in [2]) is used by using the values of I_1 corresponding to four neighboring edges of a square that contains $\psi^{-1}(y_{ij})$.
2. If $\psi^{-1}(y_{ij}) \notin \Omega$,, a constant background value (0 for a black background in **Example 4.1** and 1 for a white background in **Examples 4.2** and **4.3**) is set.

The central goal for the registration is to minimize $M(\psi)$ for $\psi \in G$. In this paper, two methods are used for optimization namely (i) the method of coarse search (that surveys the whole discretized domain for all the parameters, four in our case), and (ii) the *trust- region-reflective* method.

The latter method is used when researchers encounter the non-linear least squares problem and it yields a local optimal solution. The trust-region-reflective algorithms have been used through MatLab, see example 4.3 .

Eq. (**2.2**) denotes the general form of the least-squares optimisation (based on SSD) function for any choice of planar transformation group (i.e., G is a Lie group that acts on the plane [37], G is the rigid group for this study). This is a numerical optimization problem. Optimization is a huge field with many known algorithms [9, 38–40] whose applicability depends on the nature of the objective function. The purpose here is not to survey this field but to demonstrate some simple applications.

3. COARSE SEARCH

In this method, firstly, the domain for the matching functional is defined. This matching functional is computed for several points $\psi \in G$, see **Algorithm 4.1** for further details. This algorithm contains four nested loops, that is, the parameters of the rigid group. The values of individual parameters are set as $M_\zeta = 21, M_\gamma = 13, M_x = 11, \text{and } M_y = 11$. The total search for optimal solution (minimization in this case) is the product of all four nested loops, that is, a total of 33,033 computations for the objective function.

4. EXPERIMENTS

In this section, the implementation of **Algorithm 4.1** over synthetic data is presented. In synthetic data, the target is generated (by using known rigid transformation) from the source. Three examples are presented in which

the first example involves a pair of smooth images, whereas the other two examples are related to the registration of non-smooth images.

Example 4.1 (pair of smooth images). In this first warm-up example, 2D Gaussian blob (an example of smooth image) is considered for image registration. The Gaussian function is considered as the source of image registration. A rigid transformation, with the parameters values $\zeta = \mathrm{pi}/2, \gamma = 0.8, \mathrm{tr}_x = 0.2$ and $\mathrm{tr}_y = 0.4$, are used to generate the target. **Algorithm 4.1** yields the optimized set of parameters whose values are $\zeta_{\mathrm{opt}} = \pi/2, \gamma_{\mathrm{opt}} = 0.8, \mathrm{t}_{x_{\mathrm{opt}}} = 0.2$ and $\mathrm{t}_{y_{\mathrm{opt}}} = 0.4$. These optimised parameters are used to transform the source with a rigid transformation. The transformed source is then subtracted from the target. By doing this, attention is drawn toward the fact that how good the images are aligned (transformed source and the target). Midgrey pixels indicate a perfect match,[1] whereas the evidence of mismatch appears as black (pixel value is ≈ 0) or white (pixel value is ≈ 1). Figure 2 displays the results of registration. An excellent registration is obtained (as expected). The optimal solution is highlighted with a red circle in the bottom part of Figure 2.

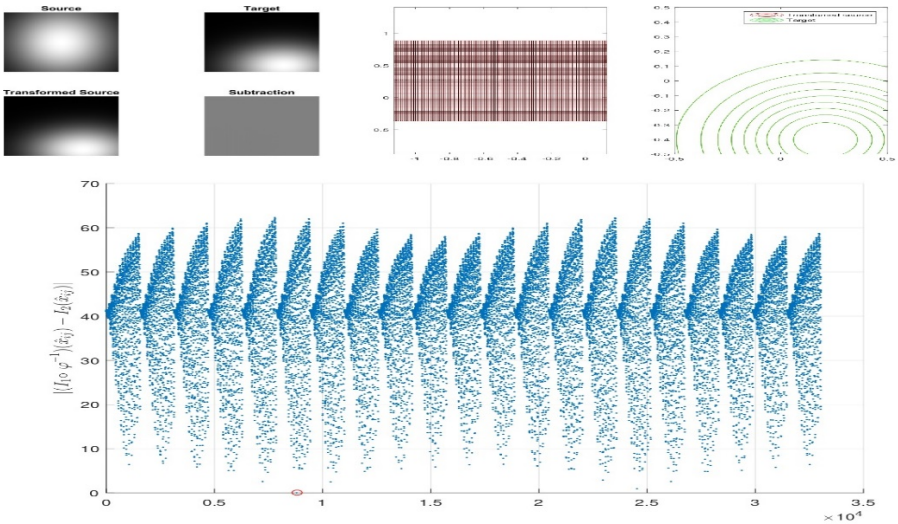

Figure.2. Image Registration is Given for **Example 4.1.** Top: Left: Source

[1] Perfect match here and elsewhere means good visual registration, i.e., there is no mismatch (apparently) between the transformed source and the target; and evidence of midgrey pixels screen when the transformed source is subtracted from its corresponding target.

(the Gaussian $\exp(-5x^2 - 3y^2)$), Target, Deformed Source, and Difference Image $\big((I_1 \circ \psi^{-1} - I_2 + 1)/2\big)$, Uniform Mid Grey Confirms that Perfect Registration between the Images is Obtained; Right: Rigid Diffeomorphism ψ^{-1} Applied to the Target Grid with the Comparison of Contour Plots of $I_1 \circ \psi^{-1}$ (the Transformed Source) and I_2 (the Target). The contour plots Have Been Made by Plotting Green Contours on Top of Red Contours. No Red Line Can Be Seen Due to Perfect Registration. Bottom: The Registration Errors Are Given. The Optimal Solution Is Identified as A Red Circle.

Example 4.2 (**pair of non-smooth images).** Image registration for non-smooth images is always challenging [9]. Consider the pair of non-smooth images. Alike the previous example, again the synthetic data is considered, that is, $\zeta = \mathrm{pi}/2, \gamma = 1.1, \mathrm{tr_x} = -0.2$, and $\mathrm{tr_y} = 0.1$ are set as the initial parameters for the known rigid transformation. The implementation of **Algorithm 4.1** produces optimized parameters that are $\zeta_{\mathrm{opt}} = \frac{\pi}{2}, \gamma_{\mathrm{opt}} = 1.1, \mathrm{t_{x_{opt}}} = -0.2$, and $\mathrm{t_{y_{opt}}} = 0.1$. After obtaining these optimized parameters, the source is transformed by following the same steps as in the **Example 4.1**. The results of image registration are given in Figure 3. Alike the previous example, a perfect registration is obtained.

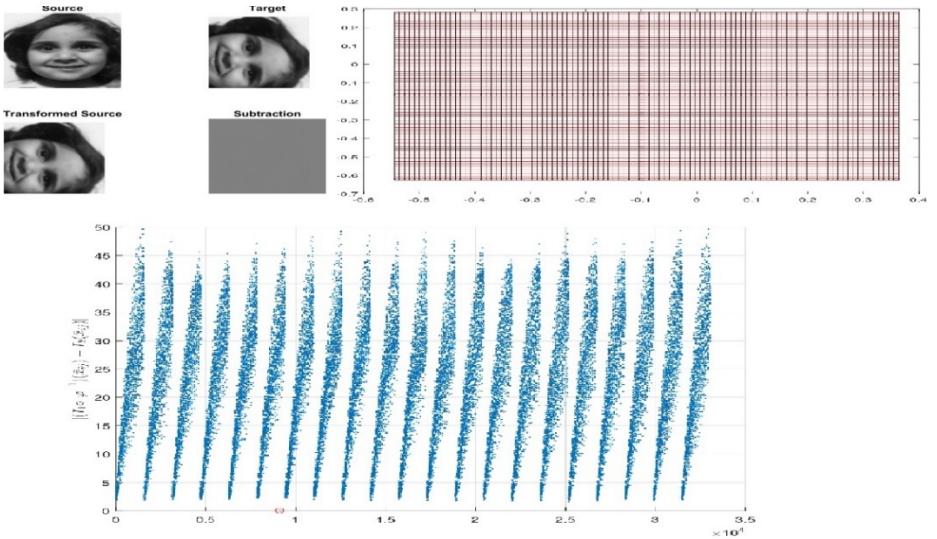

Figure 3. Implementation of **Algorithm 4.1** Over A Pair of Nonsmooth Images Used for **Example 4.2**.

Example 4.3 (pair of non-smooth images). Now consider a slightly harder example in which the target is generated from the source with the help of rigid transformation. The values $\zeta = 1.6, \gamma = 1.25, \text{tr}_x = -0.27$ and $\text{tr}_y = 0.13$ are set as parameter values for rigid transformation. Resultantly, **Algorithm 4.1** produced $\zeta_{opt} = \pi/2, \gamma_{opt} = 1.2, t_{x_{opt}} = -0.3$ and $t_{y_{opt}} = 0.1$ as optimized parameters. These parameter values are noticeably different from those values of parameters that were used to construct the target. The reason for discrepancy (in values) is due to the fact that the set of allowable values for the parameters in coarse search do not contain the exact values of the parameters that were used to generate the target. Thus, Figure 4 displays adequate but not perfect registration.

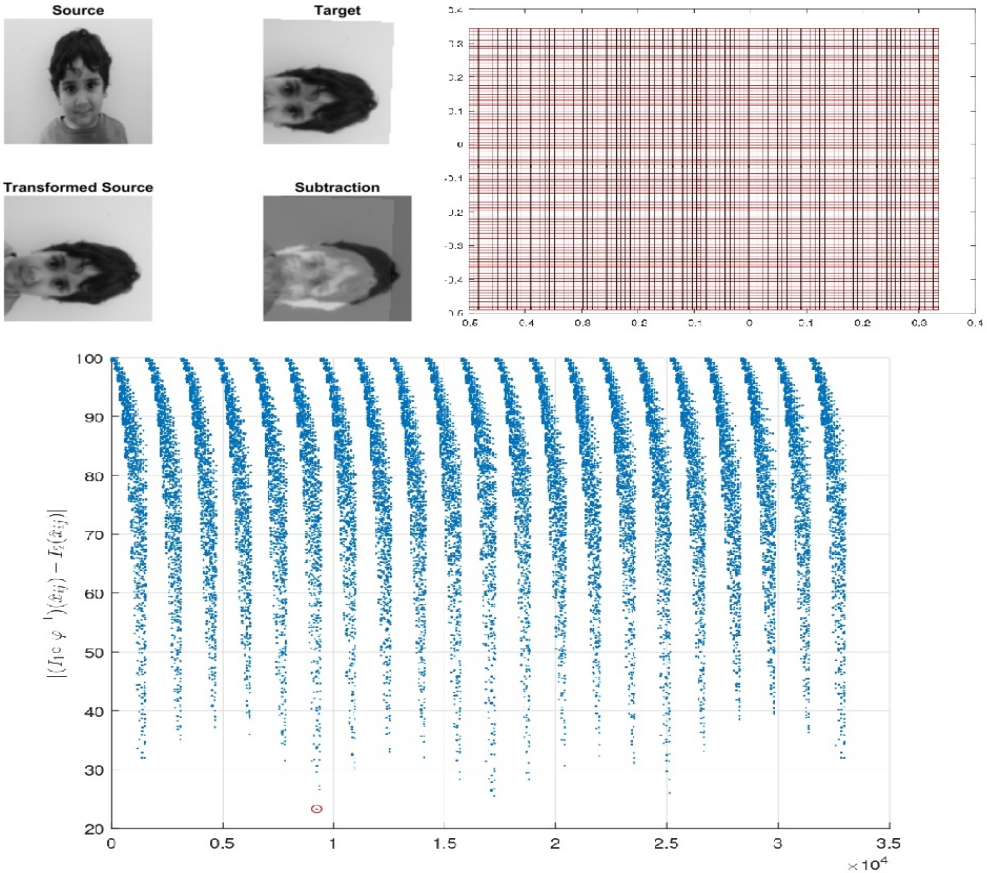

Figure 4. Result of Image Registration Using **Algorithm 4.1** for **Example 4.3**.

MatLab based optimizer **lsqnonlin** is used for the current non-linear problem. This optimizer is used for the (typical) least squares functions for optimization [2, 41].

lsqnonlin requires an initial guess for optimization. For this purpose, the above optimized parameters that were obtained at the first step of optimization (the coarse search), that is, $\zeta_{\text{ini}} = \pi/2, \gamma_{\text{ini}} = 1.2, \mathrm{t}_{\mathrm{x}_{\text{ini}}} = -0.3$, and $\mathrm{t}_{\mathrm{y}_{\text{ini}}} = 0.1$ were chosen as an initial guess. The optimizer yields a global minimum and the corresponding values of the parameters are $\zeta_{\text{opt}} = 1.6, \gamma_{\text{opt}} = 1.25, \mathrm{t}_{\mathrm{x}_{\text{opt}}} = -0.27$, and $\mathrm{t}_{\mathrm{y}_{\text{opt}}} = 0.13$. Figure 5 confirms a perfect registration.

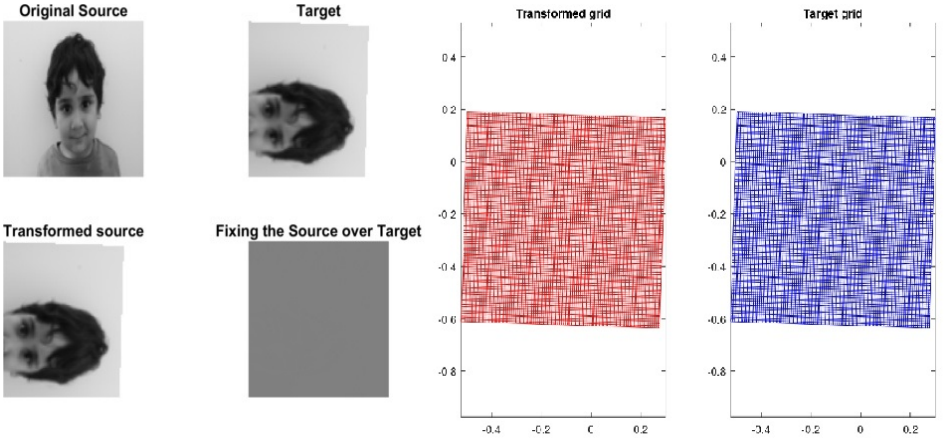

Figure 5. Results of Image Registration for **Example 4. 3** Using Lsqnonlin. Top Row: Pair of Relevant Images for the Registration. Second Row: The Transformed Source ($I_1 \circ \psi^{-1}$) And the Subtraction Between the Transformed Source and The Target. Bottom Row: The Transformed Grid and The Target Grid. These Identical Grids Indicate the Perfect Registration Between the Source and The Target.

Algorithm 4.1. Minimization of **Eq.** (**2.2**) using Coarse Search

Input : Source I_1 and target I_2

output: Warp ψ^{-1} along with the transformed image $I_1 \circ \psi^{-1}$

for $\zeta = 0{:}\,\pi/10{:}\,2\pi$ do

for $\gamma = 0.1{:}\,0.1{:}\,1.3$ do

for $tr_x = -0.5{:}\,0.1{:}\,0.5$ do

for $tr_y == -0.5{:}\,0.1{:}\,0.5$ do

Computation of deformation of source using bi-linear interpolation,

$I_1 \circ \psi^{-1}(x_{ij}) \forall y_{ij} \in S$

Compute $d = \|I_1 \circ \tilde{\psi}^{-1}(x_{ij}) - I_2(x_{ij})\|^2 \forall y_{ij} \in S$

Compute $\psi^{-1} = \tilde{\psi}^{-1}$ for the optimal solution of d,

final deformation of source: $I_1 \circ \psi^{-1}$

5. Conclusion

In this research, an algorithm for the construction of rigid diffeomorphisms has been presented. This algorithm gives an optimal solution for the objective function which calculates the discrepancy between the images (see **Eq. (2.2)**). It worked very well for the selected examples and found the optimal solution for perfect match. However, there is a deficiency in the algorithm that it gets stuck on the local minimum for some examples (not reported here). Due to this deficiency, the current authors were unable to find a perfect match (see Example 4.3). Thus, other optimization techniques are also needed to overcome this deficiency. Gradient descent (there are few more, see [42, 43]) is one of the approaches and used in **Example 4.3**.

The major benefit of the proposed algorithm is that (as it is based on coarse search) it surveys the whole domain and provides a good initial guess for more sophisticated optimization. Apparently, this method is very simple but it is always recommended to search for each parameter (over a relatively small number of values)in the whole domain. In light of modern research on optimization, it is worthy to implement coarse search because (i) it is worthless to compute the derivative at the first step (function might not be differentiable) and (ii) function might have several local minima scattered all over the domain. It becomes nearly impossible for the derivative-based optimization method (such as steepest descent) to find the global minimum. In this situation, the method of coarse search is the best option to get a better initial guess (possibly very near to the global minimum, see **Example 4.3**) in order to find the desired optimal solution for the perfect match.

REFERENCES

[1] Thompson DW. *On growth and form*. Cambridge university press; 1942.

[2] Tufail MY. *Image registration under conformal diffeomorphisms* [doctoral dissertation]. Massey university, Palmerston north, New Zealand; 2017. https://mro.massey.ac.nz/handle/10179/12459

[3] Beg MF, Miller MI, Trouvé A, Younes L. Computing large deformation metric mappings via geodesic flows of diffeomorphisms. *Int J Comput Vis*. 2005;61(2):139–57. https://doi.org/10.1023/b:visi.0000043755.93987.aa

[4] Cao Y, Miller MI, Winslow RL, Younes L. Large deformation diffeomorphic metric mapping of vector fields. *IEEE Transac Med Imag*. 2005;24(9):1216–30. https://doi.org/10.1109/tmi.2005.853923

[5] Glaunès J, Qiu A, Miller MI, Younes L. Large deformation diffeomorphic metric curve mapping. *Int J Comput Vis*. 2008;80(3):317–36. https://doi.org/10.1007/s11263-008-0141-9

[6] Grenander U, Miller MI. Computational anatomy: An emerging discipline. *Quart Appl Math*. 1998;56(4):617–94. https://doi.org/10.1090/qam/1668732

[7] Joshi SC, Miller MI. Landmark matching via large deformation diffeomorphisms. *IEEE Transac Image Proc*. 2000;9(8):1357–1370. https://doi.org/10.1109/83.855431

[8] Brown LG. A survey of image registration techniques. *ACM Comput Surv.* 1992;24(4):325–376. https://doi.org/10.1145/146370.146374

[9] Marsland S, McLachlan RI, Tufail MY. Conformal image registration based on constrained optimization. *NZIAM J*. 2020;62(3):235–55. https://doi.org/10.1017/s144618112000022x

[10] Smith SM, Jenkinson M, Woolrich MW, et al. Advances in functional and structural MR image analysis and implementation as FSL. *Neuroimage*. 2004;23:S208-S219. https://doi.org/10.1016/j.neuroimage.2004.07.051

[11] Ullah W, Siddique I, Zulqarnain RM, Alam MM, Ahmad I, Raza UA. Classification of arrhythmia in heartbeat detection using deep learning.

Comput Intell Neurosci. 2021;2021:e2195922. https://doi.org/10.1155/2021/2195922

[12] Asif M, Mairaj S, Saeed Z, Ashraf MU, Jambi K, Zulqarnain RM. A novel image encryption technique based on mobius transformation. *Comput Intell Neurosci*. 2021;2021:e1912859. https://doi.org/10.1155/2021/1912859

[13] Dayan F, Javaid M, Zulqarnain M, Ali MT, Ahmad B. Computing banhatti Indices of hexagonal, honeycomb and derived networks. *American J Math Comput Model*. 2018;3(2):38–45. https://doi.org/10.11648/j.ajmcm.20180302.11

[14] Grzeszczuk R. An Approach to classifying data with highly localized unmarked features using neural networks. *Comput Sci*. 2019;20:329–42. https://doi.org/10.7494/csci.2019.20.3.3343

[15] Gupta A. Current research opportunities for image processing and computer vision. *Computer Science*. 2019;20(4):387–410. https://doi.org/10.7494/csci.2019.20.4.3163

[16] Dabbour AA, Habib R, Saii M. Object pose estimation in monocular image using modified FDCM. *Comput Sci*. 2020;21(1):97–112. https://doi.org/10.7494/csci.2020.21.1.3426

[17] Chen K. *Introduction to variational image-processing models and applications*, 2013;90(1):1–8. https://doi.org/10.1080/00207160.2012.757073

[18] Frasczek R, Cyganek B, Wiatr K. Parallelized algorithms for finding similar images and object recognition. *Comput Sci*. 2013;14(1):113–127. https://doi.org/10.7494/csci.2013.14.1.113

[19] Zitova B, Flusser J. Image registration methods: a survey. *Image Vis Comput*. 2003;21(11):977–1000. https://doi.org/10.1016/s0262-8856(03)00137-9

[20] Glasbey CA, Mardia KV. A review of image-warping methods. *J Appl Statis*. 1998;25(2):155–171. https://doi.org/10.1080/02664769823151

[21] Kryjak T, Komorkiewicz M, Gorgon M. Real-time moving object detection for video surveillance system in FPGA. Paper presented at: *Conference on Design & Architectures for Signal & Image Processing*; November 2–4, 2011; Tampere, Finland.

https://doi.org/10.1109/dasip.2011.6136881

[22] Bartoli G. Image registration techniques: A comprehensive survey. *Visual Information Processing and Protection Group*; 2007. https://citeseerx.ist.psu.edu/document?repid=rep1&type=pdf&doi=b6d9d5785a425a86097956c508908228106863ac

[23] Goshtasby AA. *Image registration: Principles, tools and methods*. Springer; 2012.

[24] Ogiela MR. Methods of the Straightening Transformation and Analysis of Outer Contours of Objects in Medical Image Recognitio. *Comput Sci*. 1999;1(1):103–112. https://doi.org/10.7494/csci.1999.1.1.3574

[25] Ogiela MR. Fitting of tonal curve and balancing of gray levels in contrast expansion and preliminary imaging of structures in the analysis. *Comput Sci*. 2000;2:81–92. https://doi.org/10.7494/csci.2000.2.0.3580

[26] Saxena S, Singh RK. A survey of recent and classical image registration methods. *Int J Sig Proc Image Process Pattern Recog*. 2014;7(4):167–76. https://doi.org/10.14257/ijsip.2014.7.4.16

[27] Younes L. *Shapes and diffeomorphisms*. Berlin: Springer; 2010. https://doi.org/10.1007/978-3-642-12055-8

[28] Hill DL, Batchelor PG, Holden M, Hawkes DJ. *Medical image registration. Phy Med Biol*. 2001;46(3):R1. https://doi.org/10.1088/0031-9155/46/3/201

[29] Kotsas P, Dodd T. Rigid registration of medical images using 1D and 2D binary projections. *J Dig Imag*. 2011;24(5):913–925. https://doi.org/10.1007/s10278-010-9352-z

[30] Goshtasby AA. *2-D and 3-D image registration: for medical, remote sensing, and industrial applications*. John Wiley & Sons; 2005.

[31] Knaan D, Joskowicz L. Effective intensity-based 2D/3D rigid registration between fluoroscopic X-ray and CT. *Med Image Computi Comput-Assis Interven.* 2003;351–358.

[32] Livyatan H, Yaniv Z, Joskowicz L. Gradient-based 2-D/3-D rigid registration of fluoroscopic X-ray to CT. *IEEE Transactions on medical imaging*. 2003;22(11):1395–406.

https://doi.org/10.1109/tmi.2003.819288

[33] Yaniv Z. Rigid registration. *Image-Guid Interven*. 2008:159–92. https://doi.org/10.1007/978-0-387-73858-1_6

[34] Jenkinson M, Smith S. A global optimisation method for robust affine registration of brain images. *Med Image Anal*. 2001;5(2):143–56. https://doi.org/10.1016/s1361-8415(01)00036-6

[35] Modersitzki J. *FAIR: Flexible algorithms for image registration*. Society for Industrial and Applied Mathematics; 2009.

[36] Denton ER, Sonoda LI, Rueckert D, et al. Comparison and evaluation of rigid, affine, and nonrigid registration of breast MR images. *J Comput Assist Tomo*. 1999;23(5):800–805. https://doi.org/10.1097/00004728-199909000-00031

[37] Abdel-All NH, Abdel-Razek MA, Abdel-Aziz HS, Khalil AA. Geometry of evolving plane curves problem via lie group analysis. *Stud Math Sci*. 2011;2(1):51–62.

[38] Chong EK, Zak SH. *An introduction to optimization*. John Wiley & Sons; 2013.

[39] Mirjalili S, Lewis A. The whale optimization algorithm. *Adv Eng Soft*. 2016;95:51–67. https://doi.org/10.1016/j.advengsoft.2016.01.008

[40] Kirmani SK, Jamil RN. Optimization of complex geometry using tenth order partial differential equation. *Sci Inq Rev*. 2018;2(2):23–31. https://doi.org/10.32350/sir/22/020203

[41] Inc. The MathWorks. Optimization Math Toolbox: https://au.mathworks.com/help/optim/ug/lsqnonlin.html?searchHighlight=lsqnonlin&stid=srchtitle . Natick, Massachusetts, United State, 2020.

[42] Rashid M, Iqbal MA, Noor NA. DFT-mBJ study of electronic and magnetic properties of cubic CeCrO3 compound: an ab-initio investigation. *Sci Inq Rev*. 2017;1(1):27–36. https://doi.org/10.32350/sir/11/010104

[43] Iqbal MA, Erum N. Opto-Electronic investigation of rubidium based Fluoro-Perovskite for Low Birefringent Lens Materials. *Sci Inq Rev*. 2017;1(1):37–48. https://doi.org/10.32350/sir/11/010105

Scientific Inquiry and Review (SIR)
Volume 7 Issue 1, 2023
ISSN (P): 2521-2427, ISSN (E): 2521-2435
Homepage: https://journals.umt.edu.pk/index.php/SIR

Article QR

Title:	**Construction and Analysis of a Nonstandard Computational Method for the Solution of SEIR Epidemic Model**
Author (s):	Fazal Dayan, Muhammad Iqbal
Affiliation (s):	University of Management and Technology, Lahore, Pakistan
DOI:	https://doi.org/10.32350/sir.71.06
History:	Received: November 5, 2022, Revised: February 5, 2023, Accepted: February 6, 2023, Published: March 15, 2023
Citation:	Dayan F, Iqbal M. Construction and analysis of a nonstandard computational method for the solution of SEIR epidemic model. *Sci Inq Rev.* 2023;7(1):87–110. https://doi.org/10.32350/sir.71.06
Copyright:	© The Authors
Licensing:	This article is open access and is distributed under the terms of Creative Commons Attribution 4.0 International License
Conflict of Interest:	Author(s) declared no conflict of interest

A publication of
The School of Science
University of Management and Technology, Lahore, Pakistan

Construction and Analysis of a Nonstandard Computational Method for the Solution of SEIR Epidemic Model

Fazal Dayan * and Muhammad Iqbal

Department of Mathematics, School of Science, University of Management and Technology, Lahore, Pakistan

ABSTRACT

This paper is concerned with the numerical methods of susceptible exposed infectious recovered (SEIR) epidemic model of coronavirus disease 2019 (COVID-19). The model is explicated numerically with three numerical schemes, forward Euler, Runge-Kutta of order 4 (RK-4), and the proposed non-standard finite difference (NSFD) technique, respectively. In the epidemic model of infectious diseases, positivity is the main property of a consistent framework, since the negative value of a subpopulation is useless. The NSFD technique ends up being a more important and trustable numerical system than forward Euler and RK-4 techniques since it preserves positivity, stability, and convergence. On the contrary, forward Euler and RK-4 schemes do not hold these characteristics for some choices of step sizes. Numerical simulations confirmed the findings.

Keywords: convergence, NSFD method, SEIR model, stability

1. INTRODUCTION

In 1965, scientists identified the first human coronavirus case [1]. Later on, experts discovered a group of related human and animal illnesses caused by a family of viruses named coronaviruses after their crest-like appearance. People can contract seven types of coronavirus infections. COVID-19 sickness is a serious illness brought on by the SARS-CoV-2 infection [2]. The SARS-causing strain first appeared in southern China in 2002 and quickly spread to 29 different nations. By July 2003, 774 individuals had died and more than 8,000 had been infected [3]. Fever, headaches, and breathing problems, such as coughing and shortness of breath, are all brought on by coronavirus infection [4].

Middle East Respiratory Syndrome (MERS) first appeared in Saudi Arabia. Many people who were exposed to it developed difficulty in breathing. It was difficult to treat the respiratory illnesses of such people

* Corresponding Author: fazal.dayan@umt.edu.pk

and they could not recover without needing special care. People who have hidden illnesses, such as diabetes, cardiovascular disease, or risky development, are more likely to transfer recognized illnesses. Being educated about the condition and how the disease spreads is the greatest strategy to prevent and tone down its transmission.

On December 31, 2019, WHO received information regarding instances of pneumonia in Wuhan City, China with enigmatic explanations. On January 7, 2020, Chinese experts identified an original coronavirus as the cause and gave it the temporary designation '2019-nCoV' [5]. According to [6], USA and Brazil are the two nations that are most affected by COVID-19. Dhandapani et. Al provided stiff, fuzzy IRD-14 day average transmission model of COVID-19 pandemic disease [7]. To examine the factors involved in the spread of the coronavirus pandemic in Pakistan and its potential controls, S. Ullah and M.A. Khan developed a numerical model [8]. Duccio and Fanelli focused on the ephemeral aspects of the coronavirus disease 2019 in China, Italy, and France for the time period January 22 - March 15, 2020 [9]. The focus of Xiao and Ruan [10] remained on a pandemic model without a monotonic occurrence rate. The prescribed model depicts the psychological impact of specific illnesses on the local population as the number of infectious agents increase.

Since the spread of coronavirus has resulted in a pandemic, numerous mathematicians have conducted various analyses to create a model to predict its expansion [11–29].

The NSFD scheme was introduced by Mickens [23]. The construction of the NSFD mathematical model for a two-layered differential condition was the focus of Cresson and Pierret [24], who also investigated the model's various aspects, such as combination and solidness of the plan, among others. Selected mathematical models were established and tested using the RK method. Euler algorithm for requests 2 and 4 were completed. In order to account for a jungle fever model, Anguelov et al. [25] constructed the NSFD plot and investigated its dependability and constituent parts. To resolve the nonlinear Riccati differential condition, Riaz et al. [26] presented a very stable non-standard limited distinction (NSFD) strategy. By comparing the results to those of other mathematical operations, such as Euler and RK-4, the proposed model's accuracy and productivity were verified. A dynamic model for infection transmission components was proposed by Rafiq et al. [27].

A mathematical model is developed in the current study by comparing the results with prominent mathematical schemes including the Runge-Kutta approach and the Euler scheme. In order to investigate how insect vectors affect the development of plant diseases, Rafiq et al. [28] proposed a one-of-a-kind, genuinely stable, non-standard finite differentiation (NSFD) numerical arrangement. Numerical assessments were supplied and the outcomes were distinguished. In order to plan the proposed model and determine the value of the limit boundary R_0 for the model, Rafiq et al. [29] developed a model consisting of nonlinear differential conditions. To analyze the susceptible exposed infected recovered (SEIR) dynamic model of COVID-19 (coronavirus) with reference to bimodal infection transmission in vulnerable populations, Ahmed et al. [30] proposed a construction protecting nonstandard limited distinction plan. The suggested mathematical framework produced workable arrangements for the perplexing bi-modular SITR nonlinear model, combined actually consistent states, and reflected dynamic consistency with the perpetual feel of the model. The model's analysis revealed that it maintained some stability at focused consistent states. For the mathematical setup of the SEIR response dispersion pandemic model, [31] provided two innovative NSFD schemes. Moreover, [32] proposed an SIR model in a fuzzy environment. Euler, Runge Kutta of order 4 (RK-4, and the NSFD methods respectively were developed with fuzzy extensions for the solution of the model. Dayan et al. presented rumor based fuzzy model and developed an NSFD scheme for its solution [33]. Some researchers studied fuzzy epidemic models using NSFD schemes [34, 35]. Ali et al. applied the NSFD scheme for the numerical solution of a cancer disease model [36]. Alsallami et al. used Euler, RK, and NSFD methods to solve a real-world problem [37].

The remainder of this article is structured as follows. Model formulation is presented in Section 2. Section 3 discusses the model's equilibrium states, stability, and threshold analysis. Section 4 presents numerical simulation and discussion of the results, while Section 5 displays the numerical results. The novelty of the current work lies in the fact that the proposed model has not been analyzed before using the NSFD method.

2. SEIR MODEL FOR COVID-19

Consider the model

$$\frac{dS}{dt} = \Lambda - \mu S - \frac{\beta SI}{N} \quad (2.1)$$

$$\frac{dE}{dt} = \frac{\beta SI}{N} - (\mu + \epsilon)E \quad (2.2)$$

$$\frac{dI}{dt} = \epsilon E - (\gamma + \mu + \alpha)I \quad (2.3)$$

$$\frac{dR}{dt} = \gamma I - \mu R \quad (2.4)$$

2.1. Theorem

The system $(1-4)$ has a DFE point $(S_{0,}\, E_{0,} I_{0,} R_{0,}) = (\frac{\Lambda}{\mu}, 0, 0, 0)$ and an endemic equilibrium point $(S^*, E^*, I^*, R^*) = \left(\frac{\Lambda}{\mu + \frac{\beta I}{N}}, \frac{\frac{\beta SI}{N}}{(\mu+\epsilon)}, \frac{\epsilon E}{\gamma+\mu+\alpha}, \frac{\gamma I}{\mu}\right)$, respectively.

2.2. Basic Reproductive Number

By incorporating the next generation matrix (NGM) approach, the value of R_0 is determined. Let $X = [S, E]^t$, then $\frac{dX}{dt} = y(x) - z(x)$, where

$$Y(x) = \begin{pmatrix} \frac{\beta SI}{N} \\ 0 \end{pmatrix}$$

and

$$Z(x) = \begin{pmatrix} (\mu + \epsilon)E \\ (+\gamma + \mu + \alpha)I - \epsilon E \end{pmatrix}.$$

Y and Z are now the Jacobeans of the $Y(x)$ and z(x) respectively at DFEP. They are listed below.

$$Y = \begin{pmatrix} 0 & \beta \frac{\beta \Lambda}{\mu N} \\ 0 & 0 \end{pmatrix}$$

and

$$Z = \begin{pmatrix} (\mu + \epsilon) & 0 \\ -\epsilon & \gamma + \mu + \alpha \end{pmatrix}.$$

Inverse of matrix Z is

$$Z^{-1} = \begin{pmatrix} \frac{1}{(\mu + \epsilon)} & 0 \\ \frac{\epsilon}{(\mu + \epsilon)(\gamma + \mu + \alpha)} & \frac{1}{(\gamma + \mu + \alpha)} \end{pmatrix}.$$

Computing the product $Y Z^{-1}$ we get,

$$YZ^{-1} = \begin{pmatrix} 0 & \beta \frac{\beta \wedge}{\mu N} \\ 0 & 0 \end{pmatrix} \begin{pmatrix} \frac{1}{(\mu + \epsilon)} & 0 \\ \frac{\epsilon}{(\mu + \epsilon)(\gamma + \mu + \alpha)} & \frac{1}{(\gamma + \mu + \alpha)} \end{pmatrix}$$

$$YZ^{-1} = \begin{pmatrix} \frac{\beta\epsilon}{(\mu + \epsilon)(\gamma+\mu+\alpha)} & \frac{\beta}{(\gamma+\mu+\alpha)} \\ 0 & 0 \end{pmatrix}.$$

Calculating the spectral radius of YZ^{-1} we get,

$$\lambda = \frac{\beta\epsilon}{(\mu + \epsilon)(\gamma + \mu + \alpha)}.$$

The spectral radius of YZ^{-1} is equable to R_0 which is the maximal eigenvalue of YZ^{-1}.

Therefore,

$$R_0 = \frac{\beta\epsilon}{(\mu + \epsilon)(\gamma + \mu + \alpha)}. \quad (2.5)$$

2.3. Normalized Forward Sensitivity Index (NFSI)

Chitins developed the idea of sensitivity indices by calculating the sensitivity indices of R_0 [38]. A parameter's normalized forward sensitivity index (NFSI) is calculated as $\text{NFSI}(\zeta) = \frac{\zeta}{R_o} \frac{\partial}{\partial \zeta}(R_0)$.

The NSFIs of β, ϵ, β, γ, and α are clalculated as follows:

$$\text{NFSI}(\beta) = \frac{\beta}{R_o} \frac{\partial R_0}{\partial \beta} = \frac{\beta}{\frac{\beta\epsilon}{(\mu+\epsilon)(\gamma+\mu+\alpha)}} \frac{\partial(\beta\epsilon)}{(\mu+\epsilon)(\gamma+\mu+\alpha)} = \frac{(\mu+\epsilon)(\gamma+\mu+\alpha)}{\epsilon} \frac{\epsilon}{(\mu+\epsilon)(\gamma+\mu+\alpha)} = 1.$$

Similarly,

$$\text{NFSI}(\epsilon) = \frac{\epsilon}{\frac{\beta\epsilon}{(\mu+\epsilon)(\gamma+\mu+\alpha)}} \frac{\partial\beta\epsilon}{\partial\epsilon(\mu+\epsilon)(\gamma+\mu+\alpha)} = \frac{\mu}{(\mu+\epsilon)}.$$

$$\text{NFSI}(\mu) = -\frac{\gamma}{(\mu+\epsilon)(\gamma+\mu+\alpha)}, \text{ and}$$

$$\text{NFSI}(\alpha) = \frac{\alpha}{(\gamma+\mu+\alpha)}.$$

These findings unambiguously demonstrate that β is the most sensitive parameter.

2.4. Stability Analysis

The Jacobean of the system (1-4) is

$$J = \begin{pmatrix} \mu - \beta\frac{I}{N} & 0 & -\beta\frac{S}{N} & 0 \\ \beta\frac{I}{N} & -(\mu+\epsilon) & \beta\frac{S}{N} & 0 \\ 0 & -\epsilon & -(\gamma+\mu+\alpha) & 0 \\ 0 & 0 & \gamma & -\mu \end{pmatrix}$$

$$J(\xi_0) = \begin{pmatrix} \mu & 0 & -\beta & 0 \\ \beta\frac{I}{N} & -(\mu+\epsilon) & \beta & 0 \\ 0 & -\epsilon & -(\gamma+\mu+\alpha) & 0 \\ 0 & 0 & \gamma & -\mu \end{pmatrix}$$

If the absolute eigenvalues of $J(\xi_0)$ are smaller than unity, that is, $|\lambda_i| < 1$, i = 1, 2, 3. The numerical scheme converges in all cases. The eigenvalue from the aforementioned Jacobean matrix were extracted, where $\lambda_1 = \lambda_4 = -\mu$, $\lambda_2 = -(\mu+\epsilon)$, and $\lambda_3 = -(\gamma+\mu+\alpha)$.

2.4.1. Stability at Endemic Equilibrium Point. Jacobean matrix at the EE point is

$$J(E^*) = \begin{pmatrix} \mu - \beta\frac{I^*}{N} & 0 & -\beta\frac{S^*}{N} & 0 \\ \beta\frac{I^*}{N} & -(\mu+\epsilon) & \beta\frac{S^*}{N} & 0 \\ 0 & -\epsilon & -(\gamma+\mu+\alpha) & 0 \\ 0 & 0 & \gamma & -\mu \end{pmatrix},$$

where

$S^* = \frac{\Lambda}{\mu+\beta\frac{I}{N}}$ and $I^* = \frac{\epsilon E}{(\gamma+\mu+\alpha)}$.

Using the MATLAB database, the biggest eigenvalues of $J(E^*)$ were plotted. At the endemic equilibrium point, the Jacobean spectral radius has a maximum value that is smaller than unity, as is evident from the preceding figure, proving the intended assertion.

3. NUMERICAL MODELING OF SEIR MODEL FOR COVID-19

3.1. Forward Euler Method

$$S^{n+1} = S^n + h[\Lambda - \mu S^n - S^n\frac{\beta I^n}{N}] \quad (3.1)$$

$$E^{n+1} = E^n + h\left[\frac{\beta S^n I^n}{N} - (\mu+\epsilon)E^n\right] \quad (3.2)$$

$$I^{n+1} = I^n + h\ [\epsilon E^n - (\gamma + \mu + \alpha)I^n] \quad (3.3)$$

$$R^{n+1} = R^n + \mathrm{h}\ [\gamma I^n - \mu R^n] \quad (3.4)$$

3.2. Fourth Order Runge-Kutta (RK-4) Scheme

3.2.1. Step 1

$$k_1 = S^n + h[\Lambda - \mu S^n - S^n\frac{\beta I^n}{N}] \quad (3.5)$$

$$m_1 = E^n + h[\frac{\beta S^n I^n}{N} - (\mu+\epsilon)E^n] \quad (3.6)$$

$$n_1 = I^n + h\ [\epsilon E^n - (\gamma + \mu + \alpha)I^n] \quad (3.7)$$

$$p_1 = R^n + \mathrm{h}\ [\gamma I^n - \mu R^n] \quad (3.8)$$

3.2.2. Step 2

$$k_2 = h[\Lambda - \mu(S^n + \frac{k_1}{2}) - \beta\frac{(S^n + \frac{k_1}{2})(I^n + \frac{n_1}{2})}{N}] \quad (3.9)$$

$$m_2 = h[\beta\frac{(S^n + \frac{k_1}{2})(I^n + \frac{n_1}{2})}{N} - (\mu+\epsilon)(E^n + \frac{m_1}{2})] \quad (3.10)$$

$$n_2 = h\ [\epsilon(E^n + \frac{m_1}{2}) - (\gamma + \mu + \alpha)(I^n + \frac{n_1}{2})] \quad (3.11)$$

$$p_2 = \mathrm{h}\ [\gamma(I^n + \frac{n_1}{2}) - \mu(R^n + \frac{p_1}{2})] \tag{3.12}$$

3.2.3. Step 3

$$k_3 = h[\Lambda - \mu(S^n + \frac{k_2}{2}) - \beta\frac{(S^n + \frac{k_2}{2})(I^n + \frac{n_2}{2})}{N}] \tag{3.13}$$

$$m_3 = h[\beta\frac{(S^n + \frac{k_2}{2})(I^n + \frac{n_2}{2})}{N} - (\mu + \epsilon)(E^n + \frac{m_2}{2})] \tag{3.14}$$

$$n_3 = h\ [\epsilon(E^n + \frac{m_2}{2}) - (\gamma + \mu + \alpha)(I^n + \frac{n_2}{2})] \tag{3.15}$$

$$p_3 = \mathrm{h}\ \left[\gamma\left(I^n + \frac{n_2}{2}\right) - \mu\left(R^n + \frac{p_2}{2}\right)\right] \tag{3.16}$$

3.2.4. Step 4

$$k_4 = h[\Lambda - \mu(S^n + k_3) - \beta\frac{(S^n + k_3)(I^n + n_3)}{N}] \tag{3.17}$$

$$m_4 = h[\beta\frac{(S^n + k_3)(I^n + n_3)}{N} - (\mu + \epsilon)(E^n + m_3)] \tag{3.18}$$

$$n_4 = h\ [\epsilon(E^n + m_3) - (\gamma + \mu + \alpha)(I^n + n_3)] \tag{3.19}$$

$$p_4 = \mathrm{h}\ [\gamma(I^n + n_3) - \mu(R^n + p_3)] \tag{3.20}$$

3.2.5. Step 5

$$S^{n+1} = S^n + \frac{1}{6}\ [k_1 + 2k_2 + 2k_3 + k_4\ ] \tag{3.21}$$

$$E^{n+1} = E^n + \frac{1}{6}\ [m_1 + 2m_2 + 2m_3 + m_4\ ] \tag{3.22}$$

$$I^{n+1} = I^n + \frac{1}{6}\ [n_1 + 2n_2 + 2n_3 + n_4] \tag{3.23}$$

$$R^{n+1} = R^n + \frac{1}{6}\ [p_1 + 2p_2 + 2p_3 + p_4] \tag{3.24}$$

3.3. Non-Standard Finite Difference (NSFD) Scheme

To develop an explicit NSFD scheme, consider the above system as

$$\frac{df(t)}{dS} = \frac{f(t+h) - f(t)}{h} + 0(h) \qquad h \to 0.$$

S^n, E^n, I^n, and R^n are approximations. Here, h is the time step size.

$$\frac{S^{n+1} - S^n}{h} = \Lambda - \mu S^{n+1} - S^{n+1}\frac{\beta I^n}{N} \quad (3.25)$$

$$S^{n+1} = \frac{S^n + h\Lambda}{1 + h\mu + h\frac{\beta I^n}{N}} \quad (3.26)$$

$$E^{n+1} = \frac{E^n + h\frac{\beta S^n I^n}{N}]}{1 + h(\mu + \epsilon)} \quad (3.27)$$

$$I^{n+1} = \frac{I^n + h\,\epsilon E^n}{1 + h\,(\gamma + \mu + \alpha)} \quad (3.28)$$

$$R^{n+1} = \frac{R^n + h\,\gamma I^n}{1 + h\mu} \quad (3.29)$$

3.4. Stability Analysis of the NSFD Technique

The NSFD scheme of the SEIR model is carried out in this section at DFEP $(S_0, E_0, I_0, R_0) = (\frac{\Lambda}{\mu}, 0, 0, 0)$. Consider the **Eq.** (**3.25**) to (**3.28**),

$$F = S^{n+1} = \frac{S + h\Lambda}{1 + h\mu + h\frac{\beta I}{N}} \quad (3.30)$$

$$G = E^{n+1} = \frac{E + h\frac{\beta SI}{N}]}{1 + h(\mu + \epsilon)} \quad (3.31)$$

$$H = I^{n+1} = \frac{I + h\,\epsilon E}{1 + h\,(\gamma + \mu + \alpha)} \quad (3.32)$$

$$K = R^{n+1} = \frac{R + h\,\gamma I}{1 + h\mu} \quad (3.33)$$

Jacobean matrix of the **Eq.** (**3.30**) to (**3.33**) at the DFEP is as follows:

$$J(\xi_0) = \begin{pmatrix} \frac{1}{1+h\mu} & 0 & -\frac{(\frac{\Lambda}{\mu}+h\Lambda)(\frac{h\beta}{N})}{[1+h\mu]^2} & 0 \\ 0 & \frac{1}{1+h(\mu+\epsilon)} & \frac{h\beta\Lambda}{\mu N} & 0 \\ 0 & \frac{h\epsilon}{1+h(\gamma+\mu+\alpha)} & \frac{1}{1+h(\gamma+\mu+\alpha)} & 0 \\ 0 & 0 & \frac{h\gamma}{1+h\mu} & \frac{1}{1+h\mu} \end{pmatrix}.$$

The eigenvalues of the aforementioned Jacobean matrix are $\lambda_1 = \frac{1}{1+h\mu} < 1$ and $\lambda_2 = \frac{1}{1+h\mu} < 1$. The following matrix is used to compute the remaining eigenvalues.

$$J(\xi_0) = \begin{pmatrix} \frac{1}{1+h(\mu+\epsilon)} & \frac{h\beta\Lambda}{\mu N} \\ \frac{h\epsilon}{1+h(\gamma+\mu+\alpha)} & \frac{1}{1+h(\gamma+\mu+\alpha)} \end{pmatrix}.$$

The other eigenvalues are quite complicated to be calculated algebraically. Therefore, they have been calculated numerically (shown in Figure 1).

Figure 1. Eigenvalues of $J(\xi_0)$

The spectral radius of the Jacobean matrix at the DFE point has a maximum value that is less than unity, as is evident from the following figure, proving the intended assertion.

4. NUMERICAL SIMULATION OF THE SEIR MODEL

The findings are discussed in detail in this section. Additionally, Euler, RK-4, and NSFD methods in the model are compared in terms of their use.

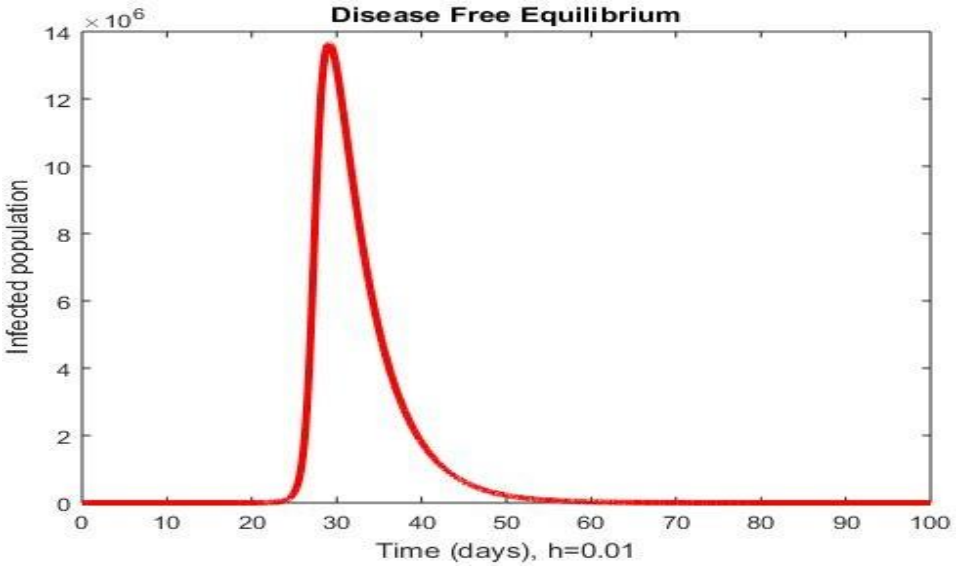

Figure 2. Infected Population using Forward Euler Scheme at h =0.0

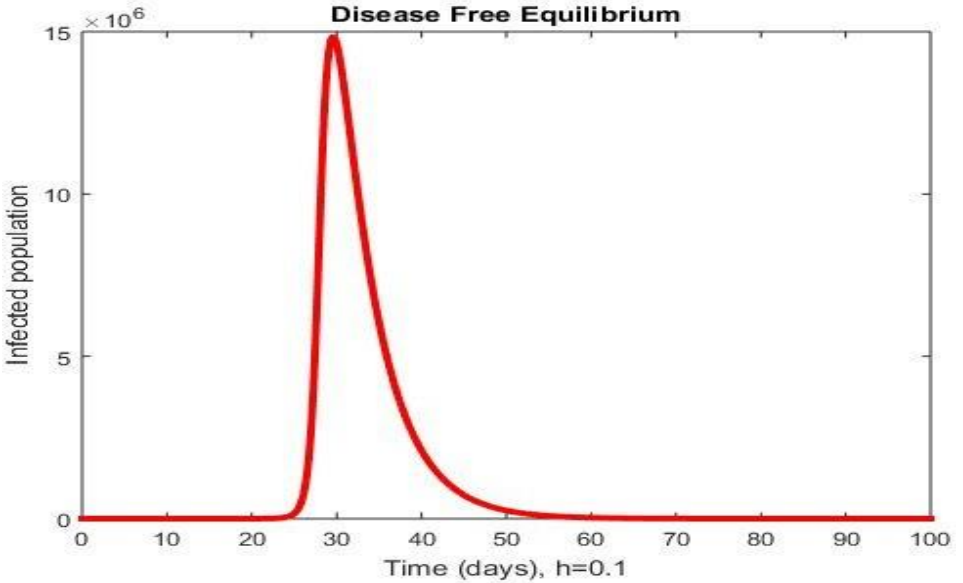

Figure 3. Infected Population using Euler Scheme at h =0.1

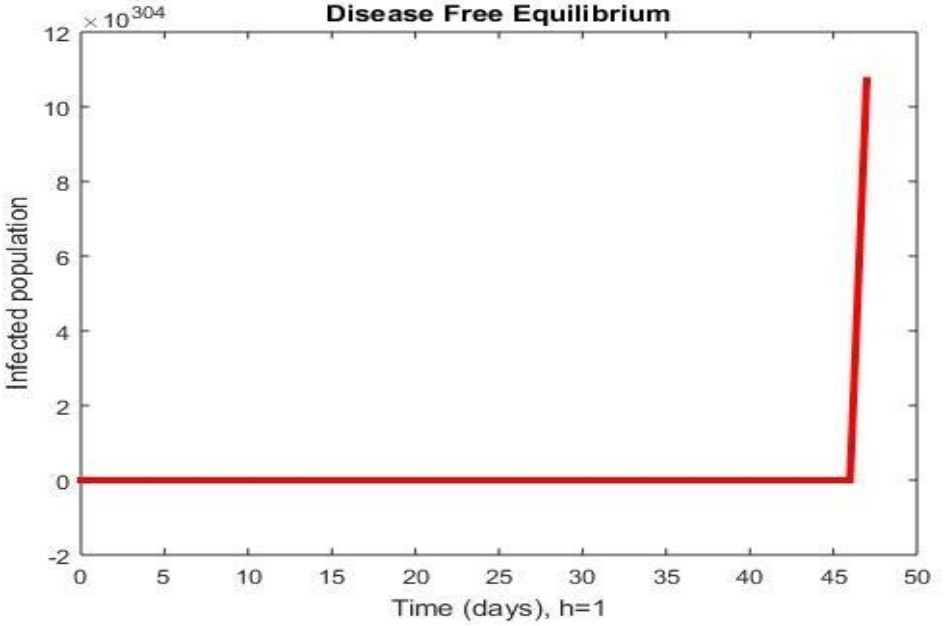

Figure 4. Infected Population using Euler Scheme at h =1

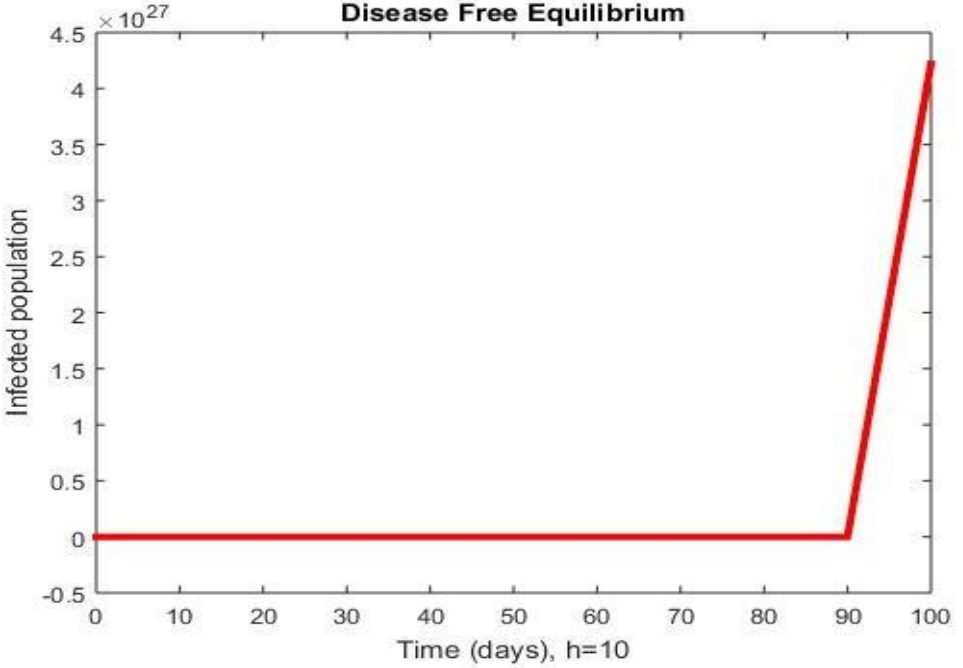

Figure 5. Infected Population using Euler Scheme at h =10

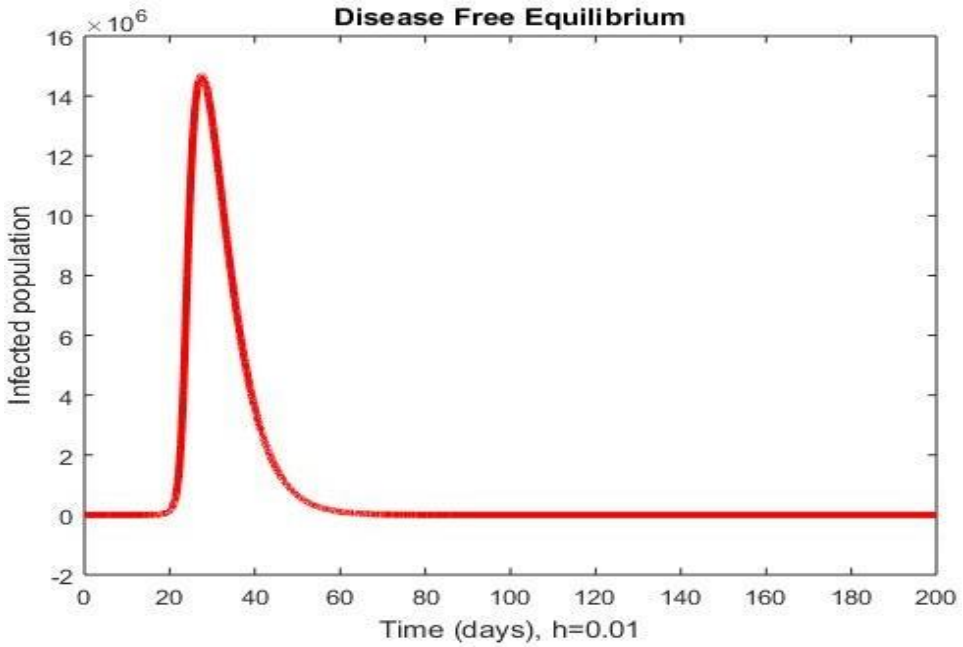

Figure 6. Infected Population using RK-4 Method at h =0.01

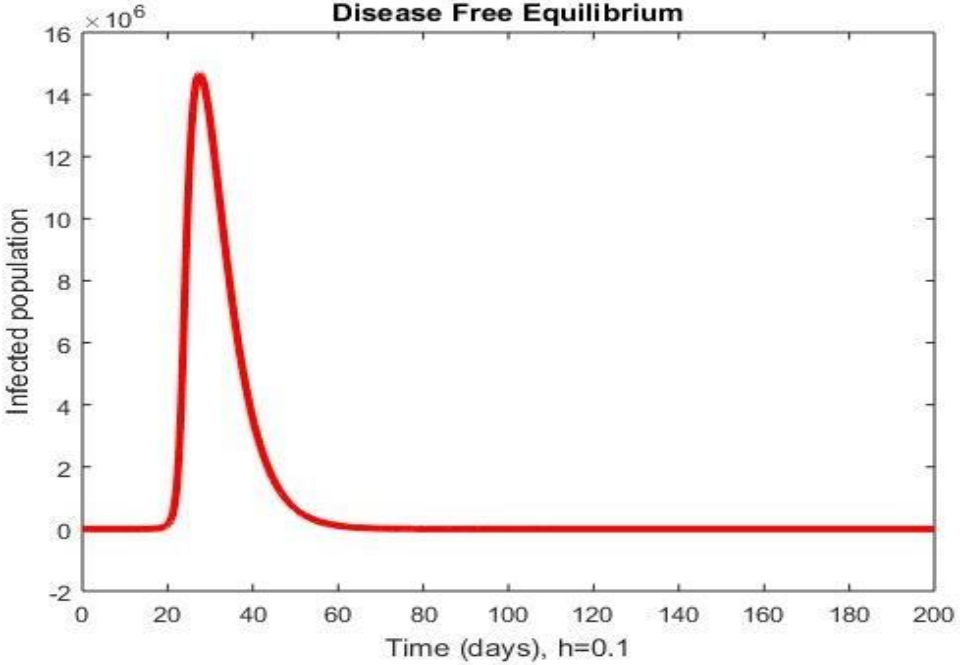

Figure 7. Infected Population using RK-4 Method at h =0.1

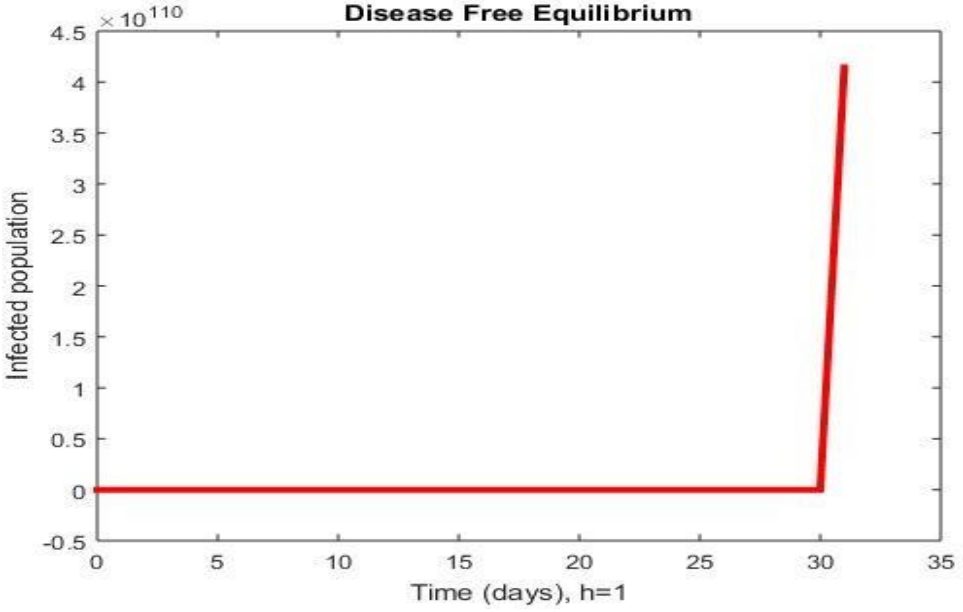

Figure 8. Infected Population using RK-4 Method at h =1

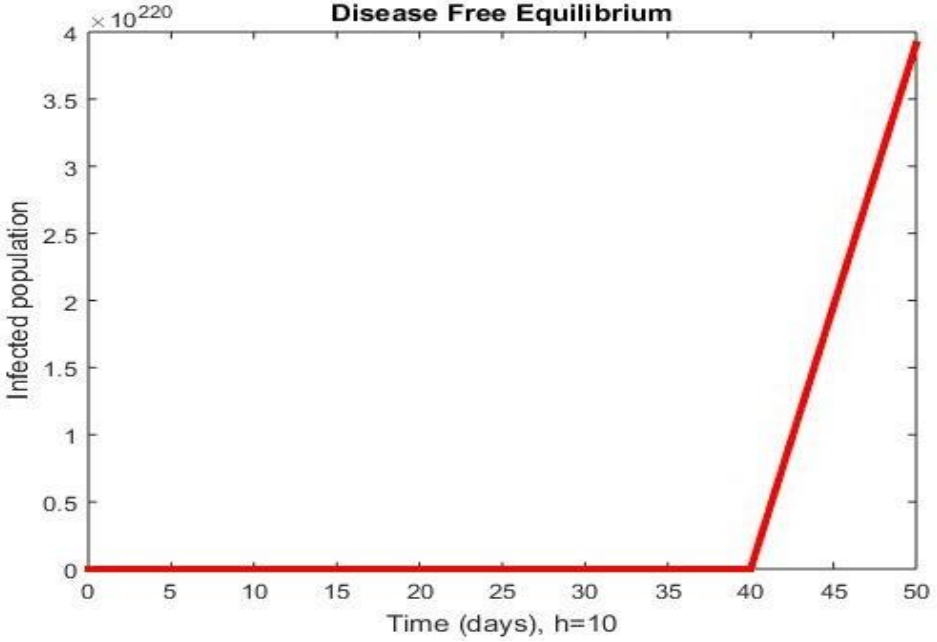

Figure 9. Infected Population using RK-4 Method at h =10

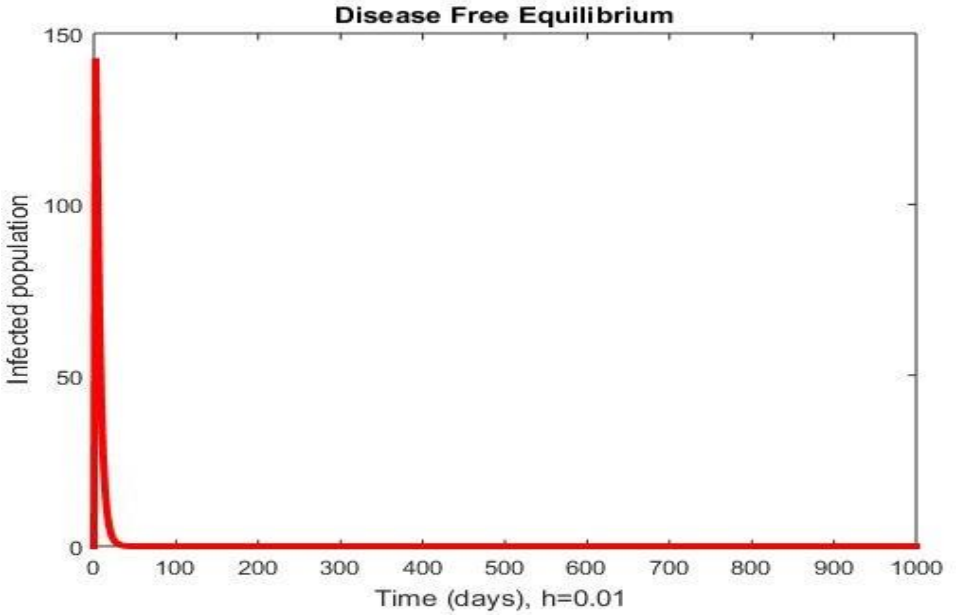

Figure 10. Infected Population using NSFD Scheme at h =0.01

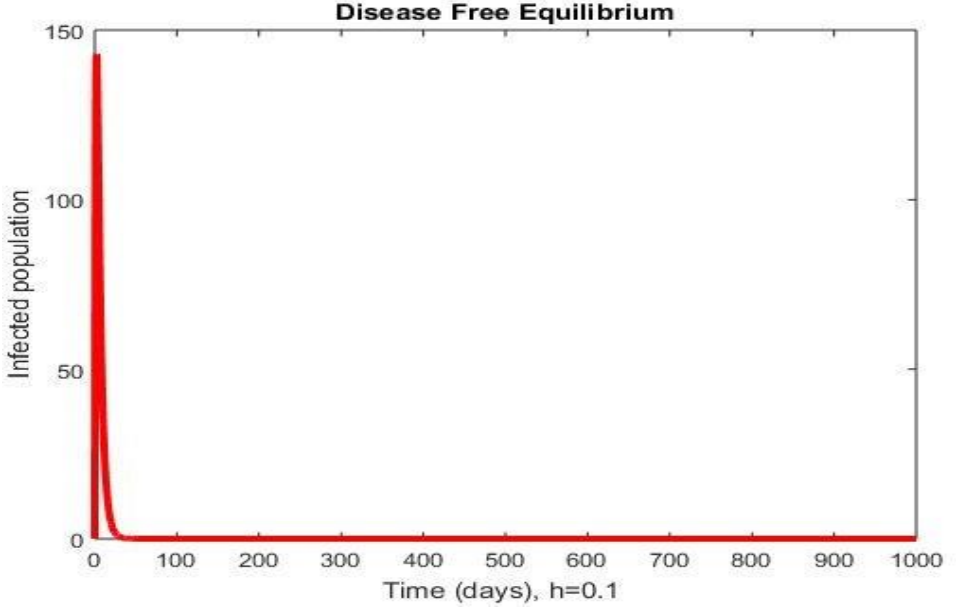

Figure 11. Infected Population using NSFD Scheme at h =0.1

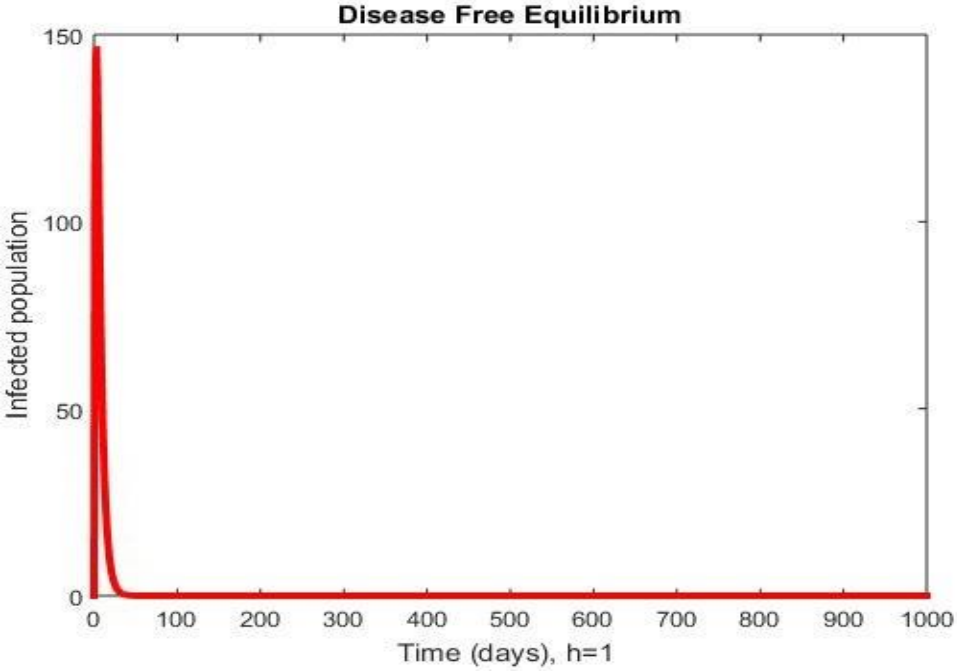

Figure 12. Infected Population using NSFD Scheme at h =1

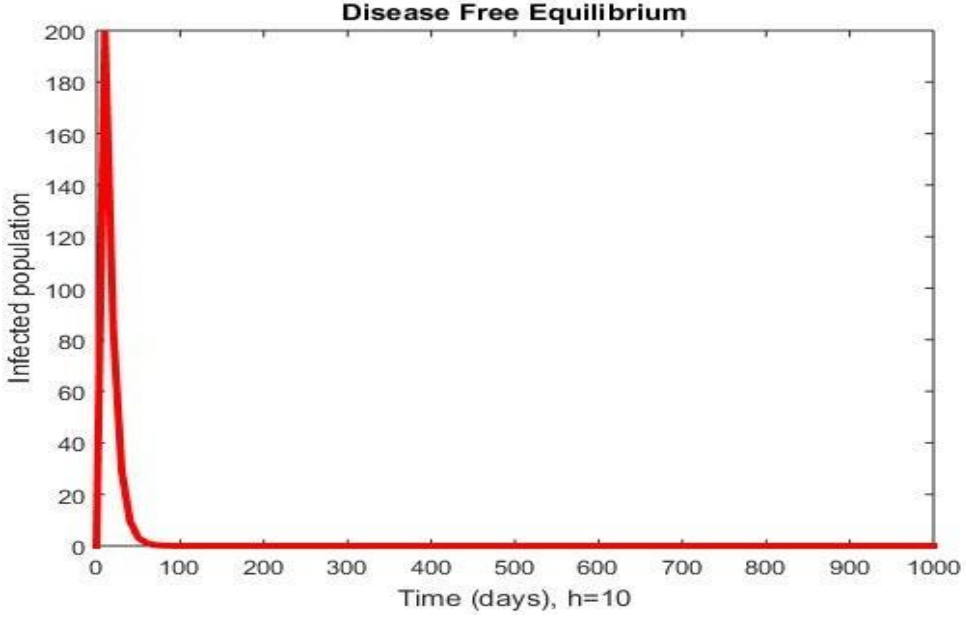

Figure 13. Infected Population using NSFD Scheme at h =10

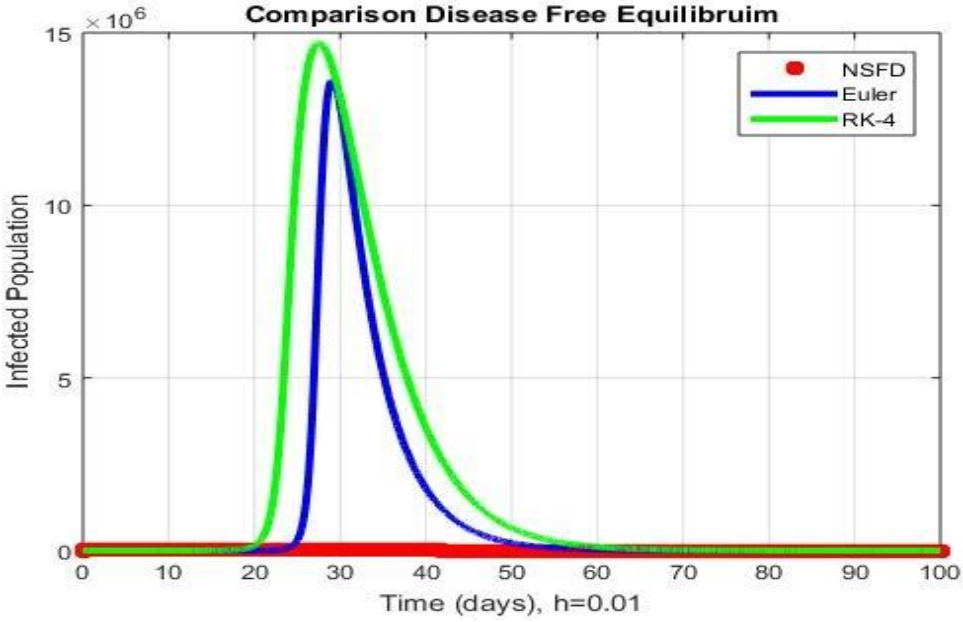

Figure 14. Comparison of Euler, RK-4, and NSFD Scheme at h=0.01

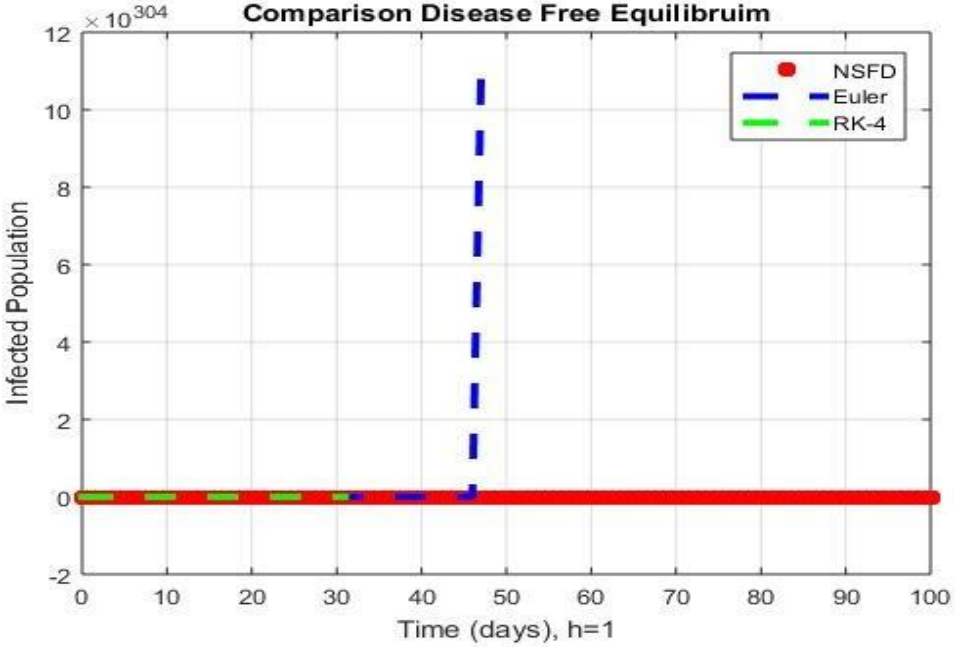

Figure 15. Comparison of Euler, RK-4, and NSFD Scheme at h=0.1

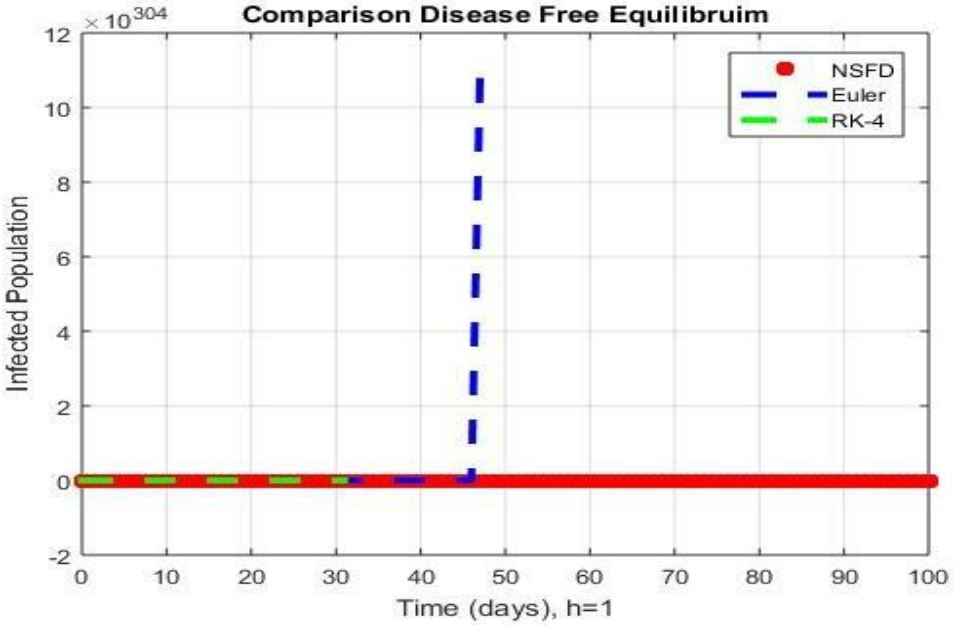

Figure 16. Comparison of Euler, RK-4, and NSFD Scheme at h=1

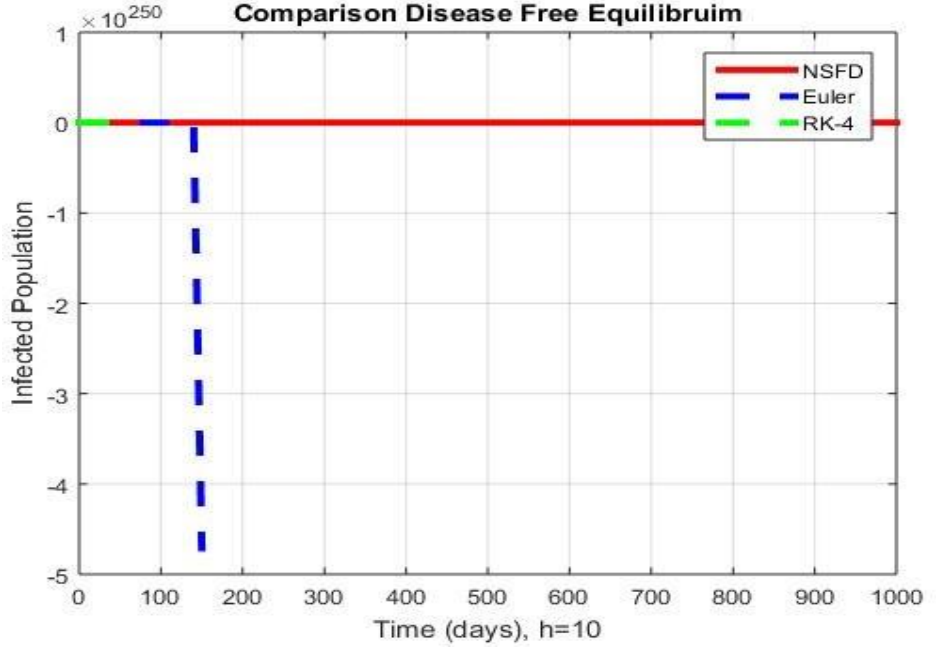

Figure 17. Comparison of Euler, RK-4, and NSFD Scheme at h=10

The behavior of the SEIR model is presented in the above graphs. Figure 2 and Figure 3 show that the Euler technique behaves favorably and converges at small step sizes ($h = 0.01$ and $h = 0.1$). In Figure 4 and Figure 5, the Euler method shows divergence at slightly large step sizes ($h = 1$ and $h = 10$). In Figure 6 and Figure 7, the RK-4 method shows convergence at small step sizes ($h = 0.01$ and $h = 0.1$). The method shows divergence as the step size increases, as shown in Figure 8 and Figure 9, respectively. In Figure 10-13, the NSFD method converges to the same equilibrium points at different step sizes. In Figure 14-17, a comparison of Euler's method, RK-4 method, and NSFD method is depicted. It is clear from the above graphs that all models show similar behaviors at small step sizes and converge to the same equilibrium points. The Euler and RK-4 methods show divergence and negative behavior as step size increases, while the NSFD method converges to the same point. Graphical depiction of behaviors demonstrates that the Euler and RK-4 methods only provide convergence solutions for small step sizes and remain inconclusive for large step sizes. The NSFD scheme, on the other hand, exhibits good behavior and also provides a convergent solution for step sizes that are extremely large.

5. CONCLUSION

The mathematical study of the SEIR model for the spread of COVID-19 was carried out in this research. For this purpose, the reproduction number R_0, sensitivity of R_0, and equilibrium points of the model were determined. It was shown that both equilibrium points have similar stability properties. In order to solve the investigated model, Euler, RK-4, and NSFD algorithms were deployed. Different time step sizes were used for numerical experiments at DFE and EE locations. The collected results were examined and compared. From the said examination, the current study concludes that the suggested method yields findings that converge to true stable states for any time step size. However, the Euler and RK-4 methods do not hold for large time step sizes. Moreover, the NSFD method is bounded, dynamically consistent, and preserves the positivity of the solution which are important requirements when modeling a prevalent disease.

REFERENCES

1. Tyrrell DAJ, Bynoe ML. Cultivation of a novel type of common cold virus in organ culture. *BMJ*. 1965;1(5448):1467–1470. http://dx.doi.org/10.1136/bmj.1.5448.1467

2. World Health Organization. Coronavirus disease (COVID-19). https://www.who.int/health-topics/coronavirus#tab=tab_1

3. Stadler K, Masignani V, Eickmann M, et al. SARS—beginning to understand a new virus. *Nat Rev Microbiol*. 2003;1(3):209–218. https://doi.org/10.1038/nrmicro775

4. Peiris JS, Lai ST, Poon LL, et al. Coronavirus as a possible cause of severe acute respiratory syndrome. *Lancet*. 2003;361(9366):1319–1325. https://doi.org/10.1016/S0140-6736(03)13077-2

5. World Health Organization. Novel coronavirus (2019-nCoV). https://www.who.int/docs/default-source/coronaviruse/situation-reports/20200121-sitrep-1-2019-ncov.pdf . Updated January 21, 2021. Accessed September 18,2021.

6. Abelson R. Brazil reported one of the highest Covid death tolls in the world. *The New York Times*. https://www.nytimes.com/2021/06/20/health/brazil-deaths-covid.html . Updated June 24, 2021. Accessed September 15, 2021.

7. Dhandapani PB, Baleanu D, Thippan J, Sivakumar V. On stiff, fuzzy IRD-14 day average transmission model of COVID-19 pandemic disease. *AIMS Bioeng*. 2020;7(4):208–223.

8. Ullah S, Khan MA. Modeling the impact of non- pharmaceutical interventions on the dynamics of novel coronavirus with optimal control analysis with a case study. *Chaos Solitons Fractal*. 2020;139:e110075. https://doi.org/10.1016/j.chaos.2020.110075

9. Fanelli D, Piazza F. Analysis and forecast of COVID-19 spreading in China, Italy and France. *Chaos Solitons Fractal*. 2020;134:e109761. https://doi.org/10.1016/j.chaos.2020.109761

10. Xiao D, Ruan S. Global analysis of an epidemic model with nonmonotone incidence rate. *Math Biosci*. 2007;208(2):419–429. https://doi.org/10.1016/j.mbs.2006.09.025

11. Lin Q, Zhao S, Gao D, et al. A conceptual model for the coronavirus disease 2019 (COVID-19) outbreak in Wuhan, China with individual reaction and governmental action. *Int J Infect Dis.* 2020:93;211–216. https://doi.org/10.1016/j.ijid.2020.02.058

12. Naveed M, Rafiq M, Raza A, et al. Mathematical analysis of novel

coronavirus (2019-nCov) delay pandemic model. *Comput Mater Continua*. 2020;64(3):1401–1414. https://doi.org/10.32604/cmc.2020.011314

13. Shatanawi W, Raza A, Muhammad Shoaib A, Abodayeh K, Rafiq M, Bibi M. An effective numerical method for the solution of a stochastic coronavirus (2019-nCovid) pandemic model. *Comput Mater Continua.* 2021;66(2):1121–1137.
14. Shahid N, Baleanu D, Ahmed N, et al. Optimality of solution with numerical investigation for coronavirus epidemic model. *Comput Mater Continua.* 2021;67(2):1713–1728. https://doi.org/10.32604/cmc.2021.014191
15. Ahmed N, Baleanu D, Rafiq M, et al., Dynamical behavior and sensitivity analysis of a delayed coronavirus epidemic model. *Comput Mater Continua*. 2020;65(1):225–241. https://doi.org/10.32604/cmc.2020.011534
16. Aba-Oud MA, Ali A, Alrabaiah H, et al. A fractional order mathematical model for COVID-19 dynamics with quarantine, isolation, and environmental viral load. *Adv Differ Equ*. 2021;106:1–19. https://doi.org/10.1186/s13662-021-03265-4
17. Gao W, Veeresha P, Prakasha DG, et al. Novel dynamic structures of 2019-nCOV with nonlocal operator via powerful computational technique. *Biology*. 2020;9(5):e107. https://doi.org/10.3390/biology9050107
18. Khan MA, Atangana A. Modeling the dynamics of novel coronavirus (2019-nCov) with fractional derivative. *Alexandria Eng J*. 2020;59(4):2379–2389. https://doi.org/10.1016/j.aej.2020.02.033
19. Atangana A, Retaraz SIG. A novel Covid-19 model with fractional differential operators with singular and non-singular kernels: Analysis and numerical scheme based on Newton polynomial. *Alexandria Eng J*. 2021;60(4):3781–3806. https://doi.org/10.1016/j.aej.2021.02.016
20. Khan MA, Atangana A, Fatmawati EA. The dynamics of COVID-19 with quarantined and isolation. *Adv Differ Equ*. 2020;2020(1):1–22. https://doi.org/10.1186/s13662-020-02882-9
21. Khan MA, Ullah S, Kumar S. A robust study on 2019-nCOV outbreaks

through non-singular derivative. *Eur Phys J Plus*. 2021;136:e168. https://doi.org/10.1140/epjp/s13360-021-01159-8

22. Rafiq M, Ali J, Riaz MB, et al. Numerical analysis of a bi-modal covid-19 SITR model. *Alexandria Eng J*. 2022;61(1):227–235. https://doi.org/10.1016/j.aej.2021.04.102
23. Mickens RE. Advances in applications of non-standard finite difference schemes. Singapore, World Scientific Publishing Company; 2019.
24. Cresson J, Pierret F. Nonstandard finite difference schemes preserving dynamical properties. *J Comput Appl Math*. 2016;303:15–30. https://doi.org/10.1016/j.cam.2016.02.007
25. Anguelov R, Dumont Y, Lubuma J, Mureithi E. Stability analysis and dynamics preserving nonstandard finite difference schemes for a malaria model. *Math Popul Stud*. 2013;(20):101–122. https://doi.org/10.1080/08898480.2013.777240
26. Riaz S, Rafiq M, Ahmad O. Non standard finite difference method for quadratic riccati differential equation. *Punjab Unive J Math*. 2015;47(2):49–55.
27. Rafiq M, Raza A, Anayat A. Numerical modeling of virus transmission in a computer network. Paper presented at: 14th International Bhurban Conference on Applied Sciences & Technology (IBCAST) 219; January 10–14, 2017; Islamabad, Pakistan. https://doi.org/10.1109/IBCAST.2017.7868087
28. Rafiq M, Ahmad W, Abbas M. et al. A reliable and competitive mathematical analysis of Ebola epidemic model. *Adv Differ Equ*. 2020;2020:e540. https://doi.org/10.1186/s13662-020-02994-2
29. Rafiq M, Ali J, Riaz MB, Jan Awrejcewicz, Numerical analysis of a bi-modal covid-19 SITR model. *Alexandria Eng J*. 2022;61(1):227–235, http://doi/doi.org/10.1016/j.aej.2021.04.102
30. Ahmed N, Tahira S, Rafiq M, et al. Positivity preserving operator splitting nonstandard finite difference methods for SEIR reaction diffusion model. *Open Math*. 2019;17(1):313–330. https://doi.org/10.1515/math-2019-0027
31. Dayan F, Ahmed N, Rafiq M, et al. Construction and numerical analysis of a fuzzy non-standard computational method for the solution of an

SEIQR model of COVID-19 dynamics. *AIMS Math*. 2022;7(5):8449–8470. https://doi.org/10.3934/math.2022471

32. Dayan F, Rafiq M, Ahmed N, et al. Design and numerical analysis of fuzzy nonstandard computational methods for the solution of rumor based fuzzy epidemic model. *Physica A.* 2022;600:e127542. https://doi.org/10.1016/j.physa.2022.127542

33. Dayan F, Ahmed N, Rafiq M, et al. A dynamically consistent approximation for an epidemic model with fuzzy parameters. *Expe Syst Appl*. 2022;210:e118066. https://doi.org/10.1016/j.eswa.2022.118066

34. Dayan F, Rafiq M, Ahmed N, Raza A, Ahmad MO. A dynamical study of a fuzzy epidemic model of Mosquito-Borne Disease. *Comput Biol Med*. 20221;148:e105673. https://doi.org/10.1016/j.compbiomed.2022.105673

35. Dayan F, Baleanu D, Ahmed N, et al., Numerical investigation of malaria disease dynamics in fuzzy environment. *Comput Mater Continua*. 2023;74(2):2345–2361.

36. Raza A, Awrejcewicz J, Rafiq M, Ahmed N, Mohsin M. Stochastic analysis of nonlinear cancer disease model through virotherapy and computational methods. *Mathematics*. 2022;10(3):e368. https://doi.org/10.3390/math10030368

37. Alsallami SA, Raza A, Elmahi M, et al. Computational approximations for Real-World application of epidemic model. *Intell Autom Soft Comput*. 2022;33(3):1923–1939.

38. Chitnis N, Hyman JM, Cushing JM. Determining important parameters in the spread of malaria through the sensitivity analysis of a mathematical model. *Bulletin Math Biol*. 2008;70:1272-1296. https://doi.org/10.1007/s11538-008-9299-0